



TECHNISCHE
UNIVERSITÄT
WIEN

Vienna University of Technology

Masterarbeit

Synthesis and Characterization of Polymer-Linker Systems for T-cell Activation

Zur Erlangung des akademischen Grades „Diplom-Ingenieur“ an der Technischen
Universität Wien, Fakultät für Technische Chemie

Ausgeführt am Institut für Angewandte Synthesechemie IAS

Eingereicht von

Stefan F. Helfert, Bsc

Matrikelnummer 0725070

Schwechatstraße 55

2514 Traiskirchen

Unter der Leitung von

Ao. Univ. Prof. DI Dr. Robert LISKA,

Univ. Ass. Mag. Dr. Claudia DWORAK

Univ.Ass. Dipl.-Ing. Dr. Eva Sevcsik

Unterschrift Betreuer

Wien, am 21 März 2017

Unterschrift Student

Danksagung

Zuerst möchte ich meinen Betreuern, Robert Liska und Claudia Dworak, danken, da sie mir die Möglichkeit gaben an diesem Projekt und in der besten Arbeitsgruppe zu arbeiten und die Durchführung dieser Diplomarbeit betreuten. Ich arbeite und forsche gerne hier und bin froh darüber auch meine Dissertation hier ausleben zu dürfen.

Außerdem möchte ich den Leuten Dank aussprechen, welche mir im Zuge meiner Arbeit analytische Hilfe zukommen ließen. Das wären, Eva Sevcsik, welche auch in diesem Projekt tätig ist, für ihre TIRF Mikroskopie Messungen, Herwig Peterlik für die SAXS Messungen an der Universität Wien, Markus Sauer und Annette Foelske-Schmitz für die gemessenen XPS Proben, Thomas Konegger für die Betreuung des von ihm selbst gebauten Dip-coaters, Davide Ret für seine vermittelten Kompetenzen am light scattering Goniometer und Roland Bittner für sein vermitteltes Wissen zur Kontaktwinkelmessung und Ellipsometrie.

Natürlich möchte ich auch der Arbeitsgruppe Fachbereich Makromolekulare Chemie des IAS TU Wien danken, für die angenehme und gesellige Zeit, während der im Labor und auch außerhalb verbrachten Zeit. Ich möchte keine einzelnen Personen nennen, ihr alle seid einfach die Besten!

Meiner Familie möchte ich danken, da sie immer mit tatkräftiger Unterstützung hinter mir standen, egal wie schwierig die Zeiten während der Studienzeit und davor waren, und sie mir immer aus der Patsche halfen, falls einmal alles schief lief.

Diese Arbeit wurde um 07:01 am Tag der Abgabe fertiggestellt. Wie immer in der letzten Minute.

Gäbe es die letzte Minute nicht,
so würde niemals etwas fertig.

Mark Twain (1835 - 1910)

Abstract

In the field of biomedical application, the generation and design of polymer brushes became very attractive due to their ability to control a number of important architectural features¹ for the creation of particular biointerfaces²⁻⁴ and applications in nanotechnologies⁴⁻⁶. In the course of this thesis, a strategy for a polymer linker system on glass substrates for T-cell activation was established, in form of end-group functionalized polymers designed for the coupling to biomolecules. For the implementation of this polymer brush system, surface-induced reversible addition fragmentation chain transfer (RAFT) polymerization was selected, delivering gentle polymerization conditions, absence of toxic catalysts, a variety of possible end-group modifications, uniform chain lengths and defined molecular weights. Acryloylmorpholine (NAM)⁷ and methoxypropylacrylamide (MPAA)⁸ were chosen as biocompatible monomers. Kinetic studies were performed on the RAFT polymerization of these monomers using 4-cyano-4-(((dodecylthio) carbonothioyl)thio)pentanoic acid (CDTPA) and 2-(((dodecylthio)carbonothioyl)thio)-2-methylpropanoic acid (DDMAT) as RAFT reagents, which were synthesized in the first step according to literature. Both RAFT reagents showed high monomer conversions within short polymerization times. The generated polymers pNAM and pMPAA were investigated on their morphology in aqueous environment with light scattering methods and small angle X-ray scattering, to predict their arrangement in a polymer brush system. It was found out that both polymers formed worm-like shaped aggregates in water and PBS buffer solution. Studies on end-group modification of pNAM and pMPAA polymers were performed by aminolysis and radical induced end-group formation. It proved, that radical induced end-group formation with 4,4'-azobis(4-cyanovaleric acid) performed in good yields and was easy to establish. For the grafting of the polymers from glass substrates by surface immobilized RAFT reagents, further studies were performed. Two approaches were tested: First, to immobilize aminopropyl triethoxysilane (APTES) on the glass surface and then couple the RAFT reagent onto it, second, to immobilize APTES modified RAFT reagents to the surface. These modifications were monitored by contact angle (CA) measurement, total internal reflection fluorescence microscopy (TIRFM), ellipsometry and X-ray photoelectron spectroscopy (XPS). With knowledge gained from these functionalization experiments, a future system for surface induced RAFT polymerization of a suitable polymer brush system will be possible.

Kurzfassung

Im Bereich der biomedizinischen Anwendungen, wurde die Herstellung und das Design von Polymer-brushes in letzter Zeit sehr attraktiv, da diese, spezielle Fähigkeiten und eine Vielzahl an wichtigen architektonischen Eigenschaften kontrollieren können. Polymer-brushes werden verwendet um spezielle Biointerfaces und Anwendungen im Nanotechnologiebereich zu realisieren. Im Zuge dieser Arbeit wurde eine Strategie für ein Polymer-Linker-System auf Glassubstraten erstellt, um T-Zellen Aktivierung zu ermöglichen. Endgruppen-funktionalisierte Polymer-brushes sollten eine mögliche Kupplung mit Biomolekülen ermöglichen. Für die Implementierung eines solchen Biointerface-Systems wurde als Methode die sogenannte oberflächeninduzierte Reversible Additions-Fragmentierungs Kettenübertragungs (RAFT) Polymerisation gewählt, da diese Methode bestimmte Vorteile mit sich bringt, wie milde Polymerisationsbedingungen, Abwesenheit von toxischen Katalysatoren, ein breites Spektrum an möglichen Endgruppen-Modifikationen, einheitliche Kettenlängen und definierte Molekulargewichte. Als biokompatible Monomere in diesem System wurden N-Acryloylmorpholin (NAM) und Methoxypropylacrylamid (MPAA) verwendet. Kinetische Studien wurden mit diesen Monomeren und den RAFT Reagenzien 4-Cyano-4-[(dodecylsulfanylthiocarbonyl)-sulfanyl]pentansäure (CDTPA) und 2-(Dodecylthiocarbonothioylthio)-2-methylpropionsäure (DDMAT) durchgeführt, welche im ersten Schritt gemäß der Literatur synthetisiert wurden. Beide RAFT Reagenzien zeigten hohe Monomerumsätze in kurzen Polymerisationszeiten. Die hergestellten Polymere polyNAM und polyMPAA wurden anschließend auf ihre Morphologie in wässriger Umgebung mittels Lichtstreuungsmethoden und Kleinwinkelröntgenstreuung untersucht, um ihre Anordnung bei Verwendung als Polymer-brushes vorherzusagen. Es wurde herausgefunden, dass beide Polymere fadenähnliche Aggregate in Wasser und in PBS Puffer Lösung formten. Studien zur Endgruppen-Modifizierung von polyNAM und polyMPAA wurden durchgeführt, mittels Aminolyse und Radikal-induzierter Endgruppen-Modifizierung. Es wurde herausgefunden, dass die radikalisch induzierte Endgruppen-Modifizierung mit 4,4'-Azobis(4-cyanovaleriansäure) mit guten Umsätzen funktionierte und leicht durchzuführen war. Für das Pfropfpolymerisieren auf der Glasoberfläche wurden weitere Studien durchgeführt. Zwei Methoden wurden getestet: Die erste war die Immobilisierung von Aminopropyltriethoxysilan (APTES) auf der Glasoberfläche mit anschließender Kupplung zu einem RAFT Reagenz, die zweite war die

Immobilisierung eines mit APTES gekuppelten RAFT Reagenzes auf die Oberfläche. Diese Modifizierungen wurden mittels Kontaktwinkel (CA) Messungen, totaler interner Reflexion Fluoreszenz Mikroskopie (TIRFM), Ellipsometrie und Röntgen Photoelektronen Spektroskopie charakterisiert. Mit den Erkenntnissen aus diesen Funktionalisierungsversuchen kann in Zukunft ein geeignetes Polymer-brush System realisiert werden.

Table of contents

Abstract	5
Kurzfassung.....	7
Introduction.....	12
1.1 Polymer brushes in the biomedical field	12
1.2 Controlled radical polymerization (CRP).....	13
1.3 RAFT polymerization	15
1.3.1 RAFT mechanism	16
1.3.2 RAFT reagents.....	18
1.3.4 End group modification	20
1.3.5 Potential applications for RAFT polymerization.....	21
1.4 Light scattering and structure analytics at macromolecular and colloidal systems.....	23
1.4.1 Static light scattering (SLS).....	24
1.4.2 Dynamic light scattering (DLS).....	27
1.4.3 Small angle X-ray scattering (SAXS)	28
1.5 Covalent surface modification and functionalization of SiO ₂ materials	29
1.6 Surface analytics	30
1.6.1 Contact angle measurement (CA).....	31
1.6.2 Ellipsometry	32
1.6.3 X-ray photoelectron spectroscopy (XPS)	33
1.6.4 Total internal reflection fluorescence microscopy (TIRFM)	34
Objective.....	36
State of the art	37
Results and discussion	44
1 Strategy for the synthesis of the polymer linker system.....	44
2 Synthesis of the RAFT reagents.....	49

2.1	Synthesis of 4-cyano-4-(((dodecylthio)carbonothioyl)thio)pentanoic acid (CDTPA).....	49
2.2	Synthesis of 2-(((dodecylthio)carbonothioyl)thio)-2-methylpropanoic acid (DDMAT)	50
3	Kinetic studies of the RAFT polymerization method	51
3.1	Reaction kinetics of RAFT polymerization of NAM and MPAA using CDTPA as CTA	52
3.2	Reaction kinetics of RAFT polymerization of NAM and MPAA using DDMAT as CTA	59
3.3	Summary of the kinetic studies of RAFT polymerization of NAM and MPAA	65
4	Analysis of pNAM and pMPAA in solution by static light scattering, dynamic light scattering and small angle X-ray scattering.....	68
4.1	SLS and DLS analysis of pNAM in water	68
4.2	SAXS analysis of pNAM in water	71
4.3	SLS and DLS analysis of pNAM in PBS buffer.....	73
4.4	SAXS analysis of pNAM in PBS buffer.....	76
4.5	SLS and DLS analysis of pMPAA in water	77
4.6	SAXS analysis of pMPAA in water	79
4.7	SLS and DLS analysis of pMPAA in PBS buffer	80
4.8	SAXS analysis of pMPAA in PBS buffer.....	81
4.9	Summary of the results of the scattering analyses	82
5	Modification of end groups	84
5.1	Aminolysis induced end group formation to thiol groups	85
5.2	Radical induced end group formation with 4, 4'-azobis (4-cyanovaleric acid) (ACVA)	87
5.3	Summary of the results for end group modification	89
6	Synthesis of a RAFT reagent with an ethoxysilane end group	91

6.1	Screening for a suitable synthesis of 2-cyano-5-oxo-5-((3-(triethoxysilyl)propyl)amino)pentan-2-yl dodecyl carbonotrithioate (Si-CDTPA).	92
6.2	Screening for a synthesis of dodecyl (2-methyl-1-oxo-1-((3-(triethoxysilyl)propyl)amino)propan-2-yl) carbonotrithioate (Si-DDMAT)	96
6.3	Screening for alternative coupling methods	99
7	Analysis of coating homogeneity using APTES for functionalization of glass surfaces	102
8	Modification of the SiO ₂ surface with RAFT reagents	108
8.1	Pre-functionalization of the surface with APTES and coupling to the RAFT reagent; pathway (1)	108
8.1.1	Analysis of the surfaces, generated by pathway (1)	110
8.2	Coupling of the ethoxysilane-RAFT reagent directly to the surface; pathway (2)	115
8.2.1	Analysis of the surfaces, generated by pathway (2)	116
8.3	Functionalization of the surface with 3-(trimethoxysilyl)propyl methacrylate (TMPMA); pathway via macro-RAFT	119
8.4	Summary of the modification pathways 1, 2 and macro-RAFT for the functionalization of SiO ₂ surfaces with CTA reagents	122
	Experimental part	126
	Summary	149
	Materials, devices, analytics	156
	Abbreviations	159
	Literature	162

Introduction

1.1 Polymer brushes in the biomedical field

In the field of biomedical application, the generation and design of polymer brushes became very attractive due to their ability to control a number of important architectural features¹ for the creation of particular biointerfaces²⁻⁴ and applications in nanotechnologies⁴⁻⁶. These systems consist of polymer chains, attached to a material's surface, like silicon⁹, glass¹⁰, gold¹¹, etc. and can be used for biomedical applications like biosensing^{12, 13} (**Figure 1**), cell culture and tissue engineering^{14, 15}, antibacterial coatings^{16, 17} and many more.

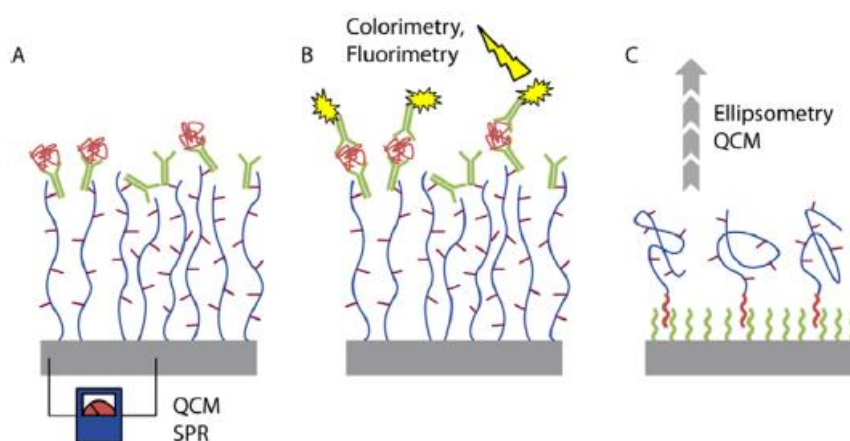


Figure 1. Examples for polymer brush based biosensing platforms; Quartz crystal microbalance (QCM); Surface plasmon resonance (SPR) for label free detection (A), label based detection (B), mass amplification (C)¹

These polymer brushes can be generated by two different approaches. First, a “grafting to” process, where an already available polymer chain is directly attached to the materials surface and second, a “grafting from” approach, where a starter compound is attached to the surface and the polymer chain grows from the surface¹⁸. The second pathway became more popular, due to a better control over architectural features¹⁹ and different methods were developed based on surface initiated controlled radical polymerization, using atom transfer radical polymerization (ATRP)¹⁰, reversible addition fragmentation chain transfer polymerization (RAFT)²⁰, nitroxide mediated polymerization (NMP)²¹ and iniferter polymerization²² for a high variety of monomers.

By changing of parameters like monomers, chain length or rather layer thickness and grafting density the interfacial properties can be tuned¹. In this thesis, the main focus is directed on the characterization of suitable polymer systems for the generation of such bioactive surfaces, concerning structure and conformation in aqueous environment. Therefore, surface induced RAFT polymerization could be applied, which is a valuable controlled radical polymerization method for the grafting of terminally functionalized polymer chains.²³

1.2 Controlled radical polymerization (CRP)

One of the drawbacks of conventional free radical polymerization (FRP) is the preparation of polymers with defined molecular weight, molecular weight distribution and complex architectures. This is based on the fact that FRP basically consists of 5 steps: Initiation, start of the chain reaction, propagation, chain termination and chain transfer. The main hindrance to get a defined molecular weight and uniform structure with FRP is termination, which is caused by a large amount of radicals being available in a polymerization mixture. Being able to control termination or reduce it, means being able to control molecular weight and molecular weight distribution. Due to that fact the so called controlled radical polymerization methods were developed over the past decades. These CRP methods are classified by a dynamic equilibrium between a dormant and an active species during polymerization, a first-order kinetic, the pre-determination of the molecular weight by the initial concentration of monomer and controlling species and the possibility to obtain polymers with a uniform chain length²⁴. **Figure 2** depicts the difference in molecular weight distribution of FRP and CRP on the basis of RAFT polymerization.

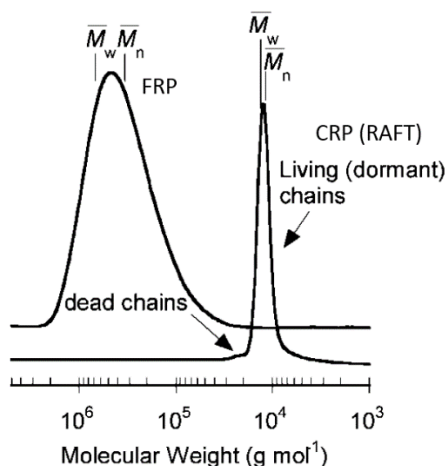
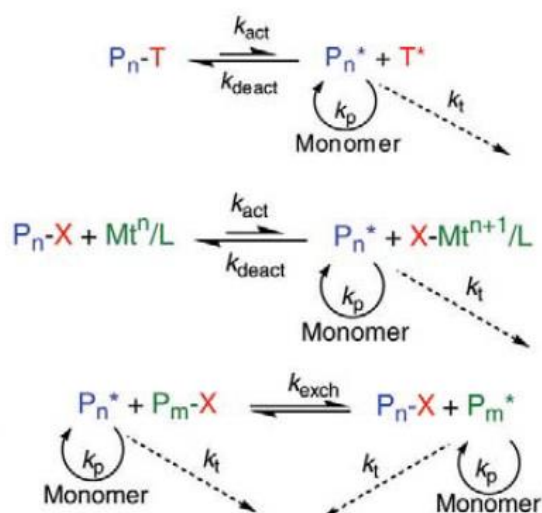


Figure 2. Comparison of molecular weight distribution of FRP and CRP on the basis of RAFT polymerization²⁵

As mentioned before, one of the basic principles of CRP is the dynamic equilibrium between an active species, which is present at a low concentration and a dormant species. The self-regulation of a CRP can be directed either by deactivation/activation process with a stable radical or an organometallic compound as it is the case for NMP or ATRP²⁶, or it can be directed by a bimolecular degenerative transfer by the addition of a transfer agent as in RAFT polymerization(**Scheme 1**).²⁷



Scheme 1. Mechanisms of the three main CRP methods; NMP (top); ATRP (mid); degenerative transfer, RAFT (bottom)²⁸

Nitroxide mediated polymerization (NMP) uses a dissociation/combination mechanism by a homolytic bond cleavage of the dormant species.²⁹ For this polymerization technique nowadays alkoxyamine compounds, like 2,2,6,6-tetramethylpiperidinyloxy (TEMPO) , are used and the polymerization can be initiated either in a unimolecular way, by usage of an alkoxyamine which decomposes in a reactive and stable radical under high temperatures, or in a bimolecular way in combination with a radical initiator.

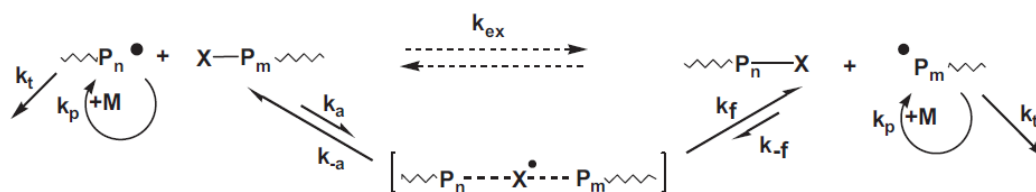
Atom transfer radical polymerization (ATRP) rests upon an atom transfer mechanism and makes use of a metal catalyst which is responsible for the homolytic cleavage of the dormant species. The process itself is very similar to the dissociation/combination mechanism mentioned before. The switch from dormant to the active species is bimolecular and results in an active radical and the used catalyst is oxidized³⁰. The polymerization environment for ATRP contains of an alkylhalide, which is homolytic cleaved by an oxidizable transition metal complex. The formed halogenide radical is added to the metal complex, and an oxidized complex is formed, whereas the formed alkylradical propagates³¹.

The topic of the degenerative transfer polymerizations, like RAFT, will be discussed in more detail in the next chapter.

1.3 RAFT polymerization

RAFT polymerization was established by the CSIRO group (Australia) in the year 1998^{32, 33} and within another French research group in 1999³⁴, so it is a quite young polymerization technique and the interest in RAFT polymerization methods increased steadily over the years³⁵.

As mentioned before, RAFT polymerization does not rely on the PRE, but on the degenerative transfer (DT) mechanism (**Scheme 2**²⁷), which is based on a thermodynamically neutral transfer reaction. Hereby, an amount of active radicals experience degenerative exchange with an inactive species via a bimolecular transfer process. These exchanges can occur via atom- or group transfer or by addition-fragmentation chemistry with unsaturated compounds²⁷.



Scheme 2. Mechanism of the degenerative transfer²⁷

In the process of DT, a short-lived intermediate radical is formed and can be considered as a transition state, however the lifetime of these intermediates can also be long enough to either retard the polymerization or participate in side reactions²⁷

RAFT polymerization makes use of thiocarbonyl compounds as so called RAFT reagents, and has a broad spectrum of compatible monomers³⁶. The advantages of RAFT over other CRP methods are: Mild reaction conditions (temperature) can be applied in contrast to NMP and in contrast to ATRP, no transition metal catalyst (toxicity) is needed³⁶. These advantages make RAFT polymerization a powerful tool in biomedical applications.

1.3.1 RAFT mechanism

The mechanism of RAFT polymerization consists of steps similar to free radical polymerization, like initiation, propagation and termination, but as mentioned before, the DT mechanism is present in this system and forms a dynamic equilibrium between the classic steps.

Initiation

The reaction has to be initiated by a radical initiator, generally thermal initiators, photoinitiators or redox initiator systems. Most common is the use of thermal azo-initiators like azobisisobutyronitrile (AIBN) or 4,4'-azobis(4-cyanovaleric acid) (ACVA).^{37, 38}

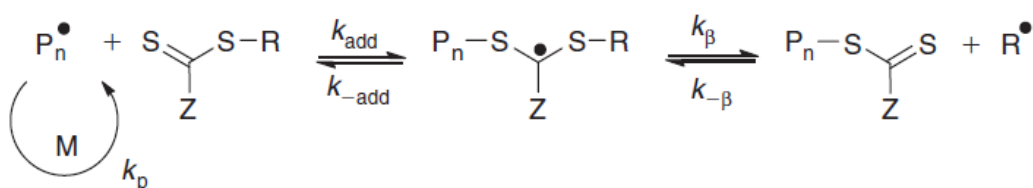
In a typical initiation process, an initiator molecule is homolytically cleaved by the particular trigger (light, heat) and forms a radical, which is able to initiate the polymerization due to addition to an olefinic group of a monomer. After the addition of an amount of monomer a polymeric radical is formed (**Scheme 3**).³⁵



Scheme 3. Initiation step of a radical induced polymerization³⁵

The Pre-equilibrium

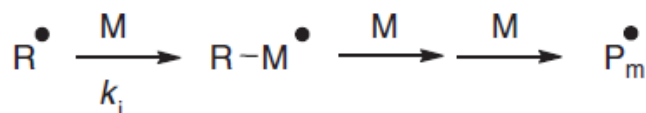
Hereby, the DT mechanism comes into operation. By use of a RAFT reagent, the polymeric radical, formed after initiation, adds to the thiocarbonyl group of the reagent and forms the particular intermediate mentioned in chapter 1.2. This intermediate decomposes subsequently into the dormant species and a new radical consisting of the leaving group R· of the particular RAFT reagent (**Scheme 4**).³⁵



Scheme 4. Reversible chain transfer and propagation in RAFT polymerization³⁵

Re-initiation

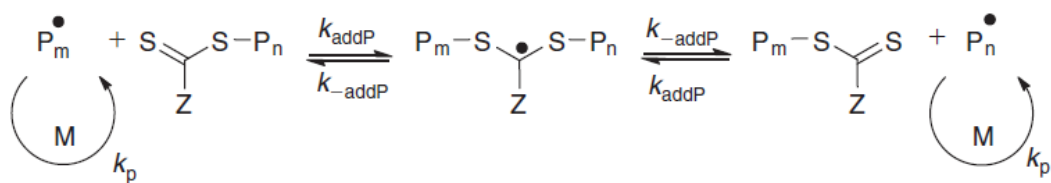
The newly formed leaving group radical is able to add to a monomer's olefinic group and initiates the polymerization again (**Scheme 5**), resulting in a new polymeric radical.³⁵



Scheme 5. Re-initiation of the RAFT polymerization³⁵

The Main equilibrium

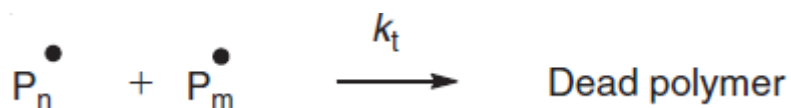
The propagating radical P_m^\bullet adds to the dormant species from the previous pre-equilibrium and forms a new intermediate, which releases the polymeric radical P_n^\bullet , from the dormant state before after fragmentation. This polymeric radical is again able to propagate by addition to new monomer units (**Scheme 6**). The equilibrium, established in this step, is the reason for the controlled growth of the polymer chains in RAFT polymerization.³⁵



Scheme 6. Main equilibrium and propagation in RAFT polymerization³⁵

Termination

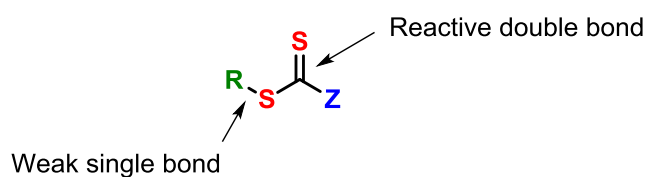
Certainly also termination processes may occur in RAFT polymerization as well as in free radical polymerization, when two polymeric radicals react with each other and terminate to so called dead chains (**Scheme 7**). But these termination processes occur very infrequently due to the fact, that the radical concentration is kept low, by the use of only small amounts of radical initiator and because a large part of radicals are existent in a dormant state.³⁹



Scheme 7. Termination process in RAFT polymerization³⁵

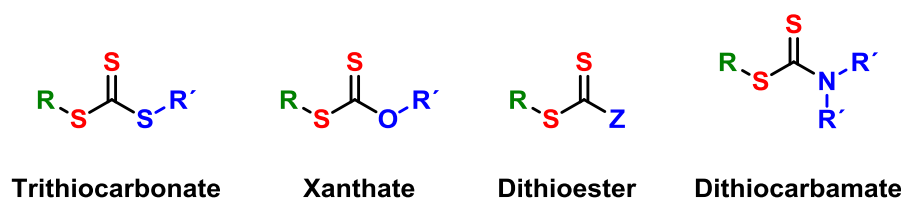
1.3.2 RAFT reagents

As mentioned before, RAFT reagents or chain transfer agents (CTAs) used in RAFT polymerization are thiocarbonyl compounds, which exhibit a weak single bond (S – R) and a reactive double bond (C = S) (**Scheme 8**).⁴⁰



Scheme 8. General structure of RAFT reagents⁴¹

Variation of the R – (green) and Z – group (blue), depicted in **Scheme 8**, makes the RAFT reagent compatible to specific monomer types and depending on the Z - group, the compound can be assigned to one of the four general structures for CTAs (**Scheme 9**).⁴⁰



Scheme 9. RAFT chain transfer agent structures⁴⁰

Hereby, the Z - group plays the key role in the reactivity of the thiocarbonyl group and the role of the R - group is to effectively fragment from the intermediate radical in the RAFT pre-equilibrium, being responsible for the re-initiation of the polymerization.⁴⁰

1.3.3 Inhibition and rate retardation

Sometimes inhibition at the beginning of the RAFT polymerization is observed, due to the slow fragmentation rate of the intermediate radical in the RAFT pre-equilibrium⁴². By determination of the kinetics and generation of a plot of the logarithmic ratio of monomer concentration at the beginning and the monomer concentration at the time t, $\ln([M]_0 / [M]_t)$ vs the time (**Figure 3**) the intersection with the t - axis provides information about the inhibition time. **Figure 3** depicts such a plot for a RAFT

polymerization of methyl acrylate with 1-phenylethyl dithiobenzoate (1-PEDB) at 60 °C as presented by the group of Perrier et al..⁴²

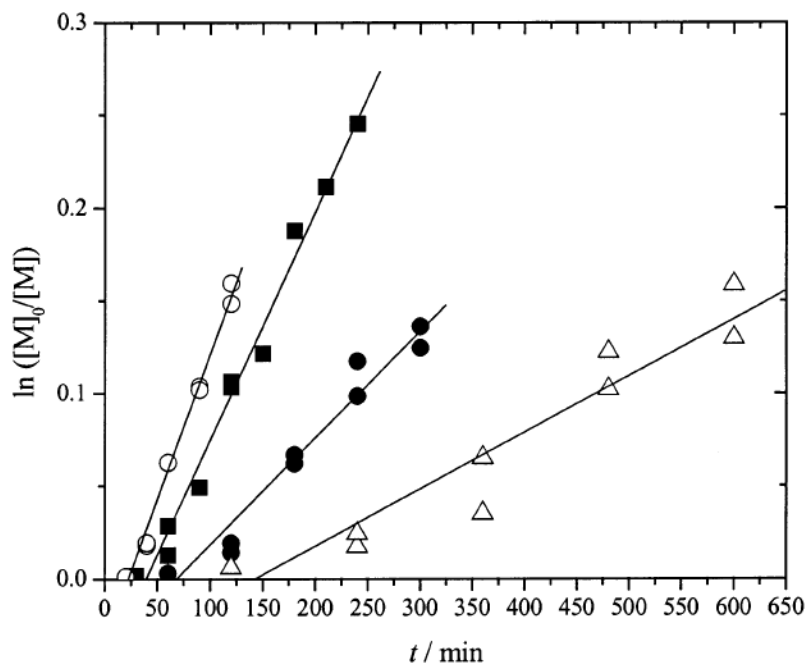


Figure 3. Pseudo-first order plot of a RAFT polymerization of methyl acrylate in bulk, with 1-PEDB as CTA in concentrations of CTA ranging from $1.9 \cdot 10^{-3} \text{ mol L}^{-1}$ (○), $3.8 \cdot 10^{-3} \text{ mol L}^{-1}$ (■), $7.7 \cdot 10^{-3} \text{ mol L}^{-1}$ (●), $17.4 \cdot 10^{-3} \text{ mol L}^{-1}$ (Δ)⁴²

From **Figure 3** it is obvious that inhibition time could increase with higher concentration of the CTA agent.

Another phenomenon, which slows down the reaction speed in RAFT polymerization, is the stabilizing of the intermediate by the Z - group. This occurrence is called rate retardation and appears most likely by use of dithiobenzoates as RAFT reagent.^{43, 44}

1.3.4 End group modification

One of the main advantages in RAFT polymerization, is that the polymer is generated between the R – group and a sulfur atom of the CTA so the thiocarbonyl groups is still present after the polymerization has stopped. With this thiocarbonyl group at the polymer end, a lot of reactions for its modification have been established (**Figure 4**).

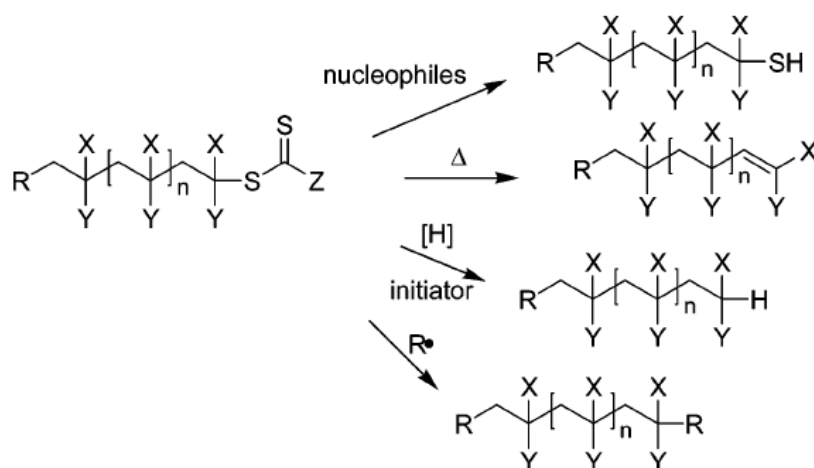


Figure 4. A small compendium of end-group modification processes ([H]; hydrogen donor)⁴⁵

Figure 4 shows the most common methods: The formation of thiols with nucleophiles, like amines, thermolysis, radical induced reduction and addition fragmentation coupling⁴⁶. There are still other reactions like hetero Diels Alder cycloadditions to the thiocarbonyl group, radical induced oxidation and many more⁴⁶. Depending on the application, different end functionalities can be introduced and, for example, coupled to a different compound or material, respectively.

1.3.5 Potential applications for RAFT polymerization

As mentioned before, due to the fact that the reactive thiocarbonyl group of the CTA is still intact, it is possible to restart the polymerization. This attempt is called macro-RAFT polymerization and could also be used for the generation of block-copolymers (**Figure 5**).

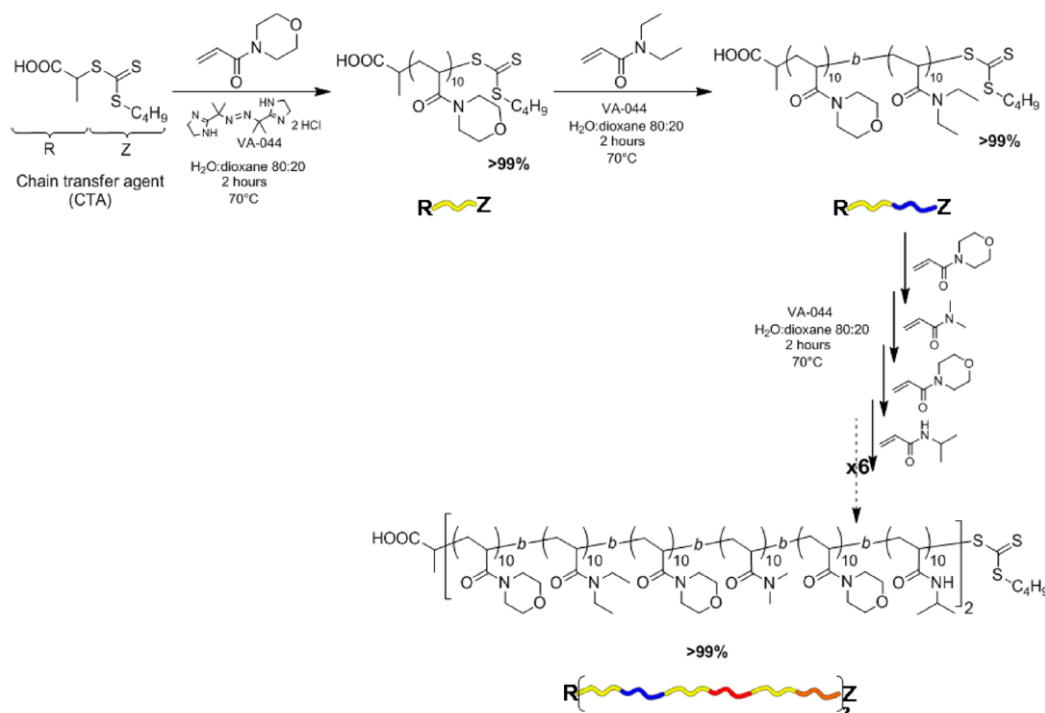


Figure 5. Strategy for the preparation of multiblock copolymers by Gody et al.⁴⁷

A lot of complex polymer architectures can be achieved using RAFT polymerization. For example, by coupling of CTAs to a multifunctional core, so called star polymers can be generated⁴⁸, by synthesis of amphiphilic block copolymers, also micelle structures can be generated⁷. RAFT polymerization can also be applied for surface modification of materials. The already generated polymer could either be attached to the materials surface in a “grafting onto” attempt⁴⁹ or the CTA can be attached to the surface and the polymerization could be performed in a “grafting from” attempt, for the generation of polymer brushes as mentioned in chapter 1.1²⁰ (**Figure 6**).

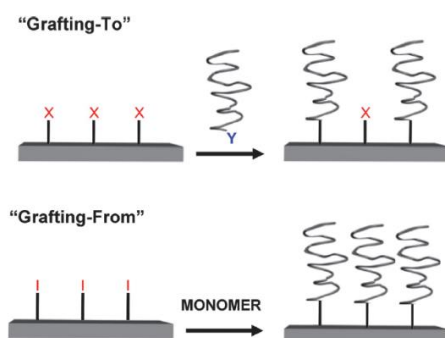


Figure 6. Difference of „grafting to“ and „grafting from“⁵⁰

These potential implementation methods make RAFT polymerization a powerful method for the creation of well-defined complex architectural structures and interfaces. Within the next chapters, methods for the structural analysis of such complex polymer architectures will be discussed.

1.4 Light scattering and structure analytics at macromolecular and colloidal systems

The effect of light scattering and colloid chemistry had its beginning in 1868 through the discovery of the Faraday-Tyndall effect (**Figure 7**). Afterwards, light scattering experiments were performed on all sorts of material but the effects of scattering are especially distinctive for colloid solutions⁵¹.

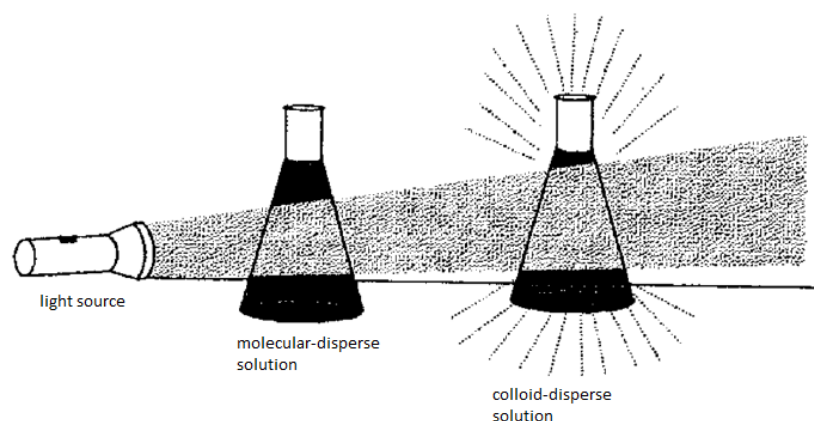


Figure 7. Faraday-Tyndall effect; scattering of light in colloid systems⁵¹

Many theories were applied, to describe all the mechanisms taking place by the interaction of electromagnetic irradiation with particles. The continuum theory (Rayleigh), fluctuation theory (Einstein and Smoluchowski), Doppler-Effect and interference theory (Mie)⁵¹ were combined to make light scattering a powerful analytical method to determine size (radius of gyration, hydrodynamic radius), shape and molecular weight (M_w) of the particles, interactions between the colloid particles (stability) and dispersity of the colloid system⁵¹. Depending on the desired information, different light scattering methods can be applied (static and dynamic light scattering).

For scattering experiments, also other electromagnetic irradiation can be applied, like X-rays. Due to the smaller wavelength of the X-ray radiation, this kind of radiation is able to penetrate the material (colloid) and can be scattered at inner atomic lattices. X-ray scattering techniques, like small angle X-ray scattering, are applied for the determination of particle geometries.⁵²

1.4.1 Static light scattering (SLS)

Due to the angle dependence of the light scattering intensity from the irradiated particles with a certain geometry, it is possible to determine geometric factors, interactions between particles and the molecular weight of the particles. A light scattering setup is depicted in **Figure 8**. The diluted colloid sample of a certain concentration is brought into a vertical polarized light beam (usually lasers), and the scattering intensity is measured by a secondary electron multiplier detector at different angles over a certain time.⁵¹

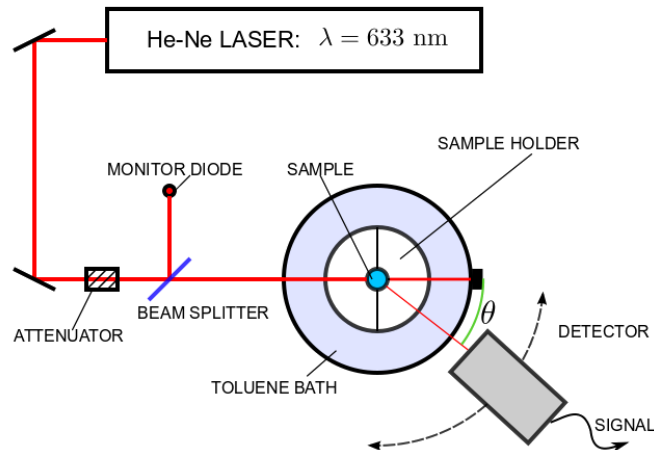


Figure 8. Experimental setup of an ALV-CGS-3 light scattering goniometer⁵³

The obtained intensity curve over time is then averaged and used for further calculations. The basic equation (after Zimm), which is used for this calculations is the virial expansion **equation 1**.⁵¹

$$\frac{R_{\theta}}{K^*c} = MP(\theta) - 2AcM^2P(\theta) + \dots \quad \text{equation 1}^{51}$$

$$\text{optical constant } K^* = \frac{4\pi^2 n_0^2}{\lambda_0^4 N_A} \left(\frac{dn}{dc} \right)^2$$

$$\text{Rayleigh ratio } R_{\theta} = \frac{(I_{\theta} - I_{\theta, \text{solvent}}) r^2}{I_0 V}$$

Here, M is the molecular weight M_w , A is the second virial coefficient, c the concentration in g mL^{-1} , n the refractive indices, (dn/dc) the refractive index increment, λ_0 the wavelength of the irradiated light, I the Intensities, Θ the scattering angle and $P(\Theta)$ the particle scattering function which is described by **equation 2**.⁵¹

$$P(\theta) = 1 - \frac{16\pi^2}{3\lambda_0^2} R_g^2 \sin^2 \left(\frac{\theta}{2} \right) + \dots \quad \text{equation 2}^{51}$$

$$\text{radius of gyration } R_g$$

By determination of the refractive index increment, and measurement of several concentrations at several scattering angles, a so called Zimm-plot (**Figure 9**) can be generated to determine the R_g , M_w , and the second virial coefficient A by extrapolation of $c \rightarrow 0$ and $\Theta \rightarrow 0$. Therefore, K^*c / R_{θ} is plotted vs $\sin^2 (\Theta / 2) + \text{constant} \cdot c$.⁵¹

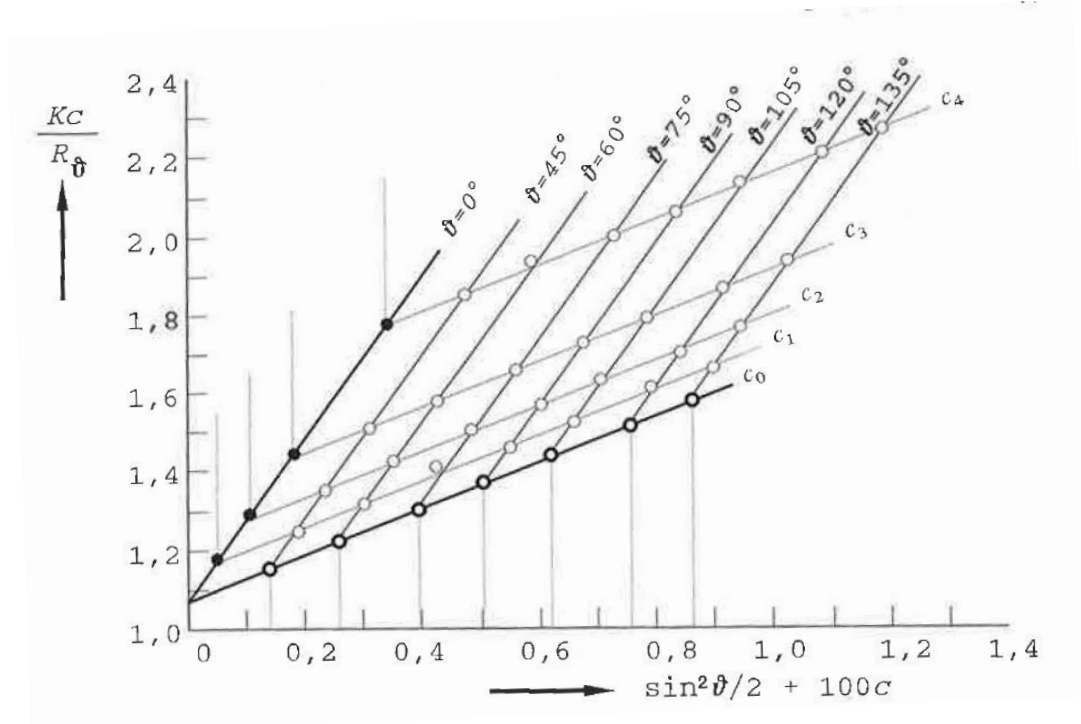


Figure 9. Zimm plot of polymer; c_{1-4} lowest to highest concentration; c_0 extrapolated infinite dilution⁵¹

In **Figure 9** the slope of the $\Theta = 0$ regression determines R_g , the slope of the $c =$ regression determines the second virial coefficient A , which describes the interaction between the particles and the intersection with the y-axis gives the molecular weight⁵¹.

By usage of the so called scattering vector q (**equation 3**), it is possible to generate a Kratky-plot, which can be used for the structural analysis of the particles.

$$\text{scattering vector } q = \frac{4\pi}{\lambda} \sin\left(\frac{\theta}{2}\right) \quad \text{equation 3}^{54}$$

Therefore, $P(R_g, q) \cdot q^2$ is plotted vs q and the shape of the particle could be determined by fitting of geometric curves.⁵⁴

1.4.2 Dynamic light scattering (DLS)

In SLS mentioned before, the scattering intensity at a certain angle is measured over time and the average is calculated. In DLS these signals are not averaged, but auto correlated. The moving and fluctuations are directly reflecting Brownian motion of the scattering particles, which is caused by thermal density fluctuations of the solvent⁵⁴. The measurement of these fluctuations is based on the Doppler-Effect⁵¹.

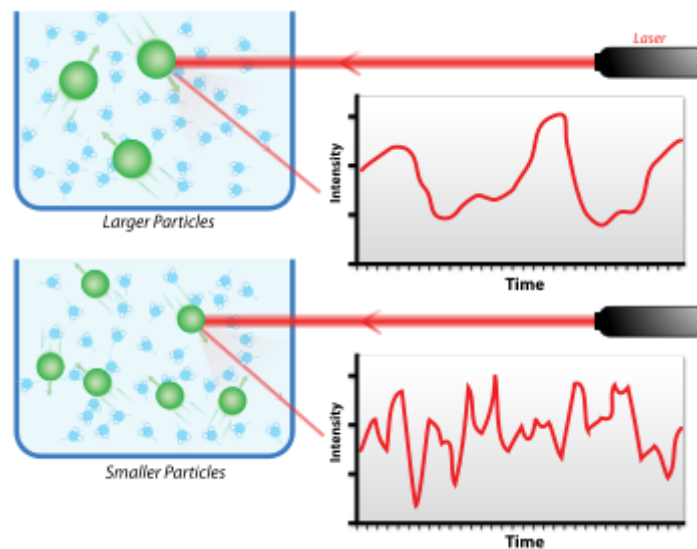


Figure 10. Hypothetical DLS spectra of large (top) and small (bottom) particles⁵⁵

An auto correlation function is used to compare the spectrum with itself to an earlier moment. This auto correlation function g (**equation 4**) can be transformed into **equation 5**, where the coefficient of diffusion can be determined. β is the amplitude of the auto correlation function, D the coefficient of diffusion, q the scattering vector. Over the Stokes-Einstein equation (**equation 6**) the hydrodynamic radius R_H can be determined⁵⁴.

$$g(\tau) = \frac{\langle I(t)I(t + \tau) \rangle}{\langle I(t) \rangle^2} \quad \text{equation 4}$$

$$g(\tau) = 1 + \beta e^{-2Dq^2\tau} \quad \text{equation 5}$$

$$D = \frac{kT}{6\pi\eta R_H} \quad \text{equation 6}$$

After the calculation of R_g from SLS and R_H from DLS, the so called ρ -ratio can be identified (**equation 7**). The ρ -ratio can give information about particle morphology in solution and ranges from 0.775 (sphere) to > 1.505 (random polymer coil) for more linear structures.⁵⁴

$$\rho = \frac{R_g}{R_H} \quad \text{equation 7}^{54}$$

1.4.3 Small angle X-ray scattering (SAXS)

Another analytical method for the determination of the particle morphology is small angle X-ray scattering. SAXS in principle, is the scattering of X-rays at colloidal particles (**Figure 11**) and is a powerful analytical tool to determine the particles shape in solution and a good supplement to light scattering experiments⁵².

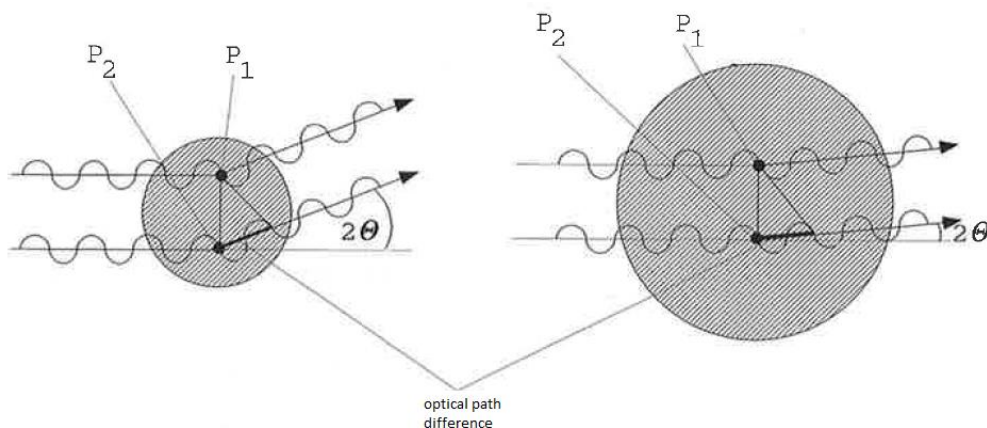


Figure 11. Schematic picture of scattering of X-rays at spherical colloidal particles of different diameter⁵²

The sample is brought in a linearized X-ray beam and the scattering at the particle will be detected on a 2D-detector in an angle range of usually $0.1^\circ - 4^\circ$ and a scattering

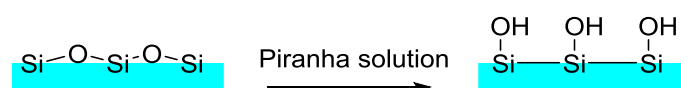
image will be generated. By mathematical fitting methods it is possible to determine the particle geometry and radius of gyration.

With these scattering methods, it is possible to analyze the conformation of free polymers in solution and these measurements could give information about the structure how an applied polymer brush system could arrange in the particular solvent.

For the establishing of a polymer brush system, first the particular surface has to be modified. This will be discussed in the following chapter.

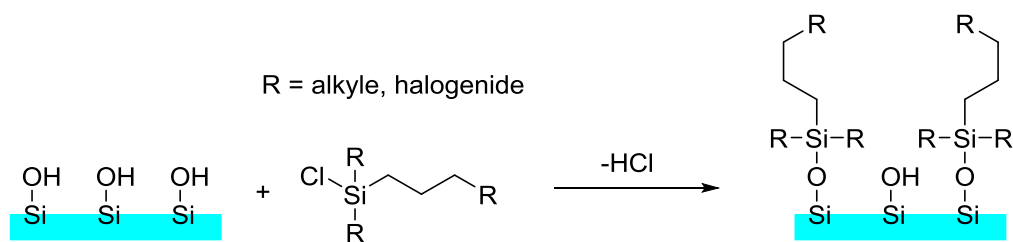
1.5 Covalent surface modification and functionalization of SiO₂ materials

For the functionalization of SiO₂ surfaces two common methods are applied: Alkoxysilanes and chlorosilanes compounds are both categorized as silanization reagents for surfaces⁵⁶. For both methods the SiO₂ surface first has to be activated. This is done by piranha solution, which is a strong oxidizing agent and removes all organic residues from the surface, whereas it hydroxylates also the surface (**Scheme 10**) and prepares a high density of silanol groups.⁵⁶



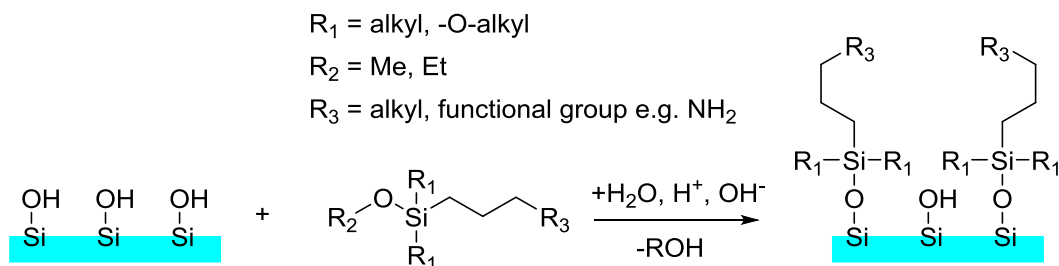
Scheme 10. Hydroxylation of the SiO₂ surface

Afterwards there are two different pathways for the silanization. First, the silanization reaction with chlorosilane compounds. The OH-groups of the hydroxylated surface react with the Si-Cl functionality and form a covalent Si-O bond through elimination of HCl (**Scheme 11**).⁵⁷



Scheme 11. Silanization via chlorosilanes⁵⁷

The second pathway is the silanization via hydrolysis of alkoxy silanes (**Scheme 12**). Because of the reactivity of the Si-Cl group, for the introduction of functional groups the modification via alkoxy silanes is favored.⁵⁸



Scheme 12. Silanization via alkoxy silanes⁵⁸

For further surface modification, alkoxy silanes with functional groups, like (3-aminopropyl) triethoxysilane, can be applied and by coupling reactions, they are modified to yield different surface characters. The characterization of these surfaces will be discussed in the next chapter.

1.6 Surface analytics

Surface modifications became quite popular in a large number of applications and processes. For the characterization of these modified surfaces a powerful set of analytical tools is needed⁵⁹. Sequentially, a small compendium of surface analytical methods will be discussed.

1.6.1 Contact angle measurement (CA)

Contact angle measurement is perhaps one of the easiest analytical methods to apply, for the characterization of a modified surface. Two different modes can be applied; static and dynamic contact angle. In static CA analysis a drop of liquid is placed on the surface and hereby, the wetting behavior is determined. In case of a surface functionalization, CA measurement can be used before and after the functionalization to determine the difference in wetting behavior. The involved forces at the boundaries between the phases are described by the Young equation⁶⁰ (**Figure 12** and **equation 8**).

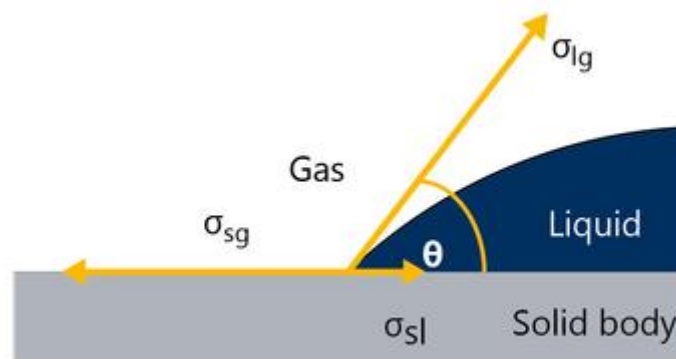


Figure 12. Schematic diagram of the contact angle⁶¹

$$\cos\theta = \frac{\sigma_{sg} - \sigma_{sl}}{\sigma_{lg}} \quad \text{equation 8}^{60}$$

This equation describes the force equilibrium between the surface tension σ_{lg} , the surface energy σ_{sg} , and the interface energy σ_{sl} on a flat surface. Two different variables of this equation can be determined very easy, by measurement of the surface tension of the liquid and the static contact angle by a goniometer. The surface energy can be divided into a polar and a dispersive share of surface energy and is determined by CA measurement of the substrate using two liquids with known shares of polar and dispersive surface tension⁶⁰. For static CA measurements, an equilibrium between the gas phase and the liquid has to be established, in the means of vapor pressure over the liquid.

The second mode for that CA measurements can be applied, is the determination of the dynamic CAs. Therefore the substrate, on which the drop of liquid was placed, is tilted until the drop starts rolling because of gravity (**Figure 13**).

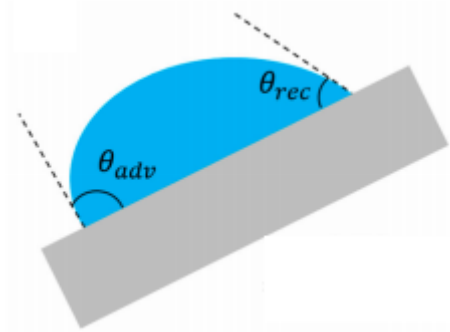


Figure 13. Schematic dynamic CA⁶²

When the drop begins to roll off, the angle in rolling direction becomes a maximum, and is called advancing CA, while the other CA becomes a minimum and is called receding CA. The difference between them is called CA-hysteresis and gives information about adhesion, wetting and energy dissipation during the droplet flow.⁶²

1.6.2 Ellipsometry

With ellipsometry it is possible to determine layer thicknesses on flat reflecting surfaces. It is a sensitive method for the analysis of single films and layer stacks. Hereby, film thicknesses from 0.1 nm – 200 μm can be determined, depending on the spectral range used and the homogeneity of the films. It is a non-invasive and non-destructive analytical method and can be applied directly on the clean surface. The basic principle of ellipsometry is, that monochromatic linearly polarized light irradiates the surface under a certain angle. There, the light will be reflected from the upper layer of the surface and also, due to refraction, of the inner layer border from the substrate, resulting in an elliptical signal arriving at the detector (**Figure 14**).⁶³

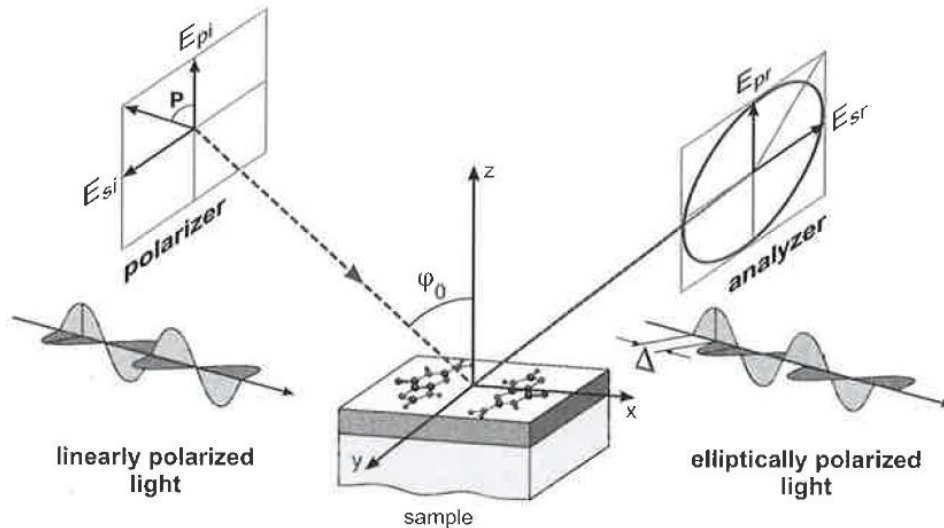


Figure 14. Schematic principle of ellipsometry⁶³

When the refractive indices of the layer materials are known, this method is very accurate in the analysis of complex layer structures.⁶³

1.6.3 X-ray photoelectron spectroscopy (XPS)

XPS is one of the most common used surface analytical method, due to the fact that it generates semi-quantitative chemical information of the atomic composition of the samples surface. The basic principle of XPS is the photoelectric effect, induced by X-ray radiation of a substrate's surface. The X-ray photon interacts with an electron with a certain binding energy, the entire photon energy is transferred to the electron, and a photoelectron is ejected from the sample with a particular kinetic energy (**equation 9**).⁶⁴

$$E_{kin} = h\nu - E_B - \phi_s \quad \text{equation 9}^{64}$$

Here, E_{kin} is the kinetic energy of the photoelectron, $h\nu$ is the energy of the X-ray photon, E_B the binding energy of the ejected photoelectron and ϕ_s is the work function term (minimum energy for the removal of a delocalized electron from the material). The kinetic energy is measured and gives direct information on the binding energy, so it

enables elemental analysis. With this method it is possible to irradiate, angle resolved, certain areas of the sample surface and from the obtained information, a depth profile with information about the atomic composition of this area can be generated. This makes XPS an essential analytical method for surface investigation.

1.6.4 Total internal reflection fluorescence microscopy (TIRFM)

TIRF microscopy, or also called evanescent wave microscopy, is a microscopic technology for the investigation of excited fluorophores near a solid surface in aqueous environments. The advantages of this technique are the minimal exposure of the sample to the excitation light, and images of very low background fluorescence. The basic principle of this technique is the total reflection of the excitation beam in an optical medium, e.g. glass cover slips, and this total internal reflection generates a thin electromagnetic field, within the aqueous sample environment beyond the optical medium's phase boundary. This electromagnetic field is called evanescent field and has the same frequency as the reflected excitation light. This field is able to penetrate the sample up to approximately 100 nm and excites the attendant fluorophores within this area (**Figure 15**).⁶⁵

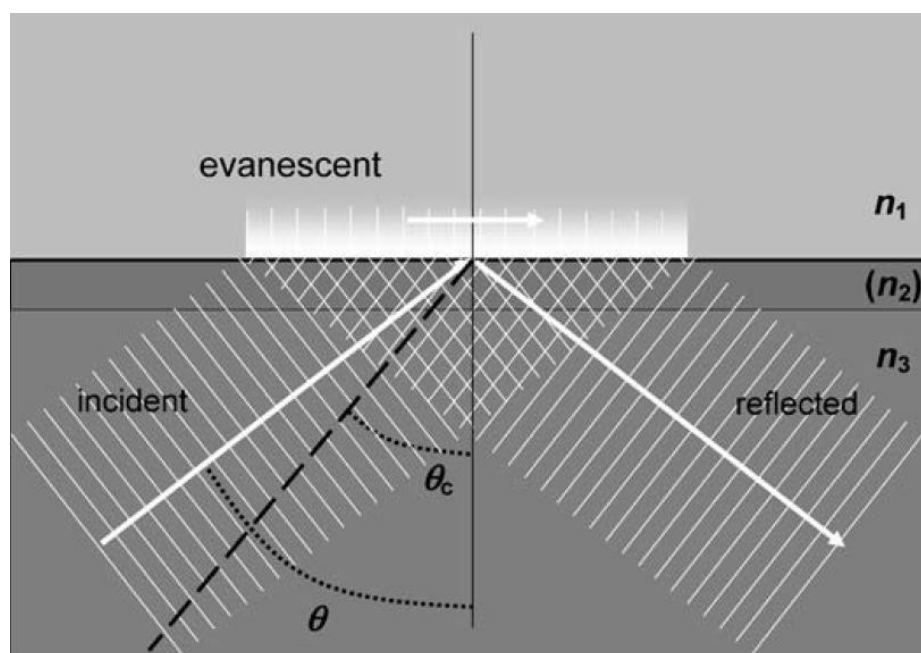


Figure 15. Total internal reflection scheme⁶⁵

By variation of the incident angle of the excitation beam in the optical medium, the penetration depth can be controlled and therefore fluorophores in the area of the phase boundary can be excited, while the excitation of the ones with higher distance will be avoided. These excited molecules in the plane area can be analyzed by microscopy and by simultaneous combination with other fluorescence techniques, TIRF technology enables various applications in chemistry, cell biology and biochemistry.⁶⁵

Objective

T cells are major players in our immune system. One protein in their plasma membrane, the T cell receptor (TCR), is able to recognize a part of a pathogen (the antigen), which is presented by another cell (antigen-presenting cell; APC), that has previously found this intruder in our body. Upon this recognition process, a tight connection between these two cells is formed, the T cell becomes activated and a series of complex events is initiated ultimately leading to immune response.

To investigate these activation events with total internal reflection fluorescence microscopy (TIRFM), the T cell has to be activated on the surface of an optical medium like glass. Two major problems occur in this research approach: First, the area around the TCR is expected to be crowded by different proteins, which are able to block the coupling of the antigen to the TCR, if the antigen is directly attached to the surface. Second, protein fouling, which occurs if proteins adsorb on the surface and aggregate.

To overcome these drawbacks, caused by direct coupling to the glass surface, a polymer linker system should be established. This system should be realized by generating uniform polymer brushes by a grafting from approach with a covalent bonded antigen as the end group, using a controlled radical polymerization method, the so called reversible addition fragmentation chain transfer polymerization. This method facilitates a polymerization under gentle temperatures, without toxic catalysts, providing low dispersities and defined molecular weights. Therefore, a RAFT reagent should be immobilized to the glass surface to graft the polymer chains directly, thus enabling a denser coating of the area. Requirements for the polymer brushes are biocompatibility, hydrophilicity, uniform chain architecture and easy access to various end groups. The end group of these polymer brushes should facilitate an easy coupling reaction to biomolecules, preferably via click chemistry reactions.

State of the art

During the last decades polymer brush platforms became of great interest, due to their ability to control important architectural features¹. These surfaces can be used in a very wide range of applications like for the design of biosensors^{13, 66}, in analytical surface chemistry⁶⁶ and in creation of specific biointerfaces.

Related to the biosciences, the monitoring of cell surface events with TIRFM on the surface of optical media is of high interest so far. The group of Sevcsik et al.⁶⁷ used streptavidin patterns, produced by micro contact printing, functionalized with a biotinylated green fluorescent protein (GFP) antibody for such studies. To adjust the surface density of GFP antibody they added various concentrations of free biotin to the incubation. Interspaces were passivated by Bovine serum albumin (**Figure 16**).

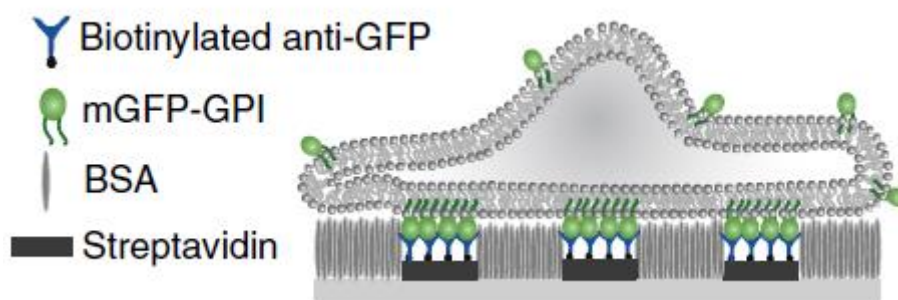


Figure 16. Streptavidin - Biotin functionalization⁶⁷

Streptavidin/Avidin and biotin is a prominent example of a noncovalent bioconjugation reaction to functionalize surfaces and an alternative to more time consuming covalent immobilization of chemical functionalities to surfaces. However, these systems lack the flexibility to vary different parameters like distance of the cell receptor from the surface or the response of the interface to changes of the environment like pH or temperature.⁶⁸

Such drawbacks caused the increasing popularity of polymer brushes in the field of biotechnology. To introduce these brush systems, controlled radical polymerization (CRP) became the most established method for surface initiated polymerization (SIP)⁶⁹. The two CRP methods commonly used at the moment are ATRP and RAFT polymerization. They are applied for the functionalization of gold surfaces, biosurfaces,

steel, particles⁷⁰ or silicon. Since ATRP uses cytotoxic metal catalysts, which are not preferred in biomedical or bioanalytical applications, RAFT polymerization gained more popularity in these kinds of fields, due to abdication of toxic catalysts and broad flexibility concerning monomer types and reaction conditions.²⁰

As a current example for the use of RAFT-generated polymer brushes on surfaces for biorelated studies, the group of Zamfir et al.²⁰ prepared a brush coating with surface-RAFT polymerization via the R-group approach. They used 4-cyano-4-((phenylcarbonothioyl)thio)pentanoic acid as the RAFT reagent and azobisisobutyronitrile (AIBN) for the generation of poly-2-hydroxyethyl methacrylate (pHEMA) brushes on silicon waver surfaces for tests about protein fouling and macro-RAFT polymerization (**Figure 17**).

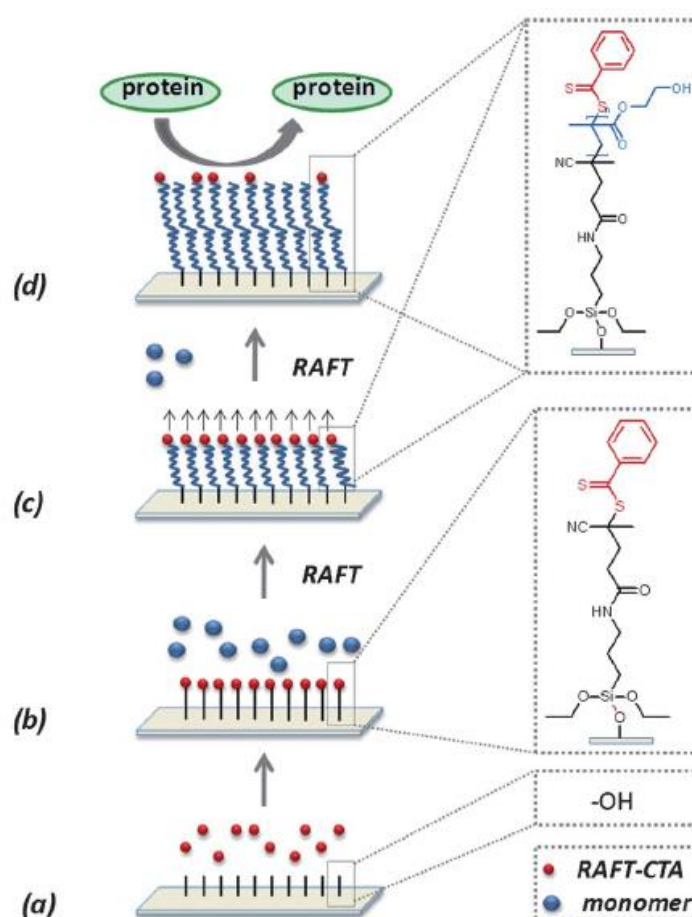


Figure 17. Surface RAFT polymerization of HEMA via the R-group approach by Zamfir et al.²⁰

In their study, the RAFT reagent was modified first by amide coupling with EDC to (3-aminopropyl) triethoxysilane (APTES) (1 h, rt, then washed with brine, dried), followed by the immobilization of this alkoxy-silanized product on a silicon wafer's surface (dry toluene, 0.02 M, 2 h at 50 °C, rt overnight). They generated the pHEMA brushes in a grafting from attempt in dioxane/water with different concentrations of sacrificial free RAFT reagent in the formulation. The surfaces were characterized by XPS, contact angle measurement and AFM.²⁰

In this context, also the group of Isahak et al.⁷¹ made use of (R)-4-(((butylthio)carbonothioyl)thio)-4-cyanopentanoic acid as the RAFT reagent and modified this reagent by amide coupling with EDC/DMAP in CH₂Cl₂ with APTES (rt, 16 h, purification by column chromatography on silica gel). They used this modified RAFT reagent for the immobilization on silica nanoparticles and generated polymer brushes with styrene sulfonate as monomer, 1,1'-azobis(cyclohexanecarbonitrile) (V40) as thermal initiator and sacrificial chain transfer agent (CTA) in water/dioxane at 90 °C. Since the brushes were synthesized on particles, DLS was chosen for the characterization of the brush length (**Figure 18**).

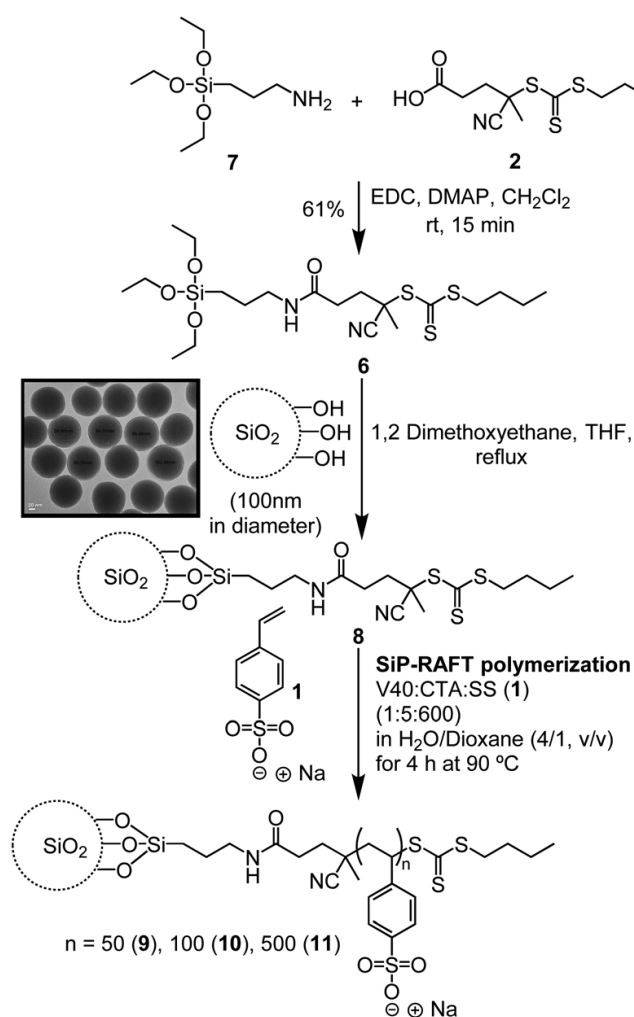


Figure 18. Synthesis of RAFT p(SS) functionalized silica nanoparticles via the R-group approach by Isahak et al.⁷¹

Apart from the brush fabrication method, also the choice of monomer type plays a key role for the properties of the modified surfaces. Stimuli-responsive brushes or so-called “smart” brushes became quite popular amongst bio-related applications, due to the fact that they are able to respond in a highly nonlinear way to one or multiple stimuli by cooperative conformational change of the macromolecules⁶⁹. Depending on the desired stimulus or bio-related properties, like protein resistance, there are sets of monomers used for such brushes (**Figure 19**).¹

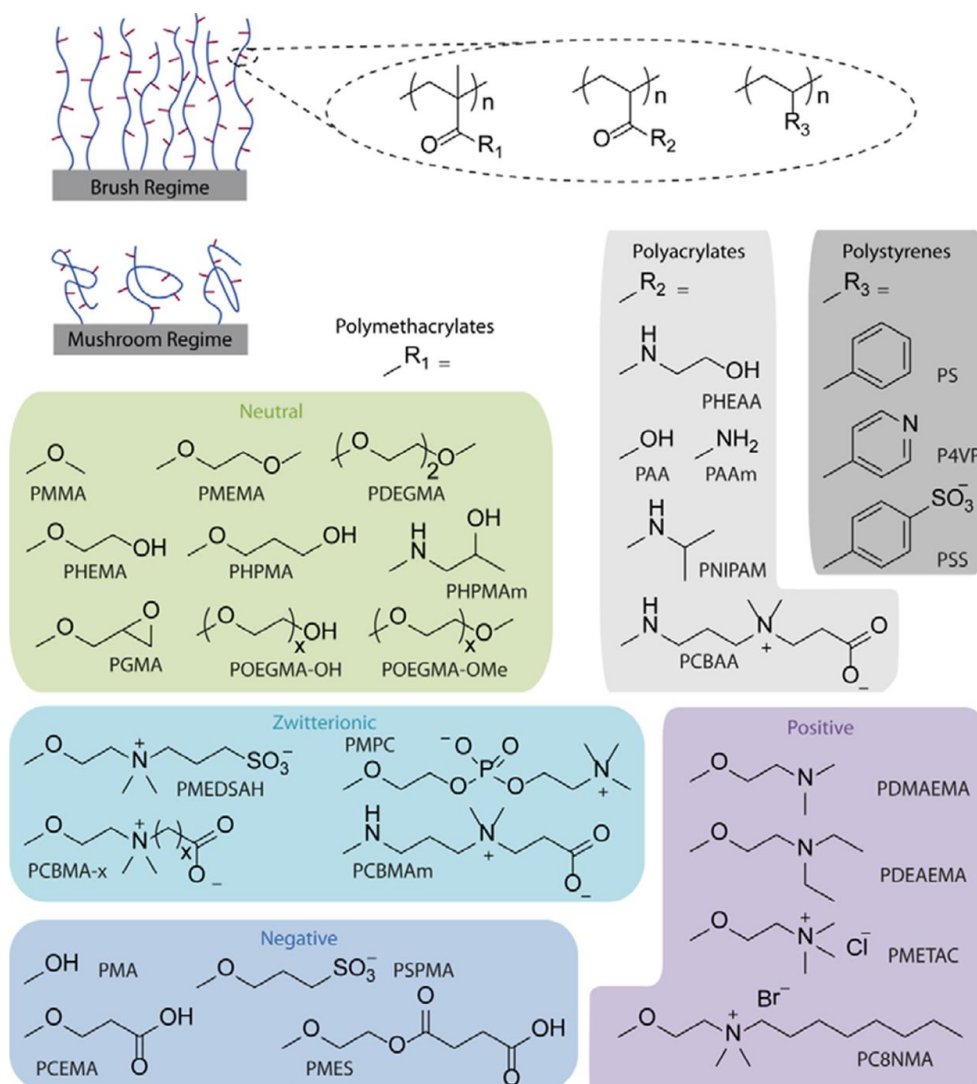


Figure 19. Chemical structures of polymer brushes most commonly used for biomedical applications¹

In the field of thermo-responsive polymer brushes poly-N-isopropylacrylamide (pNIPAM) has become one of the most extensively studied representative¹. One of the advantages of pNIPAM is a lower critical solution temperature (LCST) of ≈ 32 °C in aqueous environment, which is very suitable for responsive applications at physiologically relevant temperatures.⁶⁹

The group of Stenzel et al.⁷² synthesized stimuli-responsive pNIPAM-glycopolymer blockcopolymer brushes, using surface RAFT polymerization via the Z-group approach (**Figure 20**)

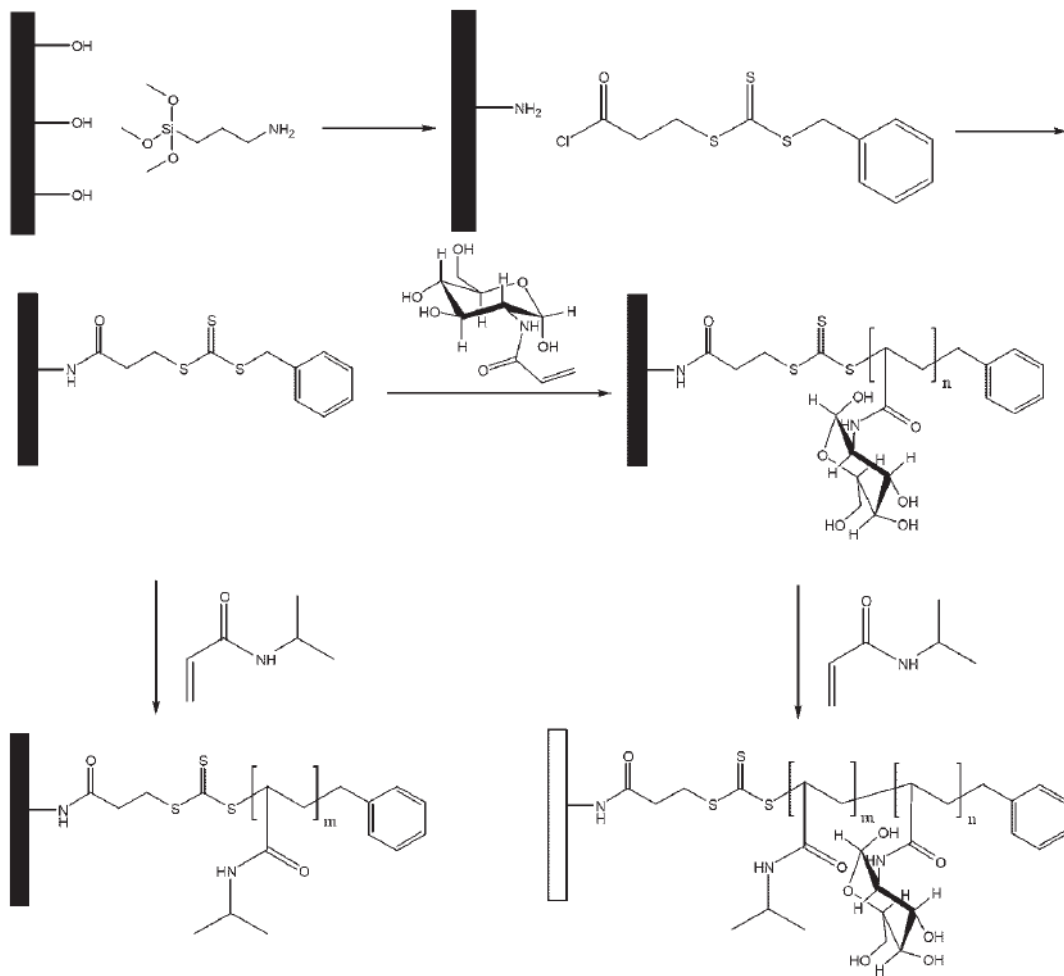


Figure 20. Synthesis of RAFT pNIPAM-glycopolymer blockcopolymer brushes on SiO₂ surfaces via the Z-group approach by Stenzel et al.⁷²

First, they functionalized the surface of a silicon wafer with amine groups, using APTES in toluene, and then coupled the acid chloride of the RAFT reagent 3-(((benzylthio)carbonothioyl)thio)propanoic acid by amide bonding to the surface. The grafting process of the brushes was carried out with 4, 4'-azobis(cyanopentanoic acid)) as thermal initiator, sacrificial RAFT reagent and NIPAM and N-acryloyl glucosamine (AGA) as monomers in deionized water/DMSO and water/ethanol⁷². They successfully synthesized pNIPAM, pAGA and pNIPAM-block-pAGA brushes on a SiO₂ surface and characterized them by contact angle measurements and ellipsometry.

Therefore, from literature, the immobilization of a RAFT reagent to a SiO₂ surface for the generation of polymer brushes, is very likely performed by condensation of alkoxy-silanes to the clean surface using APTES and amide coupling to the RAFT reagent.

To sum up, the current key aspects in the field of surface modification for biorelated applications, it can be stated, that RAFT polymerization is a highly suitable method for the generation of polymer brushes on different surfaces via the Z- and the R-approach. Concerning monomer types like acrylamides showed very promising properties with respect to biocompatibility, accessibility and also possible triggering of cell events via thermoresponsivity.

Results and discussion

The establishing of a polymer brush biointerface between a glass surface and a living organism must be well planned. The required specifications of this system were: The substrate/surface should be a glass cover slip with a thickness of 150 μm , the generated polymer brushes should display brush lengths from 10 to 50 and an end-group functionalization with the possibility for coupling to a biomolecule should exist.

1 Strategy for the synthesis of the polymer linker system

So the first strategy for a biointerface, fulfilling the aforementioned requirements, was the immobilization of a RAFT reagent via the R-group approach and then the generation of the brushes in a “grafting from” process. The thiocarbonyl group of the RAFT reagent, which should be located at the end of the polymer chain by using the R-group approach, could afterwards be modified to another functional group by a set of different reactions, depending on the intended functionality. The coupling to a biomolecule, like an antigen, should be facilitated by a click chemistry polyethylene glycol (PEG) linker (**Figure 21**).

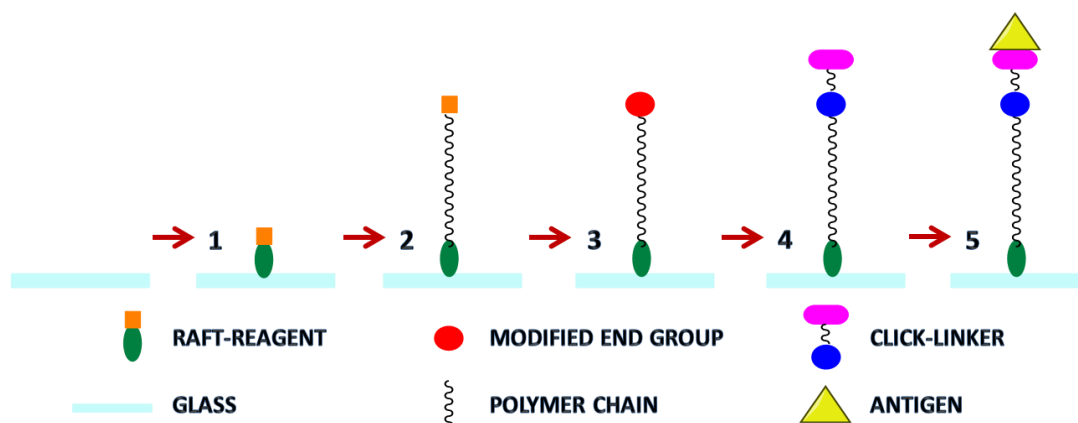
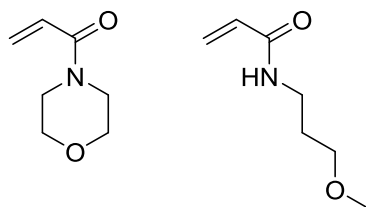


Figure 21. Strategy for the polymer linker system

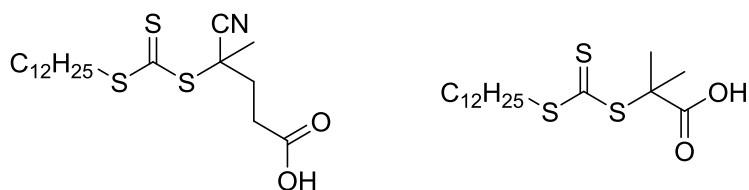
Concerning the biocompatibility and water solubility of the generated polymer brushes, two acrylamide monomers were chosen, acryloylmorpholine (NAM)⁷ and methoxypropylacrylamide (MPAA)⁸. The properties of both brush systems, one linear,

one alicyclic, should be investigated and compared to each other, because there could be a difference in rigidity of the chains.



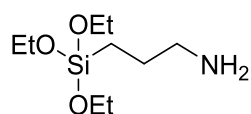
Scheme 13. Structures of the monomers NAM (left) and MPAA (right)

For the surface induced polymerization, two RAFT reagents were chosen (**Scheme 14**). 4-Cyano-4-(((dodecylthio)carbonothioyl)thio)pentanoic acid (CDTPA) and 2-(((dodecylthio)carbonothioyl)thio)-2-methylpropanoic acid (DDMAT) have both carboxylic acid functionalities for coupling reactions to the surface via the R-group approach and both of them are suitable to polymerize acrylamides according to Moad et al. and Schachner et al.^{73, 74}.



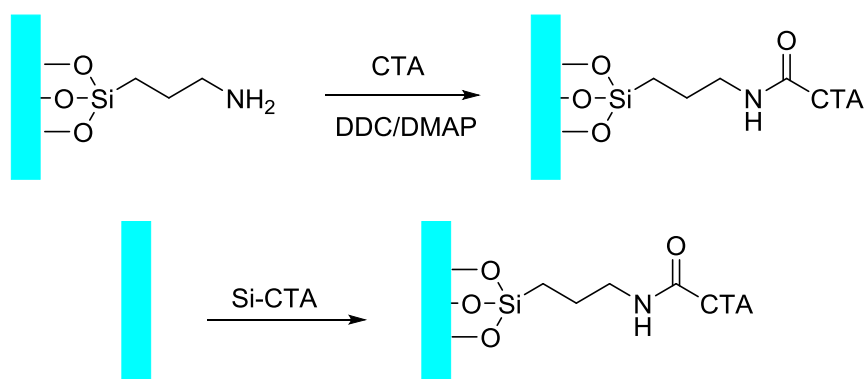
Scheme 14. Structures of CDTPA (left) and DDMAT (right)

According to previous literature, the immobilization of these RAFT reagents should be carried out by amide bond coupling with 3-(triethoxysilyl)propan-1-amine (APTES; **Scheme 15**) to the activated SiO₂ surface of the glass substrate.



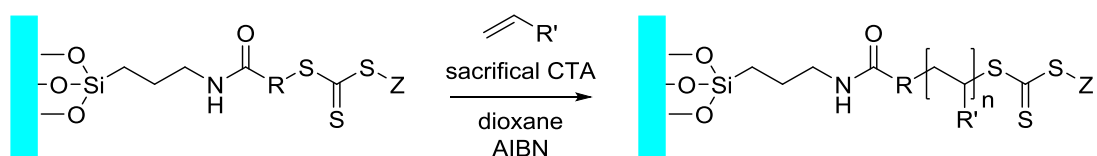
Scheme 15. Structure of APTES

This coupling approach could either be executed by first functionalizing of the surface by silanization with APTES, then amide coupling to the CTA or by first the synthesis of the alkoxy-silane functionalized CTA (Si-CTA) and then direct immobilization of this Si-CTA to the glass surface (**Scheme 16**).



Scheme 16. Immobilization approaches, prefunctionalization by APTES (top); direct functionalization with Si-CTA (bottom)

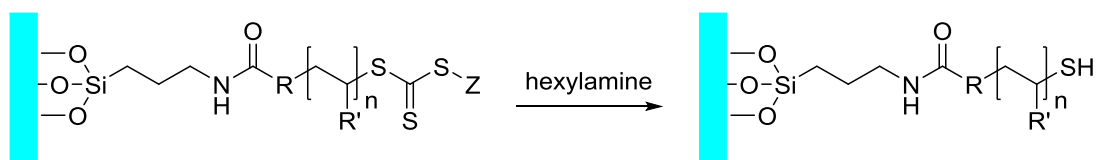
For the surface induced polymerization in a “grafting from” attempt (**Scheme 17**), azobisisobutyronitrile (AIBN) should be applied as a thermal initiator. The polymerization was planned as solution polymerization with dioxane as solvent and with an amount of so called “sacrificial” CTA in solution, otherwise a loss of control would occur²⁰ and the molecular weight (MW)- or rather the brush length distribution would become broader.



Scheme 17. Surface induced RAFT polymerization via R-group approach

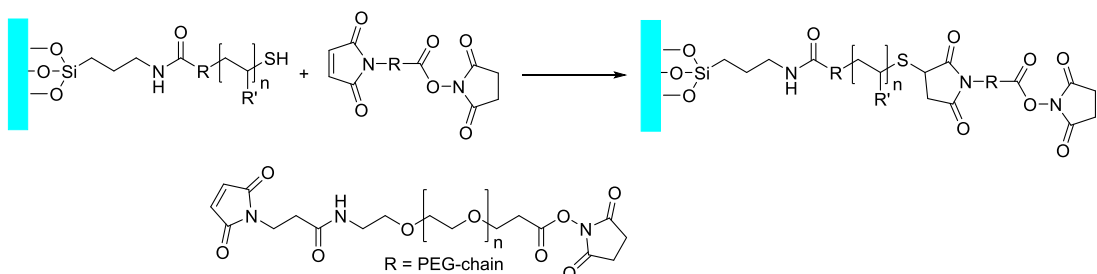
After the polymerization step, there are several options to modify the end-group. To make use of click chemistry, without toxic catalysts like copper, maleimide click

reactions⁷⁵ to a thiol functionality was an option. So it was planned to convert the thiocarbonyl endgroup to a thiol by usage of hexylamine in excess, acting as nucleophile. This reaction is called aminolysis (**Scheme 18**).⁷⁶

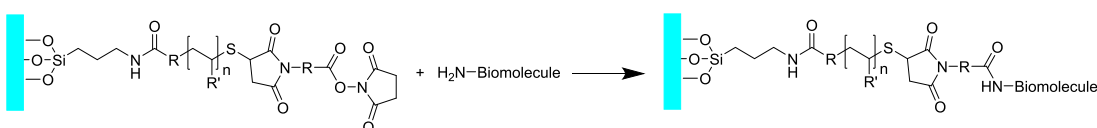


Scheme 18. Aminolysis reaction

As mentioned above, a maleimide click linker should be used to couple an antigen or biomolecule to the polymer brush thiol end group. For that purpose a maleimidopropionyl-PEG-N-hydroxysuccinimid (NHS) linker should be applied for the first tryouts (**Scheme 19**). It could be expected, that the NHS group on the linker would react with a free amine group of lysine in the antigen or biomolecule (**Scheme 20**) and the interface should be ready to use for interaction with T-cells.



Scheme 19. Maleimide click reaction with the maleimide-PEG-NHS linker



Scheme 20. NHS-coupling reaction to a biomolecule

As alternatives, also a maleimide-acrylate linker compound could be applied, by thiol-maleimide click on one side and thiol-ene click reaction on the other side of the system.

The resulting interface should then be applied for the interaction with T-cells and the studying of cell surface events via TIRF-microscopy.

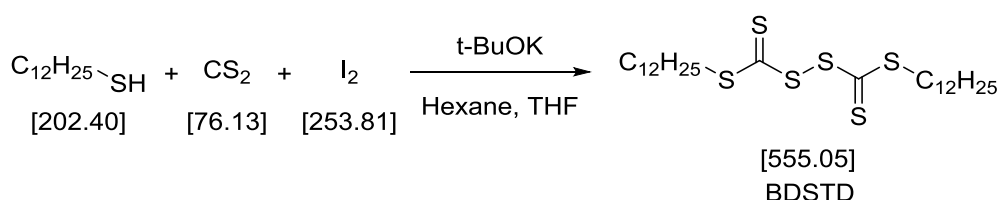
2 Synthesis of the RAFT reagents

In the first part of this work the RAFT reagents should be synthesized corresponding to literature-known procedures.

2.1 Synthesis of 4-cyano-4-(((dodecylthio)carbonothioyl)thio)pentanoic acid (CDTPA)

CDTPA was synthesized in a 2 step synthesis corresponding to the publication of Moad et al.⁷³, by the formation of bis-(dodecylsulfanylthiocarbonyl)-disulfide as intermediate.

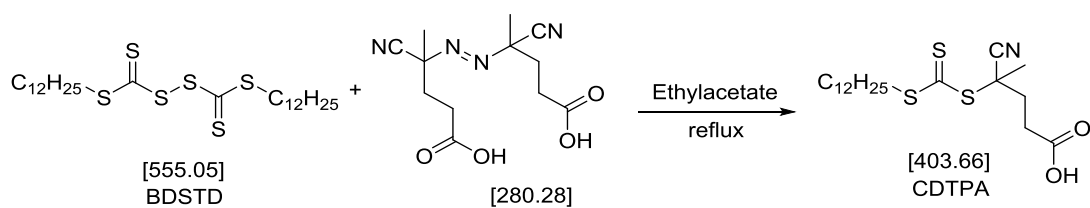
In the first step, bis-(dodecylsulfanylthiocarbonyl)-disulfide was prepared by the reaction of dodecanethiol with carbon disulfide and iodide.



Scheme 21. Synthesis of BDSTD

Therefore, potassium *tert*-butanolate was dissolved in a hexane/THF mixture and cooled down with an ice/water bath. Dodecanethiol was added dropwise and the solution became a white emulsion. This emulsion was stirred for 30 min under cooling and afterwards carbon disulfide was added dropwise to the mixture. The formed yellow foam was stirred at room temperature, then iodine dissolved in THF was added to the solution. The mixture was then stirred overnight. The solvent was removed via vacuum distillation and the product was obtained as yellow oil in 87 % yield, which crystallized at lower temperatures to an orange solid.

In the second step, BDSTD was reacted with 4,4'-(diazene-1,2-diyl)bis(4-cyanopentanoic acid) (ACVA) to obtain the targeted CTA.

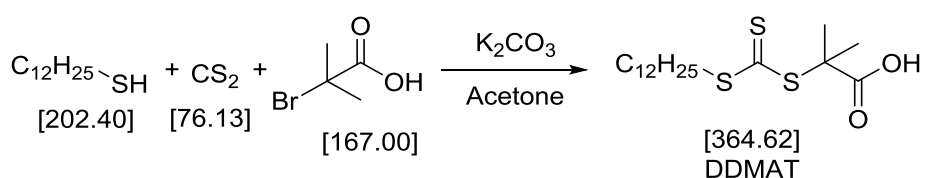


Scheme 22. Synthesis of CDTPA

BDSTD was dissolved in ethylacetate and the solution was degassed from oxygen with argon. Under inert gas atmosphere the mixture was refluxed and ACVA were added dose wise under argon counter flow. The mixture was stirred and refluxed overnight. The solvent was removed via vacuum distillation and the residue was recrystallized from diethyl ether. The product was purified via liquid column chromatography over silica with PE/EE = 1:1 to yield the product as a yellow solid in a yield of 41 %.

2.2 Synthesis of 2-(((dodecylthio)carbonothioyl)thio)-2-methylpropanoic acid (DDMAT)

DDMAT was synthesized corresponding to the literature of Skey et al.⁷⁷



Scheme 23. Synthesis of DDMAT

Dodecanethiol and potassium carbonate as base were dissolved in acetone and stirred. Then carbon disulfide was added dropwise and the mixture was stirred further. Following, 2-bromo-2-methylpropanoic acid was dissolved in acetone and added to the reaction mixture. This solution was stirred overnight and then the solvent was removed via vacuum distillation. After extractive workup, the solvent was removed via vacuum distillation and the residue was recrystallized from petroleum ether. The product purified via liquid column chromatography to yield the product as a yellow solid in a yield of 41 %.

3 Kinetic studies of the RAFT polymerization method

For the investigation of reaction kinetics, for every monomer/RAFT reagent combination, two polymers with a theoretical molecular weight of 20 000 and 40 000 g mol⁻¹ were synthesized. The polymerization was executed as solution polymerization in dioxane, with a monomer concentration of 2 mol L⁻¹ with an approximate ratio of 7.5:1 for CTA:initiator. For the monitoring of the monomer conversion, an internal standard, in this case naphthalene, was added to the formulation and samples were retrieved in noted time intervals. The taken samples, were quenched by ice cooling and removal of inert atmosphere, and analyzed by ¹H nucleus magnetic resonance (NMR).

For the determination of the monomer conversion ¹H-NMR in CDCl₃ was measured for every sample taken. In the spectrum, the peak integrals of the internal standard stay constant at 7.41 δppm, while the integral of the olefinic peak signals of the monomer constantly decreases. The monomer conversion was determined according to **equation 10**.

$$\text{monomer conversion [\%]} = \left(1 - \frac{\text{peak integral}_t}{\text{peak integral}_{t=0}}\right) * 100 \quad \text{equation 10}$$

As an example, in **Figure 22**, an overlay of the spectra at t = 0 min and t = 40 min is depicted, to show the difference of the spectra after this polymerization time.

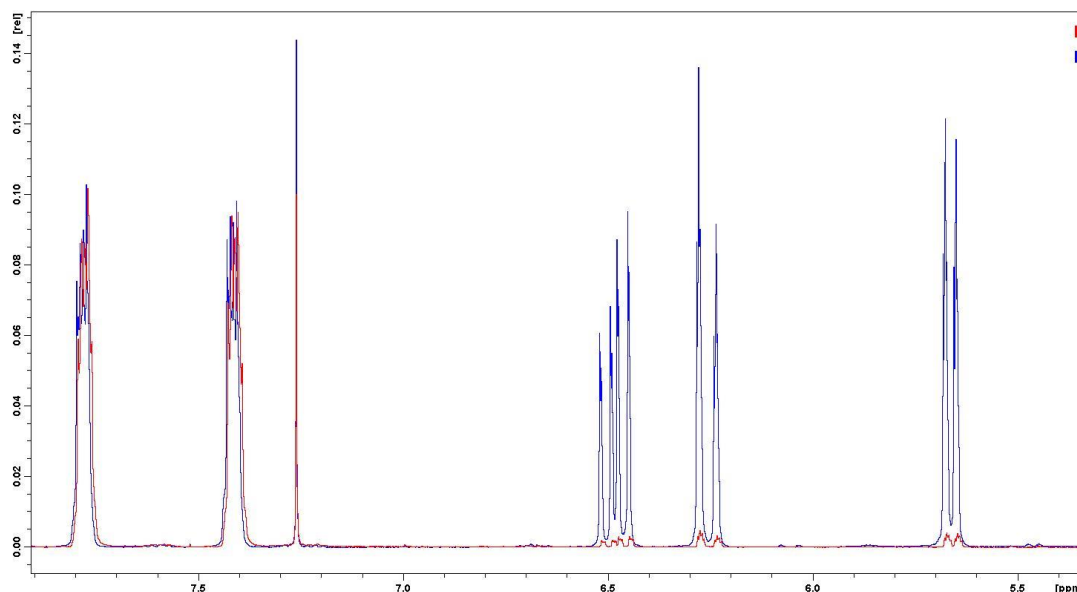


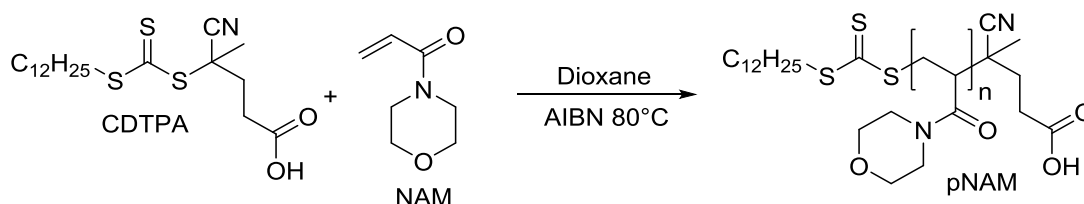
Figure 22. $^1\text{H-NMR}$ in CDCl_3 of the homopolymerization of pNAM with CDTPA at $t = 0 \text{ min}$ (blue) and $t = 40 \text{ min}$ (red)

After the maximum polymerization time was reached, the sample was quenched under ice cooling and aeration and then precipitated in petrol ether (PE). The polymer was dried and analyzed by gel permeation chromatography (GPC) with tetrahydrofuran (THF) to get also information about the molecular weight and the molecular weight distribution.

3.1 Reaction kinetics of RAFT polymerization of NAM and MPAA using CDTPA as CTA

3.1.1 Synthesis of a 20 kDa and a 40 kDa pNAM homopolymer by CDTPA as RAFT reagent and determination of the reaction kinetics by $^1\text{H-NMR}$

The first kinetic study was performed on CDTPA as CTA in combination with NAM as monomer.



Scheme 24. Synthesis of pNAM homopolymer with CDTPA

CDTPA and AIBN were weighted in a ratio of 7.1:1 and an amount of naphthalene as internal standard were dissolved in a 2 M solution of NAM in dioxane, resulting in a ratio of monomer to CTA corresponding to a 20 kDa pNAM polymer. This formulation was then degassed with argon, heated up immediately to a temperature of 80 °C under magnetic stirring and the monomer conversion was monitored by ¹H-NMR for a time of 3 h (**Figure 23**).

After the polymerization every time scale of the taken ¹H-NMR was evaluated and the monomer conversion of each sample was calculated by **equation 10**. These monomer conversions were plotted in a diagram versus the reaction time (**Figure 23**)

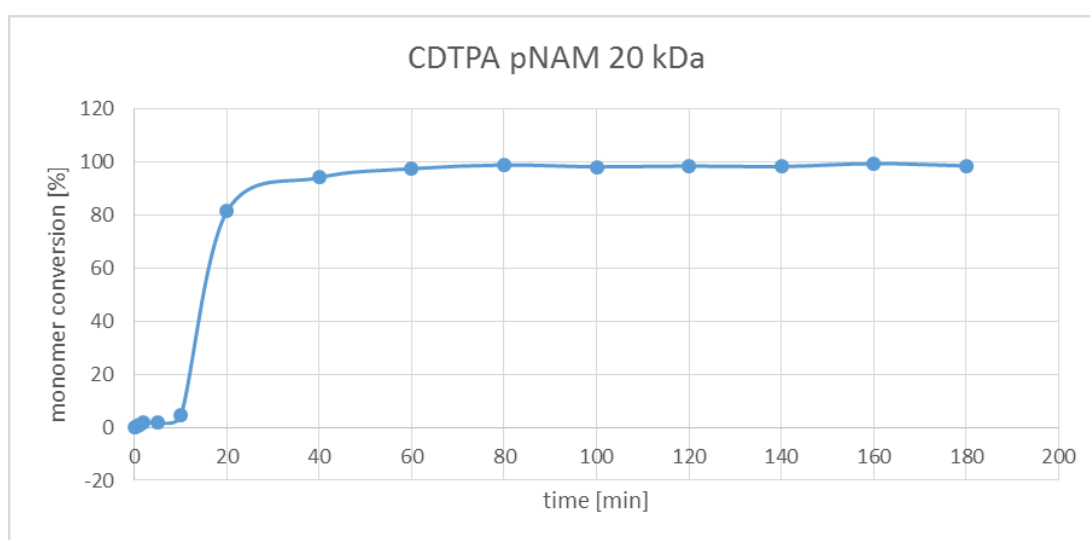


Figure 23. Polymerization kinetics I of NAM with 20 kDa CDTPA in dioxane at 80 °C

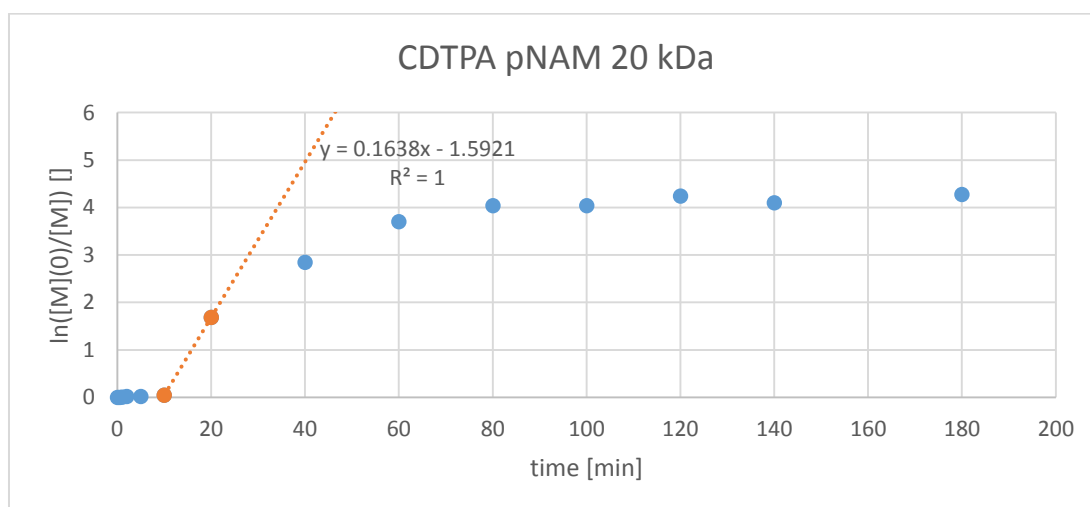


Figure 24. Evolution of the logarithmic monomer concentration over time of NAM with CDTPA in dioxane at 80 °C

Figure 23 and **Figure 24** show a small time period of 10 min in the beginning, where the conversion was quite low. The reason for that, might be the heating up of the formulation, because it was not possible to heat the formulation in a blink of an eye. A second reason could be the degradation of AIBN, which does not occur completely at once, but continuously over a period of time. Another reason could be inhibition. If re-initiation is not sufficiently fast, inhibition might occur in RAFT polymerization processes⁴⁴. But on the other hand, after 80 min the polymerization was completed with a monomer conversion of 99 %. The reaction kinetics of this RAFT polymerization should follow a pseudo-first order kinetic. This cannot be seen in **Figure 24**, due to fact that between the measurement interval between 10 and 20 min a monomer conversion step from 4 to 81 % occurred and from the approximation a conversion of > 90 % was reached 10 min later. However, the measurement was taken 20 min later with a conversion of 94 % and the linearity could not be plotted by use of this measurement point.

After finalization of the polymerization, the polymer was isolated by precipitation in PE and analyzed. The eluogram from GPC (**Figure 25**) showed a molecular weight M_n of 8 224 g mol⁻¹ and M_w of 11 241 g mol⁻¹ related to polystyrene (PS) standards, therefore a dispersity of $\mathcal{D} = 1.37$. Dispersities below 1.5 are common for polymers, prepared by controlled radical polymerization, so the RAFT polymerization of NAM with CDTPA was successful.

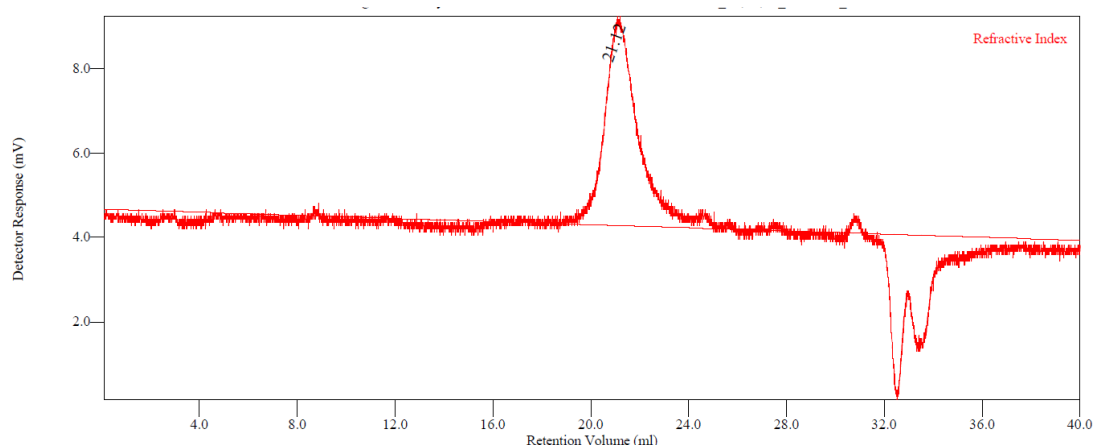


Figure 25. GPC-Eluogram of pNAM 20kDa with CDTPA; THF

To compare the results of the kinetic studies, also a 40 kDa polymer was synthesized, and the reaction kinetics were investigated with the same method as for the 20 kDa polymer. The ratio of monomer to CTA used, was 277.7:1 and the ratio of CTA to AIBN was set to 6.6:1.

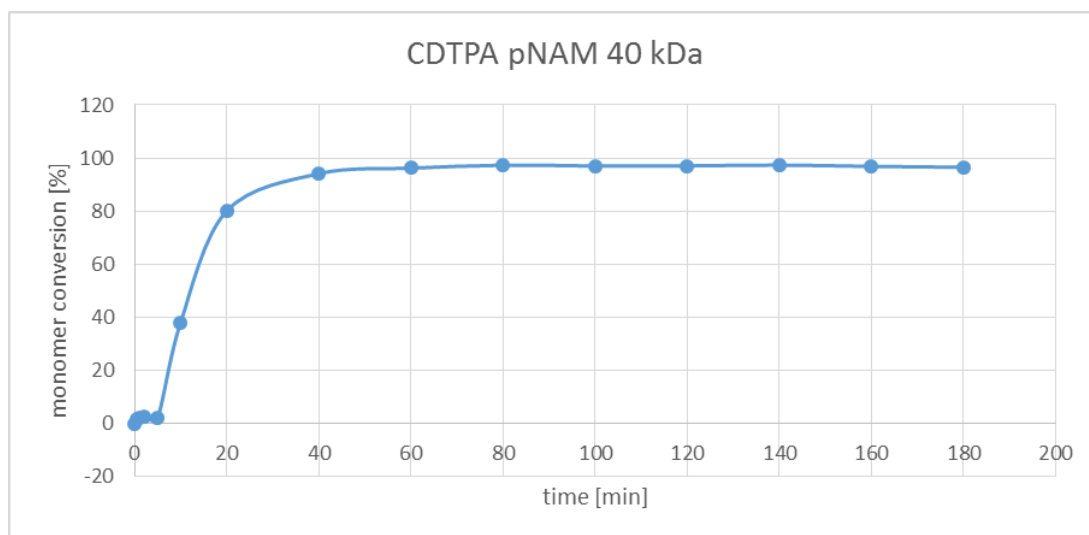


Figure 26. Polymerization kinetics II of NAM with 40 kDa CDTPA in dioxane at 80 °C

Figure 26 shows less inhibition time, compared to the data of the polymerization with a target MW of 20 kDa. The reason for that might be the lower concentration of CDTPA in the formulation, because a higher molecular weight was aspired. So the RAFT equilibrium favored re-initiation. In an overlay of both kinetic studies (**Figure 27**), a difference in inhibition time of approximately 7 min could be identified.

For this attempt, a monomer conversion of 97 % was reached, with $M_n = 16\,638\text{ g mol}^{-1}$ and $M_w = 22\,627\text{ g mol}^{-1}$, and a Đ of 1.36 according to PS standards.

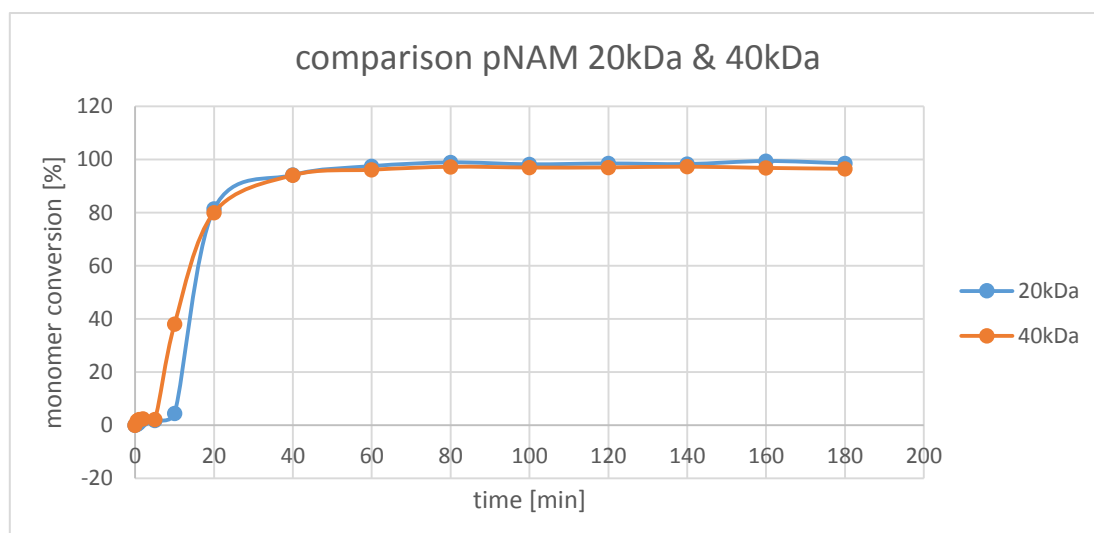
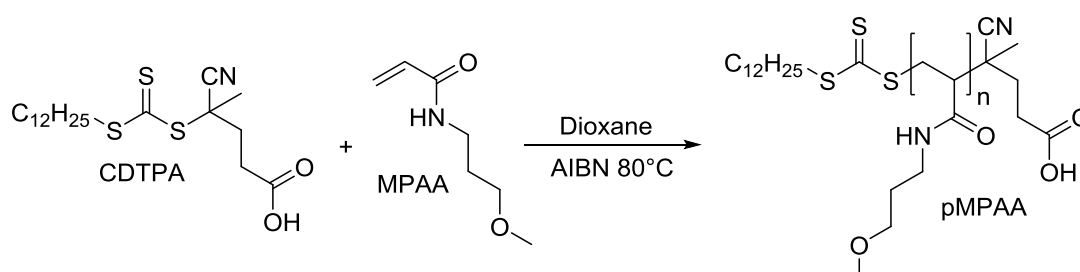


Figure 27. Comparison of the 20 kDa and 40 kDa polymerization of NAM with CDTPA

For the determination of the reaction kinetics of the MPAA RAFT polymerization with CDTPA as CTA, the same general procedure as explained in the beginning of chapter 3 should be used. Again, polymers with theoretical molecular weights of 20 kDa and 40 kDa should be synthesized.

3.1.2 Synthesis of a 20 kDa and 40 kDa pMPAA homopolymer by CDTPA as RAFT reagent and determination of the reaction kinetics by $^1\text{H-NMR}$

After the investigation of the polymerization of NAM, the other mentioned monomer MPAA was applied for further kinetic studies.



Scheme 25. Synthesis of pMPAA homopolymer with CDTPA as CTA

CDTPA and AIBN were weighted in a ratio of 7.4:1 into a penicillin flask. An amount of naphthalene as internal standard were dissolved in a 2 mol L⁻¹ solution of MPAA in dioxane, resulting in a ratio of monomer to according to a 20 kDa pMPAA polymer. This formulation was then degassed with argon and heated up immediately to a temperature of 80 °C. The monomer conversion was monitored by ¹H-NMR and plotted versus the reaction time (**Figure 28**).

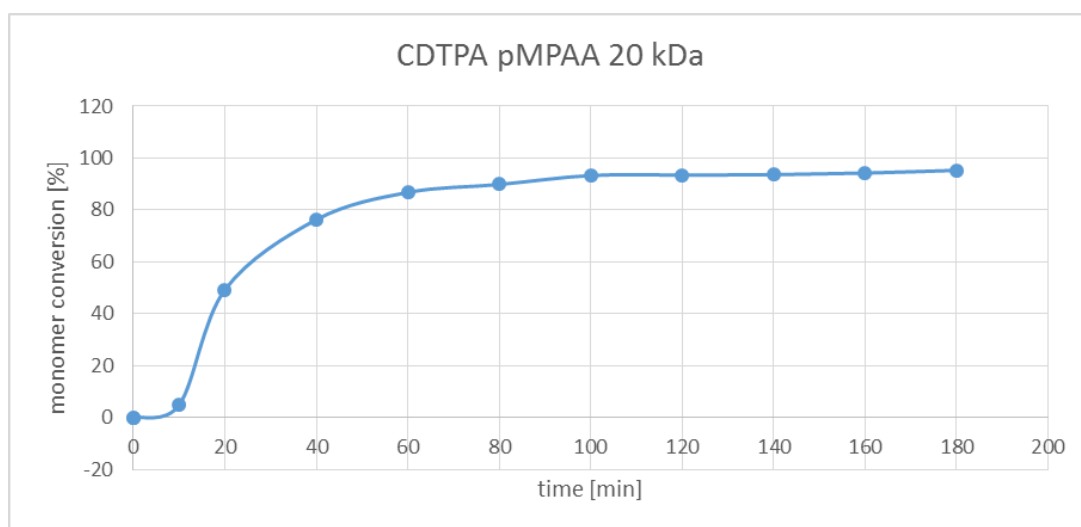


Figure 28. Polymerization kinetics I of MPAA with CDTPA in dioxane at 80 °C

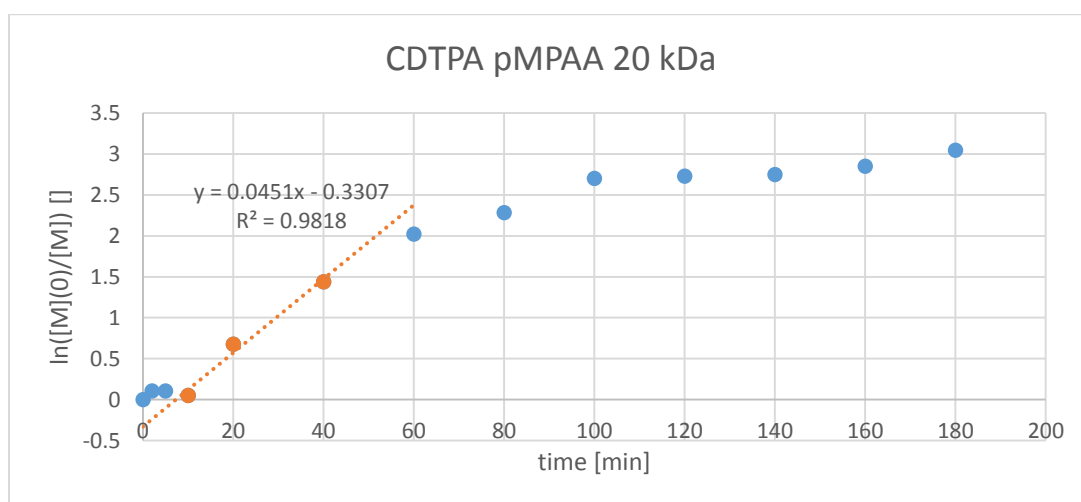


Figure 29. Evolution of the logarithmic monomer concentration over time of MPAA with CDTPA in dioxane at 80 °C

At the beginning, again a time interval of approximately 7 min for inhibition occurred, then the polymerization started with a steep rate of monomer conversion in a pseudo-first order kinetic (**Figure 29**). In the case of the composition CDTPA and MPAA, the reaction velocity is slower compared to NAM. It took about 100 min to reach almost the maximum monomer conversion of 95 % (determined at 180 min). A $M_n = 8\,720\text{ g mol}^{-1}$, $M_w = 11\,675\text{ g mol}^{-1}$ and a dispersity of $\bar{D} = 1.34$, determined by GPC, gave validation of accomplishment of a RAFT polymerization.

For the synthesis of the 40 kDa pMPAA polymer the ratio of monomer to CTA for this RAFT polymerization, was according to the target MW and the ratio of CTA to AIBN was set to 7.7:1.

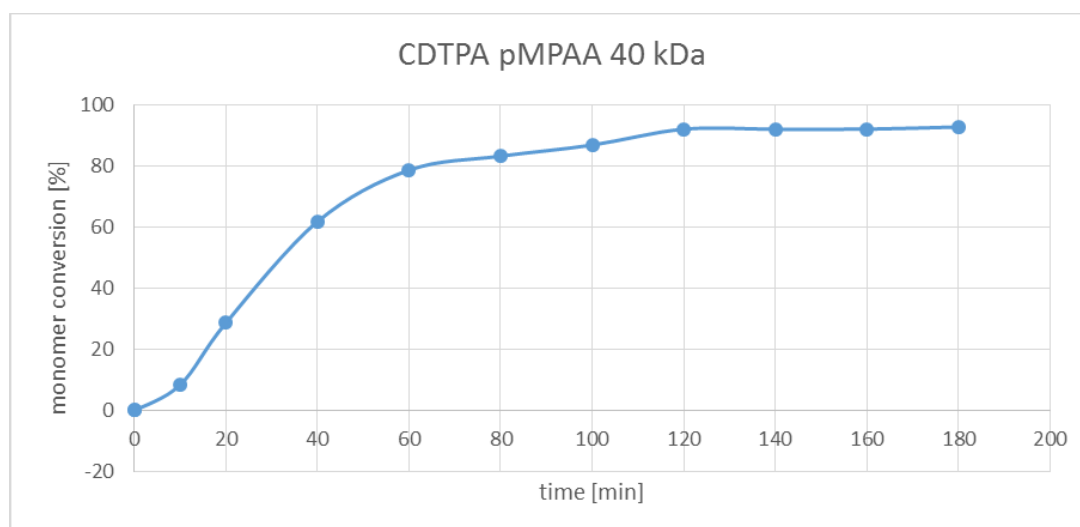


Figure 30. Polymerization kinetics II of MPAA with CDTPA in dioxane at 80 °C

As seen before, for pNAM with a MW of 40 kDa, the RAFT polymerization started with a lesser inhibition period. For the polymerization of a 40 kDa pMPAA polymer the approximate maximum monomer conversion of 93 % (determined after 180 min) was reached after 120 min with a $M_n = 13\,428\text{ g mol}^{-1}$, $M_w = 20\,050\text{ g mol}^{-1}$ and $\bar{D} = 1.49$ according to PS standards. In the overlay **Figure 31**, the difference of approximately 3 min in inhibition time of these two polymerizations, can be determined.

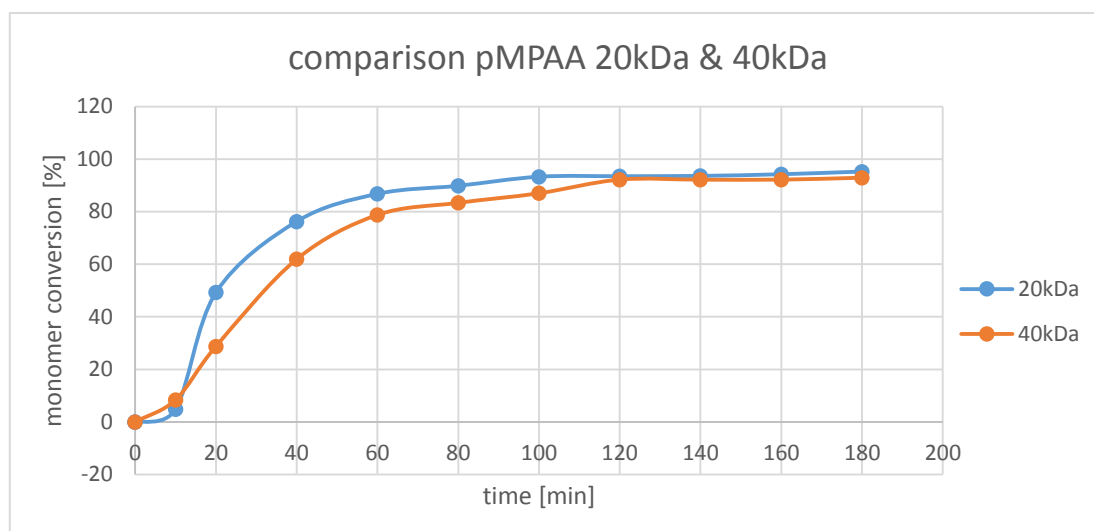
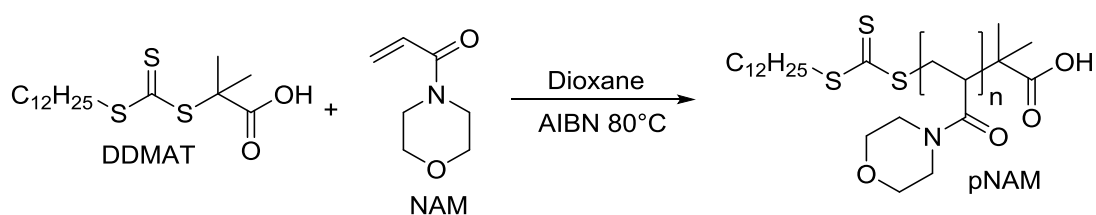


Figure 31. Comparison of the 20 kDa and 40 kDa polymerization of MPAA with CDTPA

3.2 Reaction kinetics of RAFT polymerization of NAM and MPAA using DDMAT as CTA

3.2.1 Synthesis of a 20 kDa and 40 kDa pNAM homopolymer with DDMAT as RAFT reagent and determination of the reaction kinetics by ¹H-NMR

After the kinetic studies of CDTPA as CTA, the kinetic of the other chosen RAFT reagent DDMAT was investigated in combination with NAM.



Scheme 26. Synthesis of pNAM homopolymer with DDMAT

The ratio of monomer to CTA for this RAFT polymerization, was according to a 20 kDa pNAM polymer and the ratio of CTA to AIBN was 5.7:1 in dioxane as solvent and at a temperature of 80 °C.

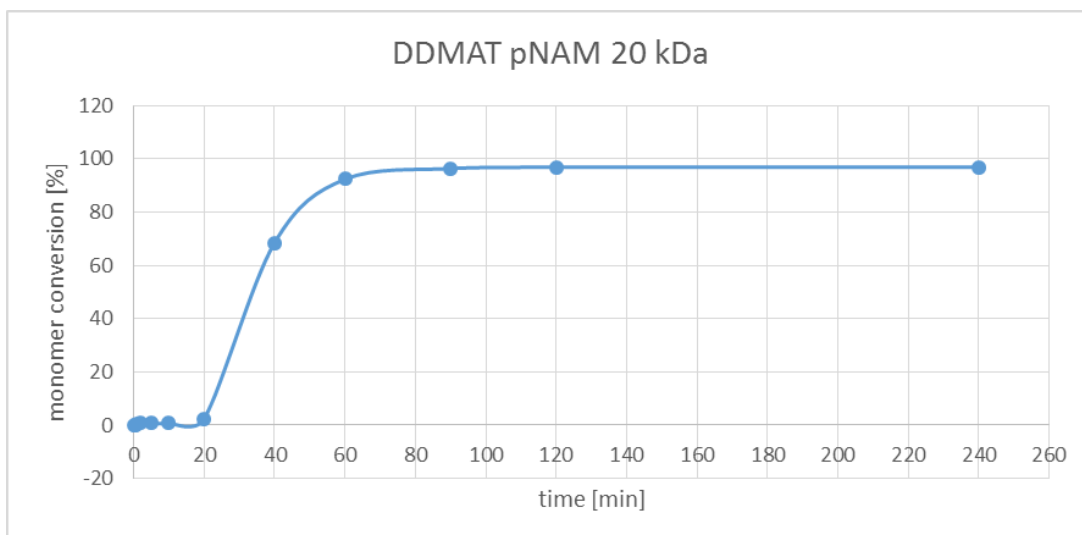


Figure 32. Polymerization kinetics I of NAM with DDMAT in dioxane at 80 °C

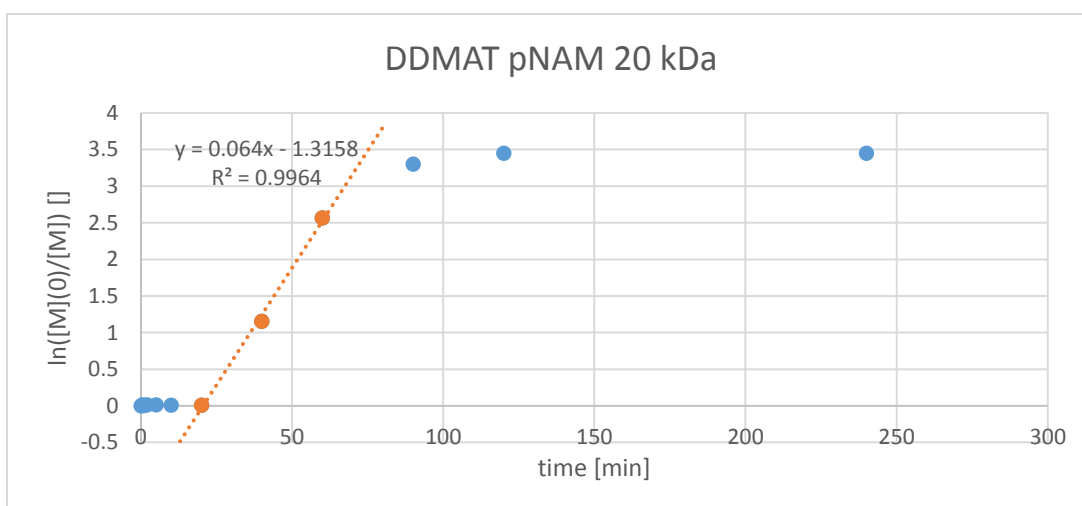


Figure 33. Evolution of the logarithmic monomer concentration over time of NAM with DDMAT in dioxane at 80 °C

DDMAT as RAFT reagent in combination with NAM as monomer showed a longer time of inhibition compared to the polymerization of NAM 20 kDa with CDTPA. The polymerization started after 20 min, but then the reaction proceeded fast, with a pseudo-first order kinetic (**Figure 33**). Conversions above 90 % were reached after 60 min and the polymerization ended in a maximum monomer conversion of 97 % after 240 min with $M_n = 8\,911 \text{ g mol}^{-1}$, $M_w = 12\,103 \text{ g mol}^{-1}$ and \bar{D} of 1.36 according to PS standards.

For the synthesis of the 40 kDa pNAM polymer, the ratio of monomer to CTA used, was according to the target degree of polymerization and the ratio of CTA to AIBN was 8.16:1 in dioxane as solvent and a temperature of 80 °C.

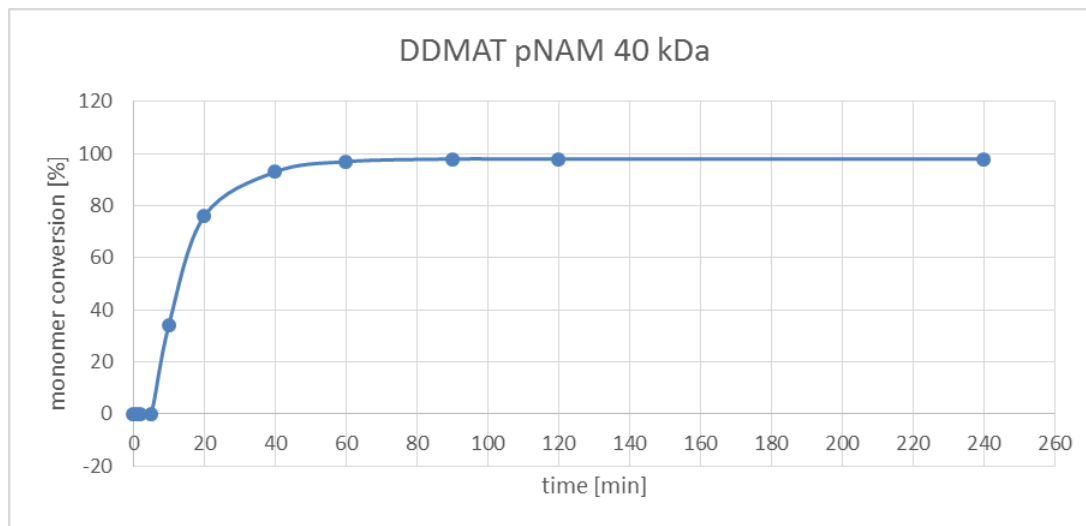


Figure 34. Polymerization kinetics II of NAM with DDMAT in dioxane at 80 °C

For the polymerization with a higher ratio of monomer to CTA, DDMAT worked out significantly faster. The inhibition time was less than 10 min and conversions above 90 % could be reached after 40 min reaction time. For this polymerization a dispersity of $\bar{D} = 1.37$ according to PS standards, $M_n = 16\,358\text{ g mol}^{-1}$, $M_w = 22\,454\text{ g mol}^{-1}$, and an end monomer conversion of 98 % was reached. In the comparison of these two kinetics (**Figure 35**), the difference of approximately 16 min can be appointed.

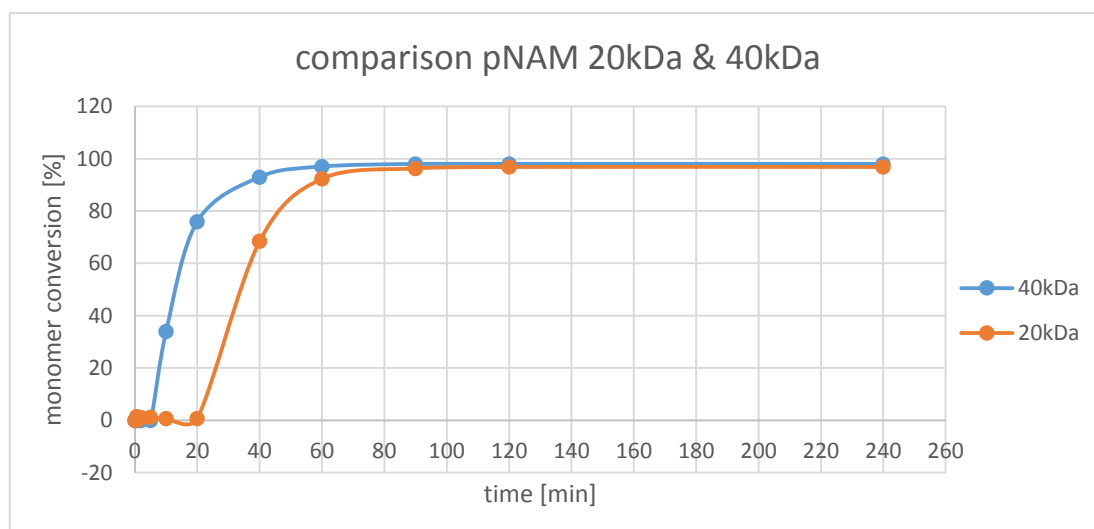
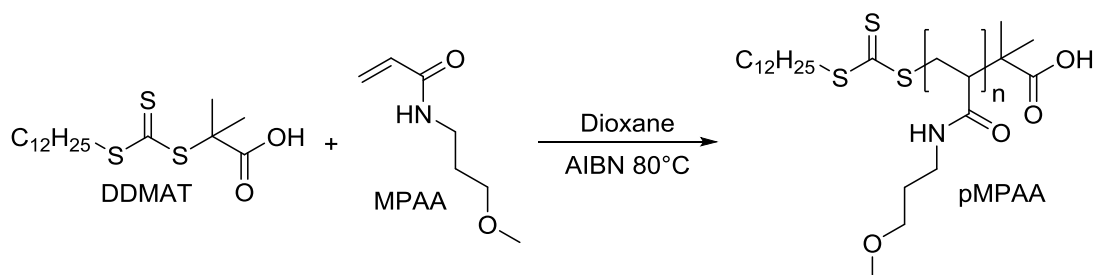


Figure 35. Comparison of the 20 kDa and 40 kDa polymerization of NAM with DDMAT

3.2.2 Synthesis of a 20 kDa and 40 kDa pMPAA homopolymer by DDMAT as RAFT reagent and determination of the reaction kinetics by $^1\text{H-NMR}$

After the investigation of DDMAT in combination with NAM, the kinetic behavior of DDMAT in combination with MPAA was analyzed.



Scheme 27. Synthesis of pMPAA homopolymer with DDMAT

For the synthesis of the 20 kDa pMPAA polymer, the ratio of monomer to CTA used, was according to the target MW and the ratio of CTA to AIBN was 8.12:1 in dioxane as solvent and a temperature of 80 °C was applied.

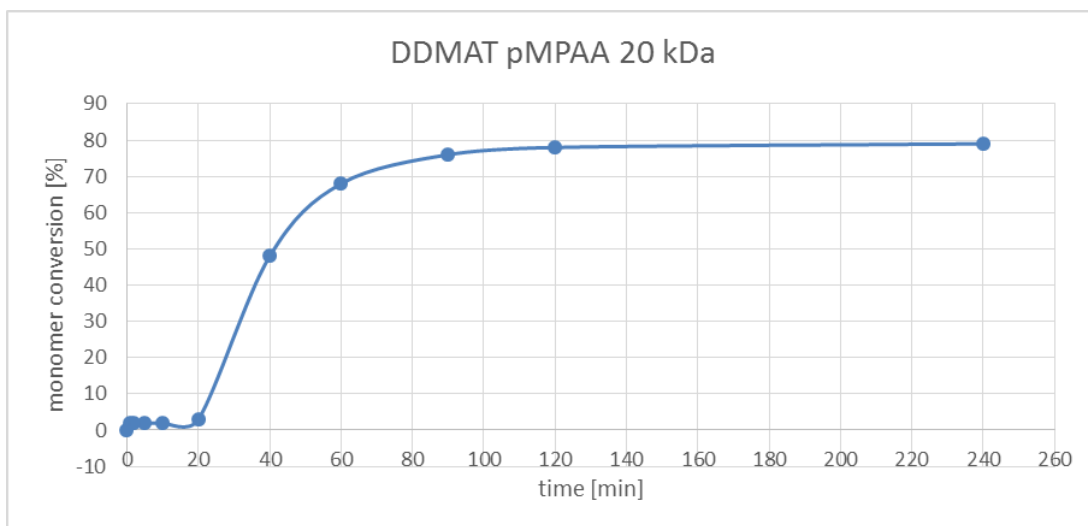


Figure 36. Polymerization kinetics I of MPAA with DDMAT in dioxane at 80 °C

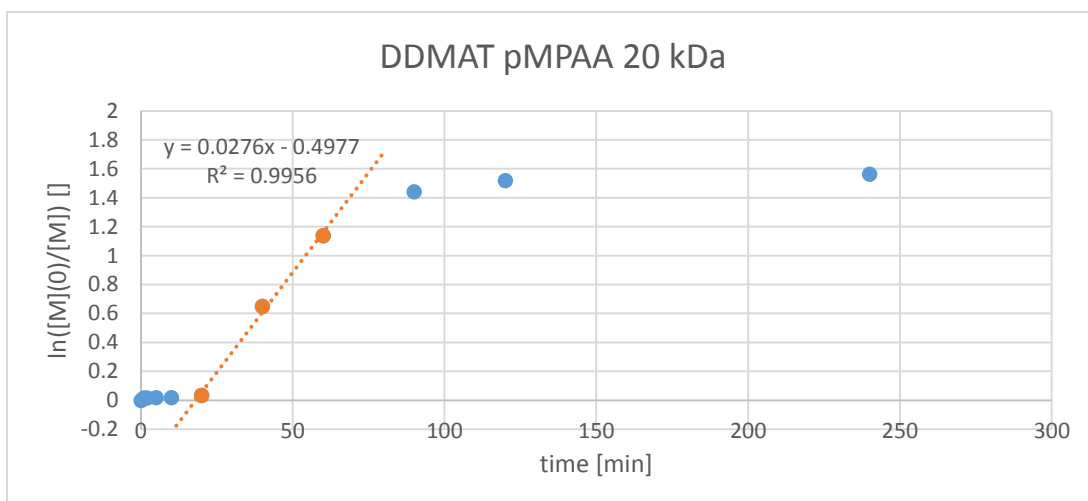


Figure 37. Evolution of the logarithmic monomer concentration over time of MPAA with DDMAT in dioxane at 80 °C

DDMAT did not show the same excellent results in combination with MPAA as with NAM, due to the lower monomer conversion of 79 % after 4 h polymerization time, but exhibited a pseudo-first order kinetic after an inhibition time of 18 min (**Figure 37**). For this attempt a $M_n = 7\,714 \text{ g mol}^{-1}$, $M_w = 11\,174 \text{ g mol}^{-1}$ and a dispersity of $\mathcal{D} = 1.45$ (PS Standards) was achieved.

The ratio of monomer to CTA used for the 40 kDa pMPAA polymer, was according to the target MW and the ratio of CTA to AIBN was 8.19:1 in dioxane as solvent and a temperature of 80 °C was applied.

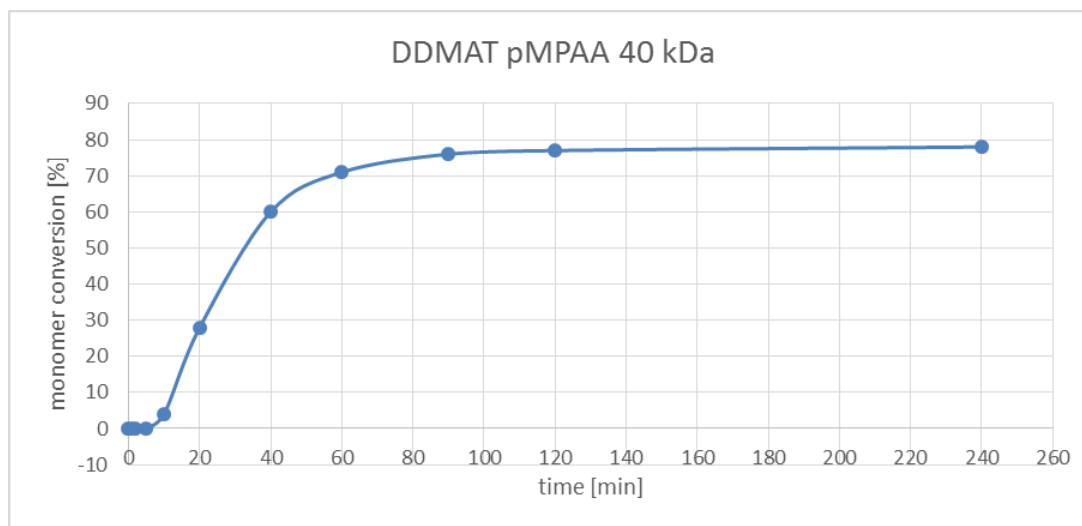


Figure 38. Polymerization kinetics II of MPAA with DDMAT in dioxane at 80 °C

For the higher ratio of monomer to CTA, the familiar effect of lower inhibition time occurred again. In the synthesis of a 40 kDa polymer only a monomer conversion of 78 % was achieved, similar to the pMPAA polymerization with a target MW of 20 kDa. For this polymerization a $M_n = 11\,248\text{ g mol}^{-1}$, $M_w = 19\,004\text{ g mol}^{-1}$ and a dispersity $\bar{D} = 1.67$, which represented a value too high for satisfying CRP conditions. The difference in inhibition time of these two polymerizations was approximately 11 min, which was determined by the comparison of these two kinetic graphs (**Figure 39**).

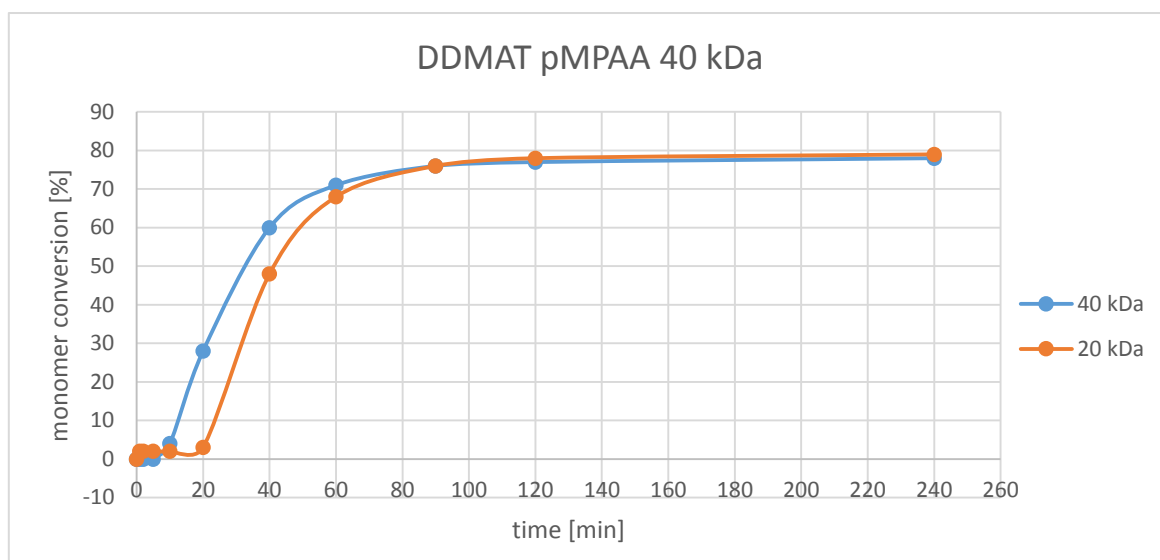


Figure 39 Comparison of the 20 kDa and 40 kDa polymerization of MPAA with DDMAT

3.3 Summary of the kinetic studies of RAFT polymerization of NAM and MPAA
 For the chosen monomers, both RAFT reagents, CDTPA and DDMAT, showed a good performance. High monomer conversion and low dispersities could be reached within reasonable polymerization times. Because of the longer inhibition time at the beginning, and the lower monomer conversion by the usage of MPAA as monomer, CDTPA should be favored over DDMAT for further investigations of surface initiated RAFT polymerization of the two monomers. **Figure 40** emphasizes these results, showing the comparison of the data for the polymerizations with 20 kDa target molecular weight.

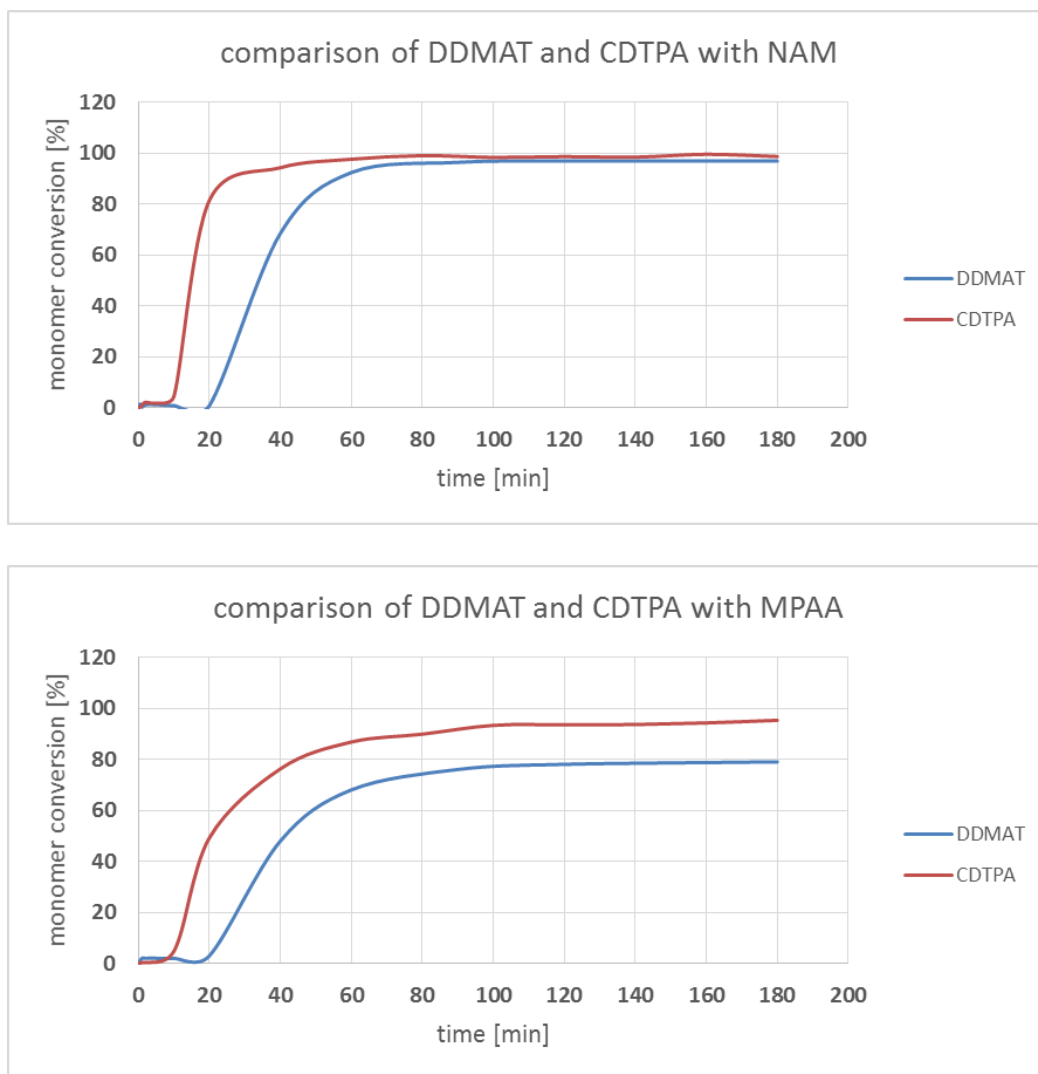


Figure 40. Comparison of CDTPA and DDMAT as RAFT agents for the two acrylamide monomers in their kinetical behavior

From the perspective of dispersity and molecular weight (**Table 1**), CDTPA performed very constant for both monomers, NAM and MPAA, with PDIs of $\bar{D} < 1.5$ regardless which monomer was used. On the other hand, DDMAT showed similar results with NAM, but in combination with MPAA higher PDIs were obtained. For the 40 kDa pMPAA polymer synthesized with DDMAT already a dispersity of $\bar{D} = 1.67$ was determined. From the point of dispersity CDTPA was superior to DDMAT as well. In **Table 1** the difference in molecular weight of the measurements via $^1\text{H-NMR}$ and GPC could be seen. The reason for that, is the use of polystyrene standards, which have a different morphology in THF than the generated polymers.

Table 1. Final results of the kinetic studies of RAFT polymerization of pNAM and pMPAA with CDTPA and DDMAT as CTA

Monomer	CTA	Target MW [kDa]	Monomer conversion [%]	M _{NMR} [kDa]	M _{n,GPC} [kDa]	M _{w,GPC} [kDa]	PDI []
NAM	CDTPA	20	99	19.8	8.2	11.2	1.37
	CDTPA	40	97	38.4	16.6	22.6	1.36
	DDMAT	20	97	21.2	8.9	12.1	1.36
	DDMAT	40	98	40	16.4	22.5	1.37
MPAA	CDTPA	20	95	18.9	8.7	11.7	1.34
	CDTPA	40	93	36.8	13.4	20.1	1.49
	DDMAT	20	79	17.5	7.7	11.2	1.45
	DDMAT	40	78	31.9	11.2	19.0	1.67

4 Analysis of pNAM and pMPAA in solution by static light scattering, dynamic light scattering and small angle X-ray scattering

To investigate the behavior of the polymer brush system in aqueous environment and its aggregation behavior, light scattering experiments of the free polymer in milli-Q water and phosphate buffered saline (PBS) buffer should be carried out. For this measurements a dilution series of the RAFT polymers was generated and analyzed by a goniometer with a Helium/Neon Laser. For the SLS measurement the scattering signal was measured 3 times for 30 s from an angle of 30 ° to 130 ° in an interval of 10 ° at a temperature of 25 °C. DLS measurements were performed simultaneous and calculated by the generated data. For a better structural analysis SAXS measurements were also applied. By fitting approximations of geometric constructs in the scattering image, the shape of the particles in solution was determined.

4.1 SLS and DLS analysis of pNAM in water

First a pNAM polymer (pNAM20k) with a theoretical molecular weight of 21.6 kDa (determined by monomer conversion with $^1\text{H-NMR}$) was synthesized using CDTPA as RAFT reagent, under the same conditions as used for the kinetic studies. pNAM itself is soluble in water, so a dilution series of 5 concentrations from 0.5 mg mL^{-1} to 3 mg mL^{-1} of pNAM20k in milli-Q water was applied. With this dilution series the refractive index increment $\left(\frac{\partial n}{\partial c}\right)_T$ of 0.165 mL mg^{-1} was determined via a modified refractive index (RI) detector and then analyzed with a light scattering goniometer. The generated data was analyzed via a Zimm plot (**Figure 41**).

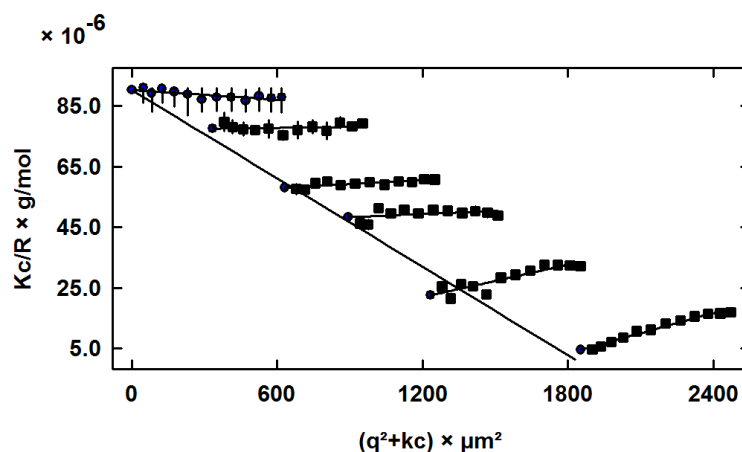


Figure 41. Zimm plot of a pNAM dilution series in water

From the Zimm plot (**Figure 41**) it could be derived, that the second virial coefficient A_2 (slope of the linear regression in concentration direction; $A_2 = -1.5 \cdot 10^{-5} \text{ mol dm}^3 \text{ g}^{-2}$) was negative. That implies the aggregation of the polymer particles in aqueous solution, and that the solution was not stable. The next abnormality was the changing slope value of the linear regression in angle direction, which made it difficult to determine the M_w and R_g . An approximation for the determination of R_g was applied by just using one concentration of approximately 3 mg mL^{-1} . With this, the shape analysis, a so called Kratky plot could be generated from this static light scattering data (**Figure 42**) and approximations through simple geometric constructs could be fitted.

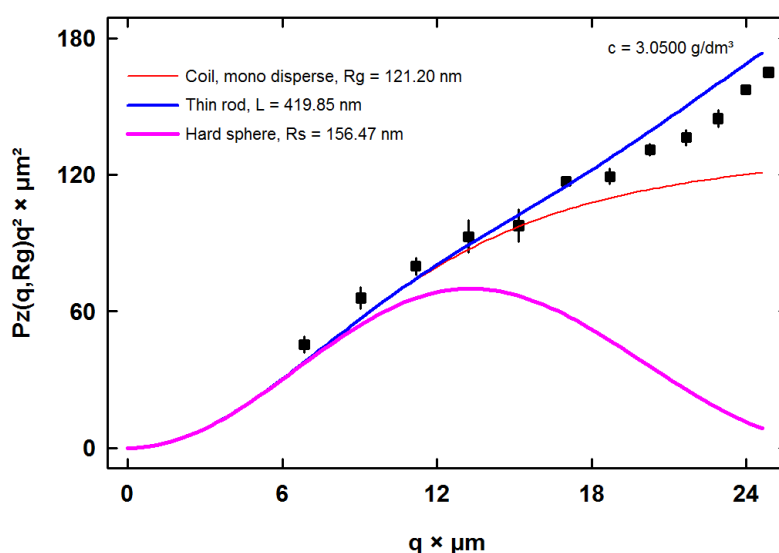


Figure 42. Kratky plot of pNAM (3 mg mL^{-1}) in water

As identifiable in the Kratky plot **Figure 42**, the best fit was found for a thin rod similar geometric form. However, it matched the graph not perfectly, but it could be labeled as a worm-like structure. The only conspicuousness was that, lengths of $L = 420 \text{ nm}$ or $R_g = 121 \text{ nm}$ are theoretically impossible for a polymer of 21 kDa molecular weight. The reason for that abnormality was certainly aggregation and since the used concentration was the highest of the dilution series⁷⁸. Another fact to mention is, that by usage of a lower concentration, it was not possible to determine any shape by Kratky plotting (**Figure 43**).

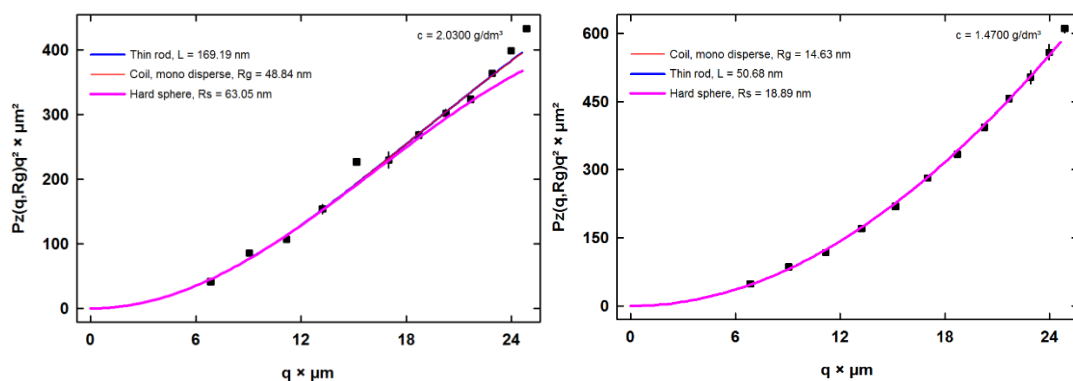


Figure 43. Kratky plot for pNAM in water; 2 mg mL^{-1} (left); 1.5 mg mL^{-1} (right)

Nevertheless, it was obvious from the plot with the highest concentration and largest particles⁷⁸ in **Figure 42**, that the formed aggregates exhibited worm-like shape. Due to the factor of aggregation, another experiment by determination of the hydrodynamic radius R_H by dynamic light scattering and dynamic Zimm plotting, was applied. By the comparison of R_g and R_H , the form could be predicted. For this experiment, a lower concentration, 1.5 mg mL^{-1} , was chosen, and SLS and DLS measurements were done simultaneous from the same sample at the same time (**Figure 44**).

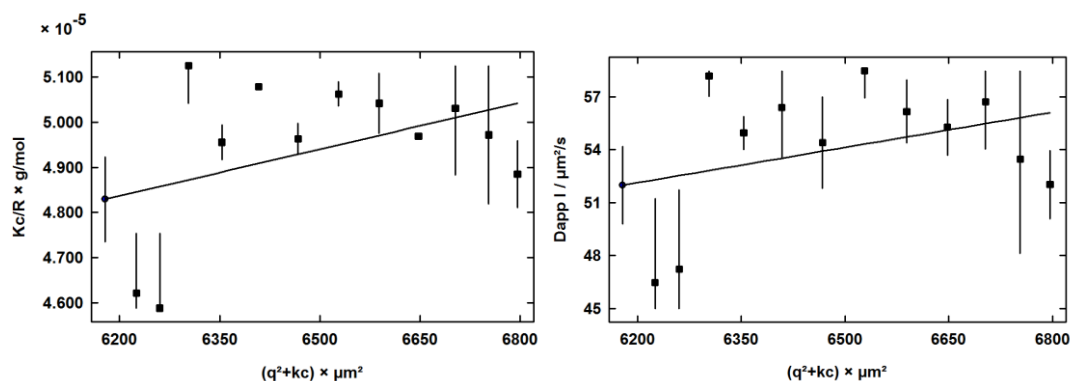


Figure 44. Left: Zimm plot of pNAM (1.5 mg mL^{-1}); right: dynamic Zimm plot pNAM (1.5 mg mL^{-1})

The value R_g / R_H determined from this experiment was $14.63 \text{ nm} / 4.72 \text{ nm}$, which gave calculated a value of ≈ 3 . A ratio of > 2 defines worm-like to rod-like polymer chains⁷⁹, so this experiment also confirmed the assumptions of worm-like structure mentioned before.

4.2 SAXS analysis of pNAM in water

For a better understanding of the polymer shape in solution, SAXS measurements were performed additionally. For this measurements a dilution with a concentration of $6 \text{ mg pNAM mL}^{-1}$ was provided, and filled, void-free, into cylindrical quartz cuvettes with a diameter of 1.5 mm. The sample was irradiated with X-rays for a time of 6 h and the background of the solvent (measured also for 6 h) was then subtracted from the measured scattering image (**Figure 45**).

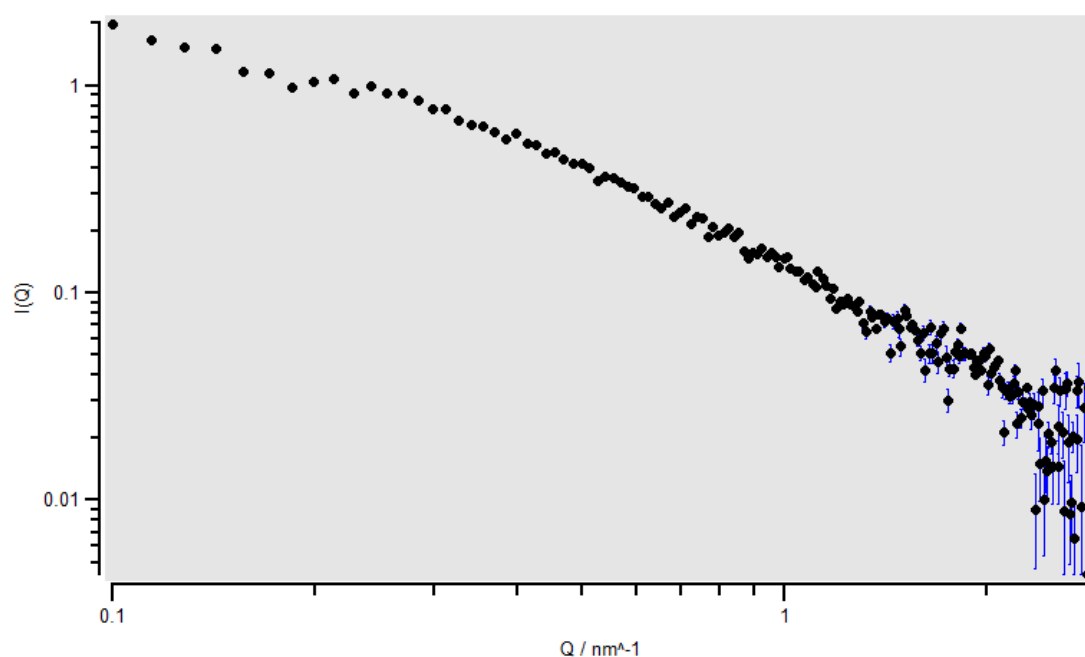


Figure 45. SAXS scattering image of pNAM (6 mg mL^{-1}) in water

Here, of course, aggregation occurred as well; the small bump at a scattering vector of 0.2 nm^{-1} indicated this phenomenon. In the next step, various curves for geometric forms were plotted in the diagram, until the regression exhibited the lowest variance of fit and normal distributed residuals.

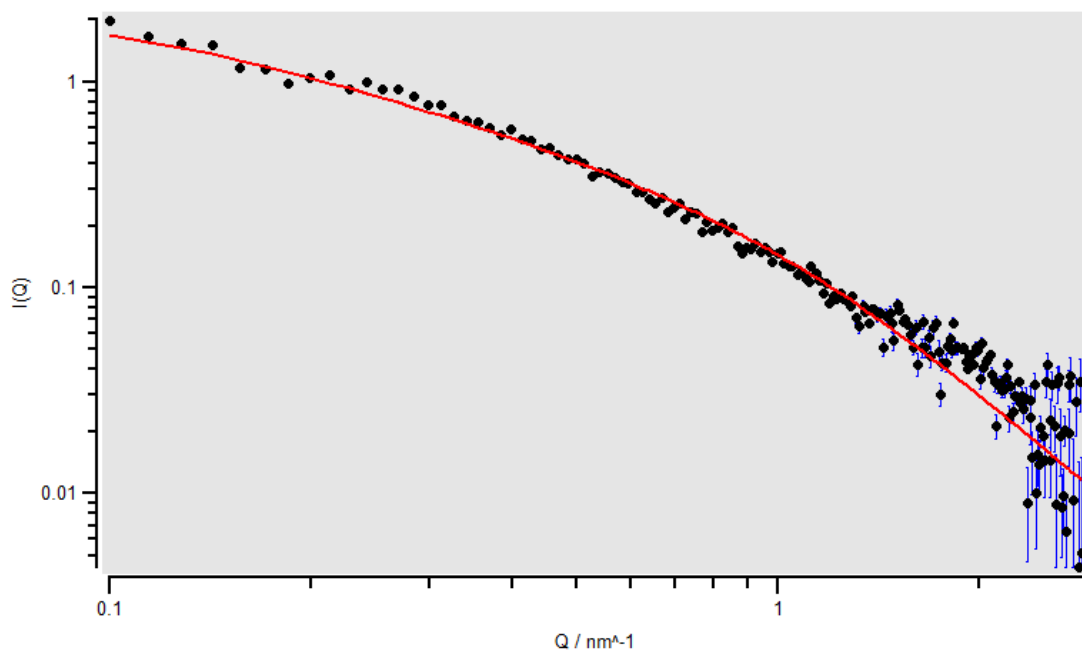


Figure 46. Mathematical fit of pNAM (6 mg mL^{-1}) in water; Kholodenko worm⁸⁰

The best fit is depicted in **Figure 46** and gave the structure of the Kholodenko worm (**Figure 47**)⁸⁰, which is categorized in the field of worm-like polymer structures, with a variance of fit of $1.6 \cdot 10^{-4}$. Other geometric constructs, like sphere, coil, worm-like and thin rod were also tried, but the best fit was achieved by Kholodenko worm, and for this attempt the distribution of the residuals (**Figure 48**) for this regression, was absolutely in range.

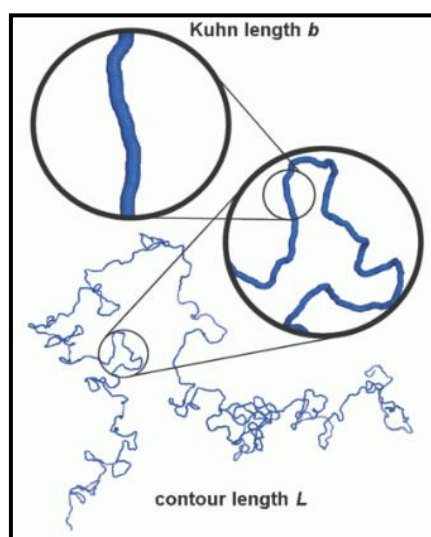


Figure 47. Kholodenko worm structure⁸¹

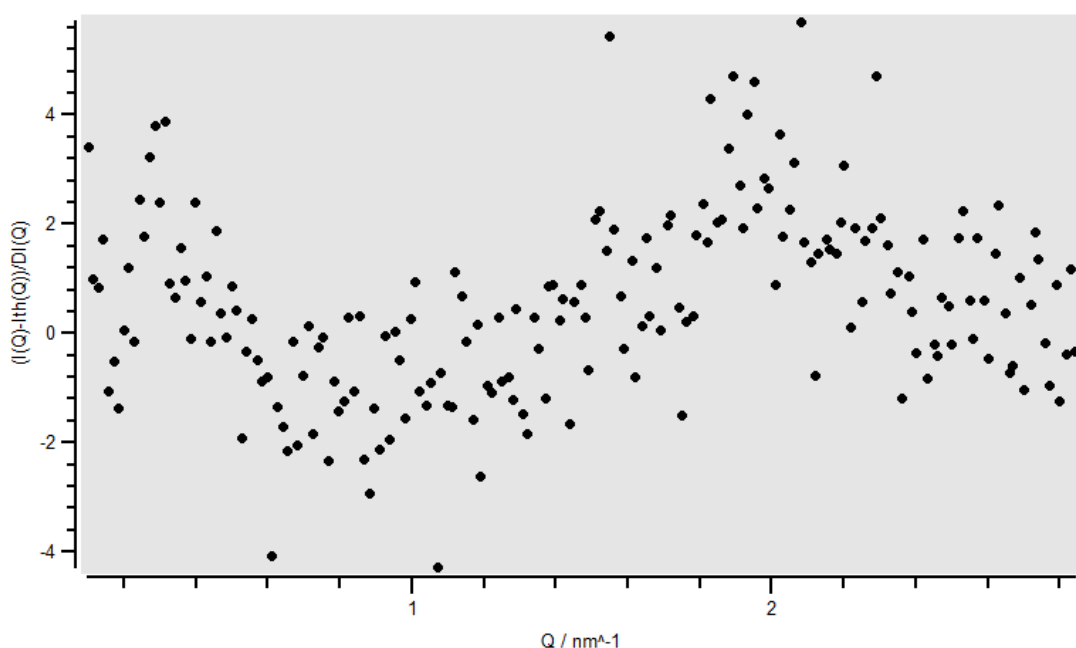


Figure 48. Distribution of the residuals; Kholodenko fit of pNAM in water

Despite of the aggregation, over the time of 6 h, the shape of the particles was a worm-like structure. The SAXS experiment, confirmed the assumptions from the SLS and DLS measurements for the structure of pNAM in water, so it is possible to expect the polymer morphology in solution as a worm-like conformation.

4.3 SLS and DLS analysis of pNAM in PBS buffer

Naturally, it was of interest to see, if the properties in aqueous solution were the same also for PBS buffer as solvent, because for applications with bio organisms, the usage of PBS is very common. The dilution series were prepared from the same pNAM polymer, pNAM20k, synthesized for the measurements in water, and the concentrations for this dilution series were nearly the same ($0.5 - 2 \text{ mg mL}^{-1}$), for reasons of comparison (**Figure 49**).

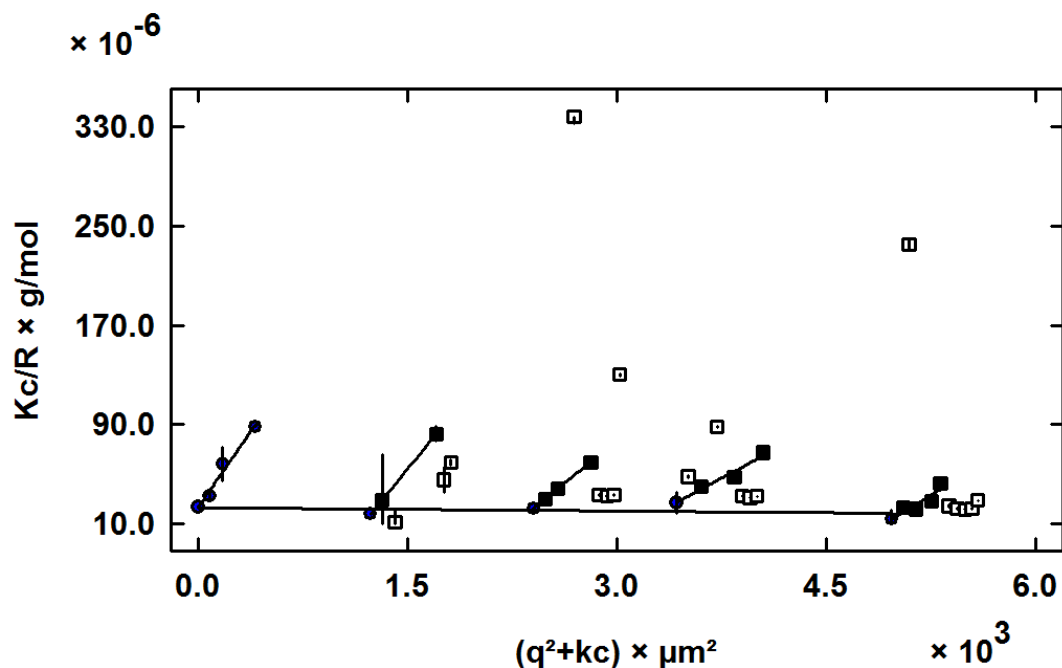


Figure 49. ZIMM Plot of pNAM in PBS

For the measurement in PBS, a very poor scattering image for pNAM was obtained. This caused the removal of various measurement points due to possible aggregation processes during the measurement. What could be determined from the beginning, was a high R_g of 143.5 nm, indicating aggregation, because the polymer could not be as spacious as calculated. For an ideal rod-like carbon chain backbone of the same amount of monomer units, the length would be 37.4 nm^{82, 83} with use of C – C bond length and cosinus of 90 ° minus sp^3 hybridized carbon binding angle divided by 2 . But the second virial coefficient A_2 was not as negative as for the measurement in water, only $A_2 = - 1 \cdot 10^{-6} \text{ mol dm}^3 \text{ g}^{-2}$ (measurement in water $A_2 = - 1.5 \cdot 10^{-5} \text{ mol dm}^3 \text{ g}^{-2}$), which was 10 times lower than in water. It could be possible that the aggregation process was so fast, that the dissolved sample aggregated even in the very small amount of time before the measurement start and during the measurement until a point of maximum aggregation. Therefore, a behavior like in theta solvated state could be possible.

For the determination of the shape in solution the ratio of R_g / R_H was used first. R_H was determined by dynamic Zimm Plot (**Figure 50**) using the concentrations 1 and 2 mg mL^{-1} , which gave the lowest variance in the result $R_H = 54.88 \text{ nm}$.

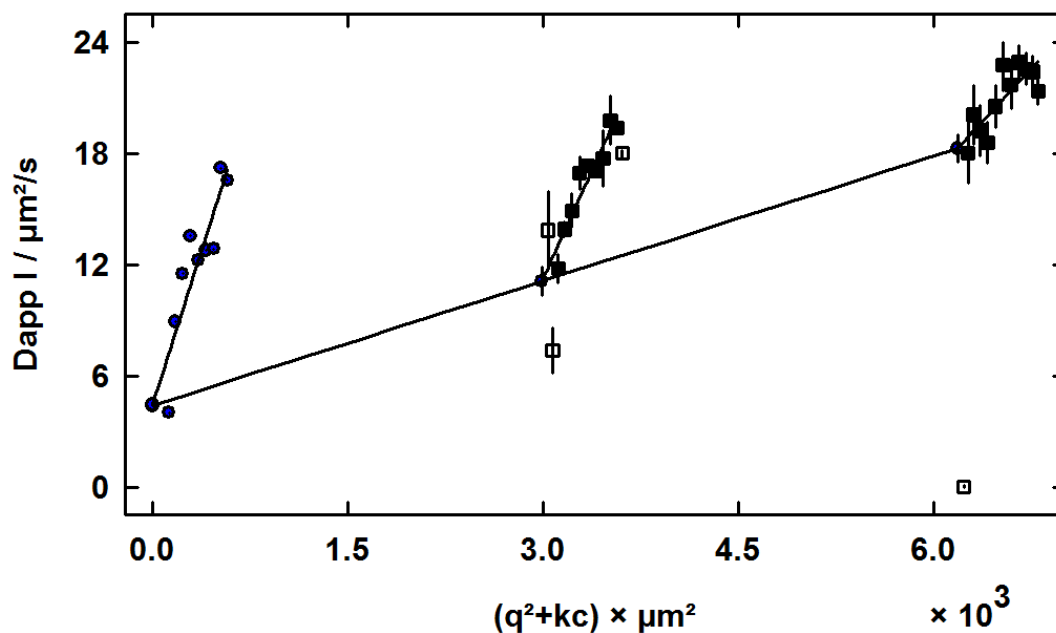


Figure 50. Dynamic Zimm plot pNAM (1 and 2 mg mL⁻¹)

This R_H from DLS measurement and R_g from SLS Zimm plot calculation ($R_g = 143.5$ nm), gave a ratio of 2.6 and indicated a wormlike structure. Furthermore a Kratky plot was generated from the data, used in the Zimm plot (**Figure 51**), and due to less data points, the regression was not that accurate but hinted at a wormlike structure.

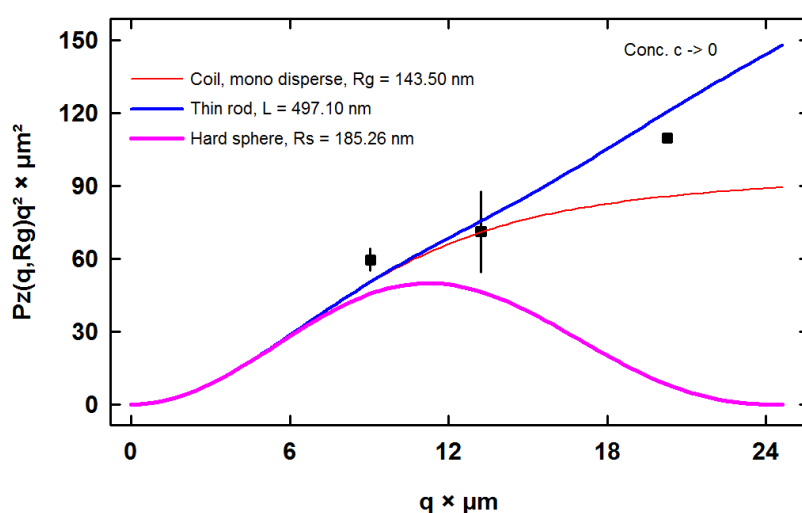


Figure 51. Kratky plot of pNAM in PBS buffer solution

In the case of pNAM in PBS buffer, the following SAXS experiment gave more structural information about the conformation in solution.

4.4 SAXS analysis of pNAM in PBS buffer

For the shape analysis with SAXS for pNAM in PBS, again a concentration of 6 mg mL^{-1} was measured by the same method as described for the measurement in water. As discussed in chapter 4.2, again the Kholodenko worm fit was the best regression with a variance of fit of $5.6 \cdot 10^{-4}$ (**Figure 52, Figure 53**).

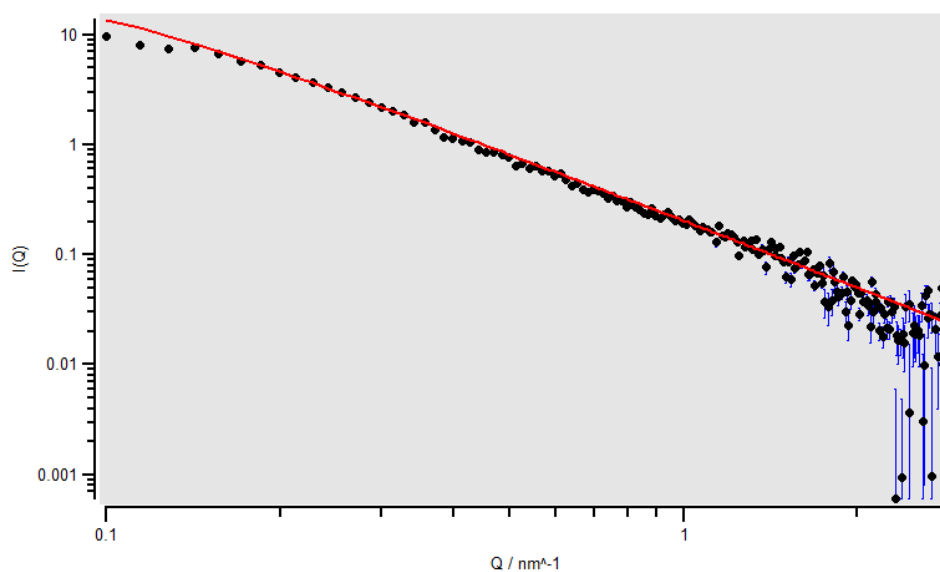


Figure 52. SAXS scattering image of pNAM (6 mg mL^{-1}) in PBS; Kholodenko worm fit

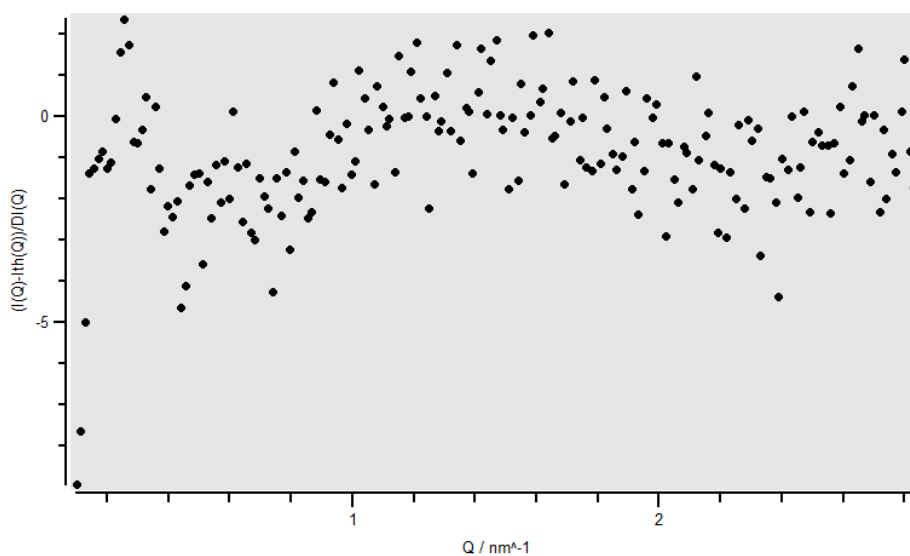


Figure 53. Distribution of the residuals; Kholodenko fit pNAM in PBS

4.5 SLS and DLS analysis of pMPAA in water

Here again, first a pMPAA (pMPAA20k) Polymer with a theoretical molecular weight of 20 kDa (determined from monomer conversion by $^1\text{H-NMR}$) was synthesized using DDMAT as RAFT reagent, under the same conditions used for the kinetic studies. pMPAA itself was also dissolvable in water, so a dilution series of 5 concentrations from 0.5 mg mL^{-1} to 3 mg mL^{-1} in milli-Q water was applied, the refractive index increment $\left(\frac{\partial n}{\partial c}\right)_T$ of 1.616 mL mg^{-1} was determined and the polymer was analyzed with SLS and DLS. The generated data from SLS was analyzed via a Zimm plot (**Figure 54**).

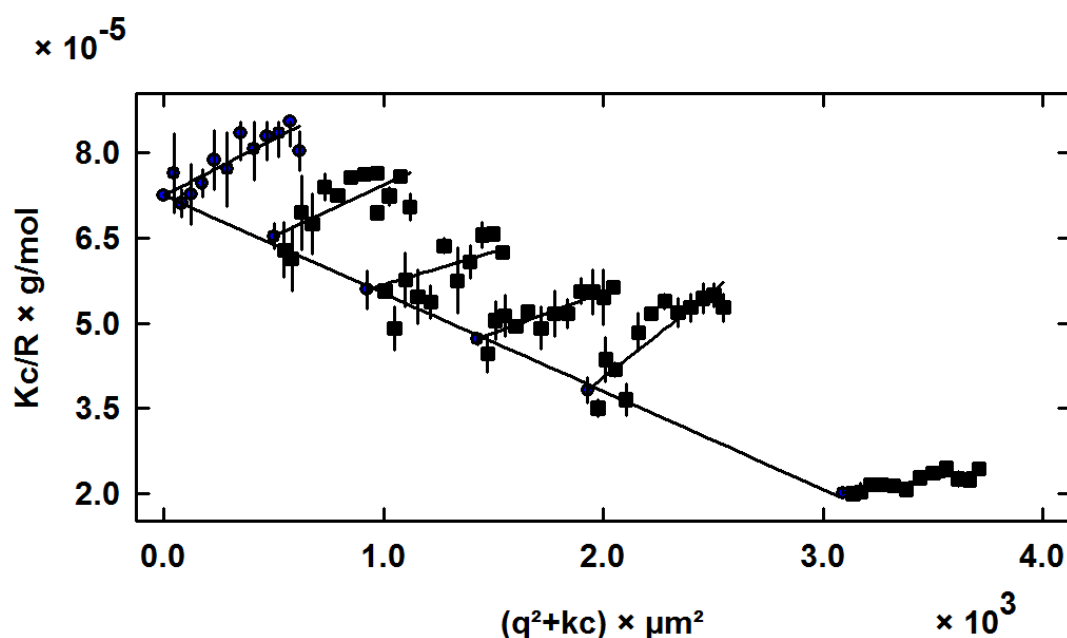


Figure 54. Zimm plot of a pMPAA dilution series in water

For pMPAA in water, the same phenomenon like for pNAM in water occurred. The second virial coefficient $A_2 = -8.5 \cdot 10^{-6} \text{ mol dm}^3 \text{ g}^{-2}$, determined by the slope of the linear regression in concentration direction within the Zimm plot, was negative. That implied, that pMPAA in water formed in almost the same manner no stable colloidal solution and led to aggregates. In comparison to the measurement of pNAM in water, the linear regressions in angle direction had positive slopes. Thus it was possible to calculate R_g and M_w , in an approximate way, because of aggregation. But from the

evaluation of the Zimm plot values for $R_g = 29 \text{ nm}$ ($\pm 10.3 \%$) and $M_w = 1.38 \cdot 10^4 \text{ g mol}^{-1}$ ($\pm 2.1 \%$) were obtained.

For the analysis of the shape of these pMPAA particles, it was not possible to obtain a Kratky plot, in a way, which was performed for pNAM in water. **Figure 55** shows Kratky plots for the whole dilution series as well as for particular concentrations.

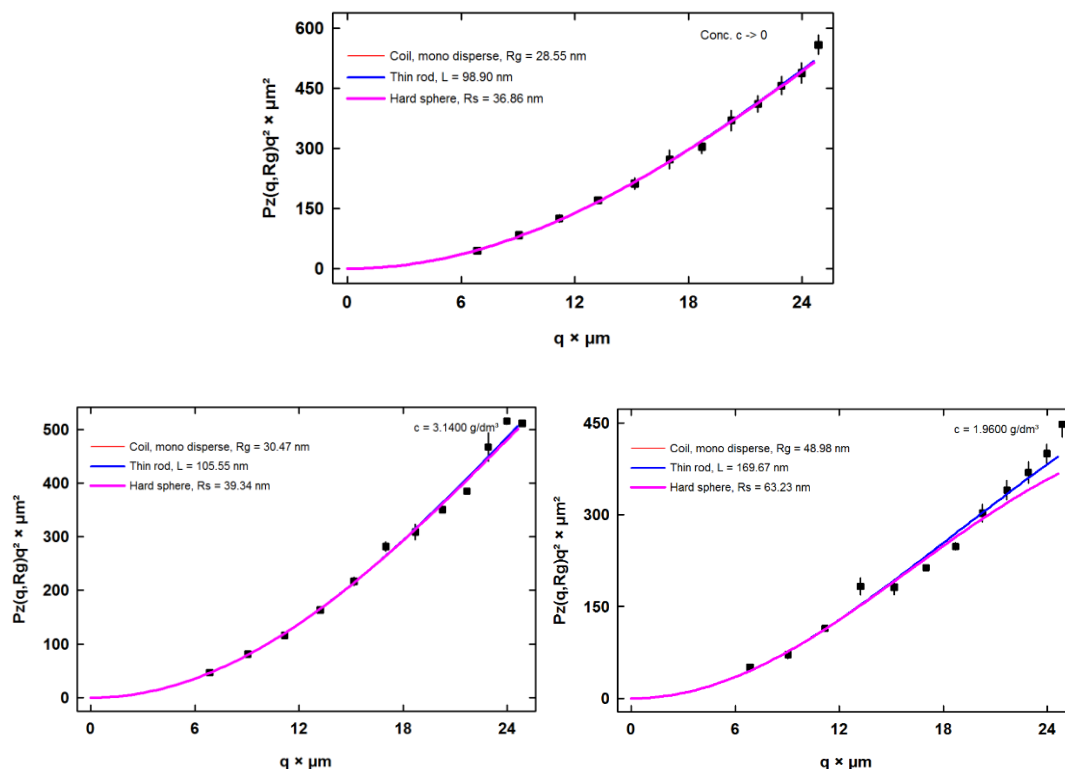


Figure 55. Kratky plots for pMPAA in water; whole dilution series $c \rightarrow 0$ (top); single measurement $c = 3 \text{ mg mL}^{-1}$ (left); single measurement $c = 2 \text{ mg mL}^{-1}$ (right)

In comparison to the pNAM particles in water from the previous measurements, the formed aggregates were too small to give proper structural information. What could be determined in a more precise way, was the ratio of R_g to R_H . The hydrodynamic radius could be determined via dynamic Zimm plot from the DLS measurement (**Figure 56**) and R_g could be determined by classic Zimm plot from the SLS measurement.

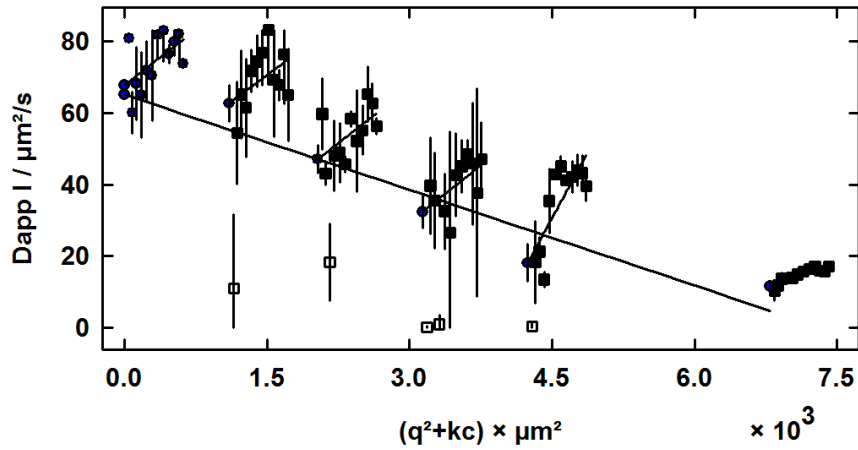


Figure 56. Dynamic Zimm plot of the dilution series of pMPAA in water

From these experiments, a ratio $R_g / R_H = 4.86$ was calculated, which confirmed the linear conformation of the polymer in solution.

4.6 SAXS analysis of pMPAA in water

SAXS measurement for pMPAA20k, the same as for the SLS/DLS analysis was used in a 6 mg mL^{-1} solution in milli-Q water. Also for pMPAA the Kholodenko worm-like structure fitted best with a variance of fit $9.7 \cdot 10^{-5}$ (**Figure 57** and **Figure 58**)

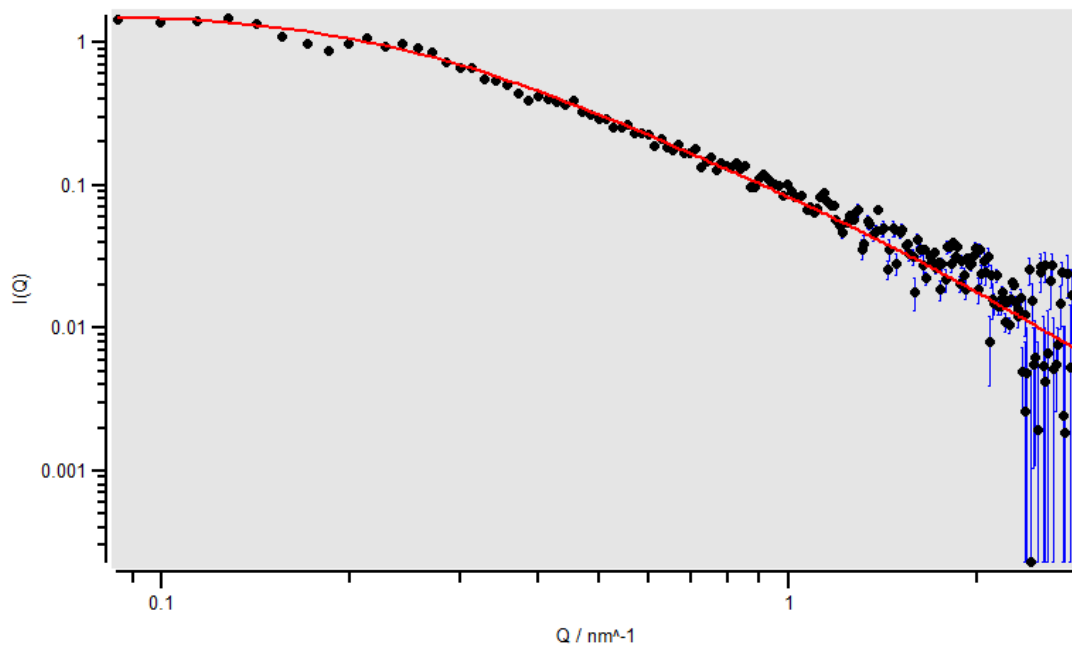


Figure 57. SAXS scattering image of pMPAA (6 mg mL^{-1}) in water; Kholodenko worm fit

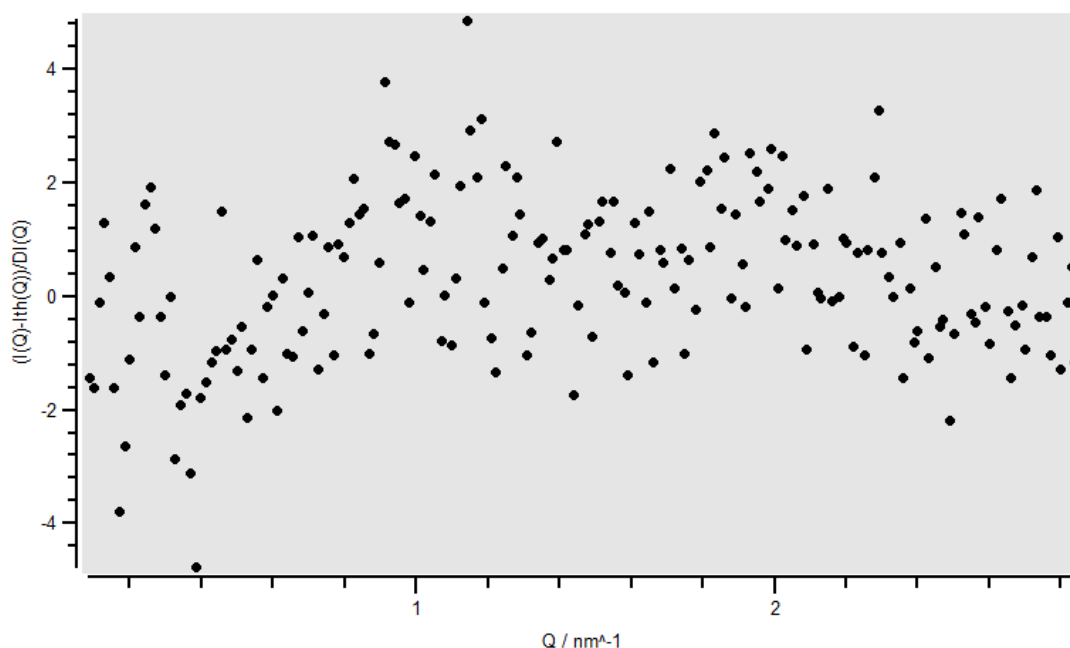


Figure 58. Distribution of the residuals; Kholodenko fit of pMPAA in water

4.7 SLS and DLS analysis of pMPAA in PBS buffer

For the measurement of pMPAA20k in PBS, again a dilution series from 0.5 – 3 mg mL⁻¹ was applied and here also a broad distributed scattering image, like for pNAM20k in PBS, was generated (**Figure 59**).

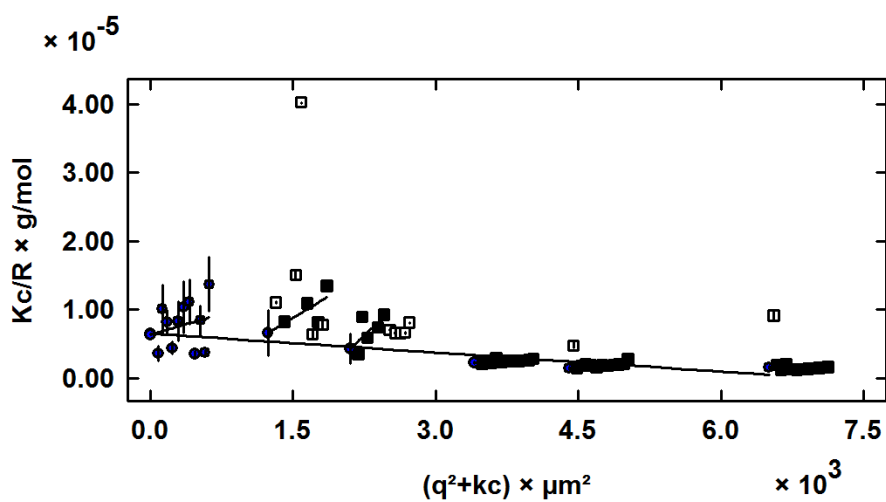


Figure 59. Zimm Plot of pMPAA in PBS

From the calculation via Zimm plot, the values $R_g = 43.5$ nm, and a negative $A_2 = -1 \cdot 10^{-6}$ mol dm³ g⁻² were generated, which again indicated aggregation in solution, but the second virial coefficient in water was 8.5 times lower than in PBS. To determine the shape of the particles, the Kratky plot gave no satisfying result, so the ratio of R_g / R_H of the measurement of $c = 2$ mg mL⁻¹ was used for an approximation (**Figure 60**).

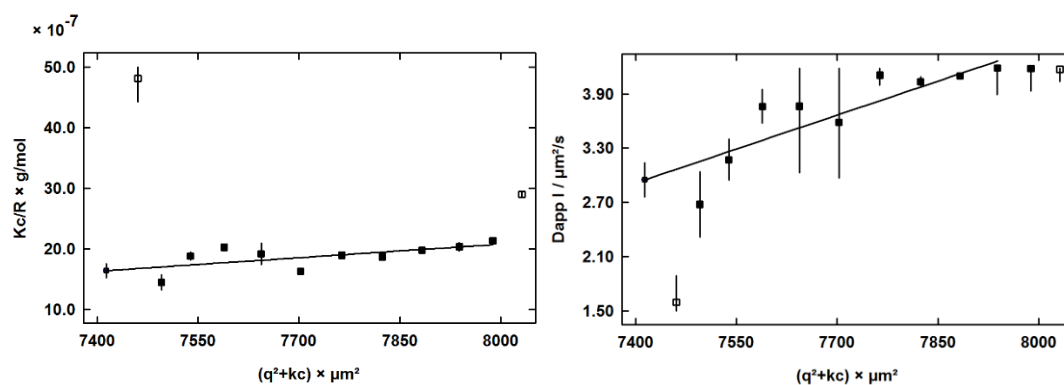


Figure 60; 2 mg pMPAA mL⁻¹ in PBS; Zimm plot (left); dynamic Zimm plot (right)

The calculated approximation of R_g / R_H was a value of 2.25, which indicates again a wormlike structure for the aggregates in solution. However, the SAXS experiment could give better information about this experiment.

4.8 SAXS analysis of pMPAA in PBS buffer

In the SAXS measurement for pMPAA20k, the same compound as for the SLS/DLS analysis was used in a 6 mg mL⁻¹ solution in PBS. Also for pMPAA the Kholodenko worm-like structure fitted best with a variance of fit of $2.2 \cdot 10^{-4}$ (**Figure 61** and **Figure 62**).

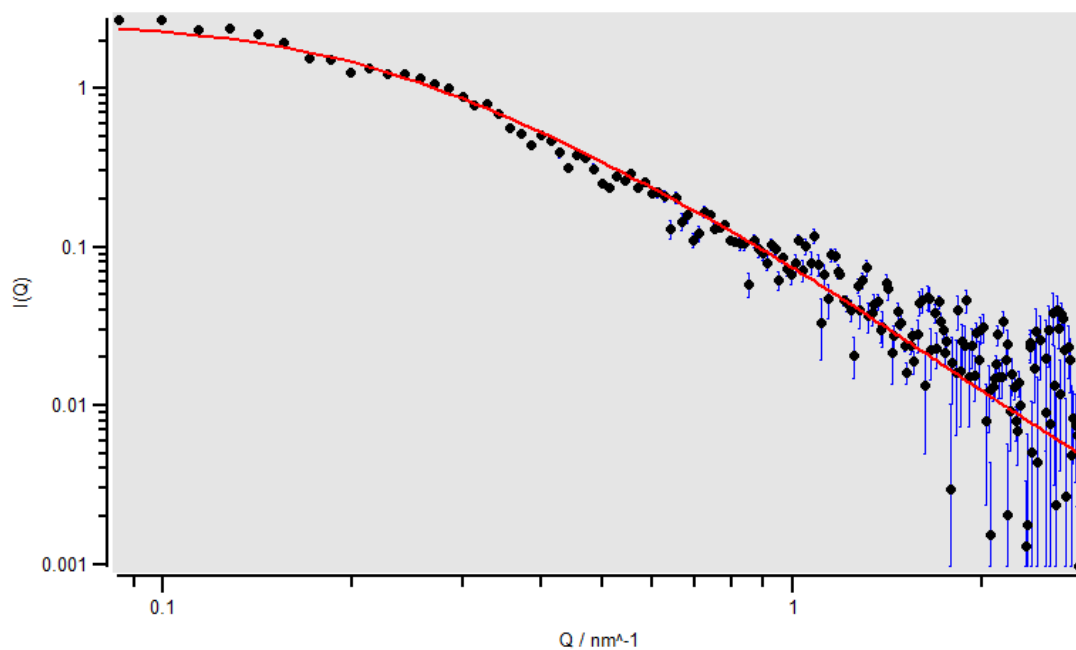


Figure 61. SAXS scattering image of pMPAA (6 mg mL^{-1}) in PBS; Kholodenko worm fit

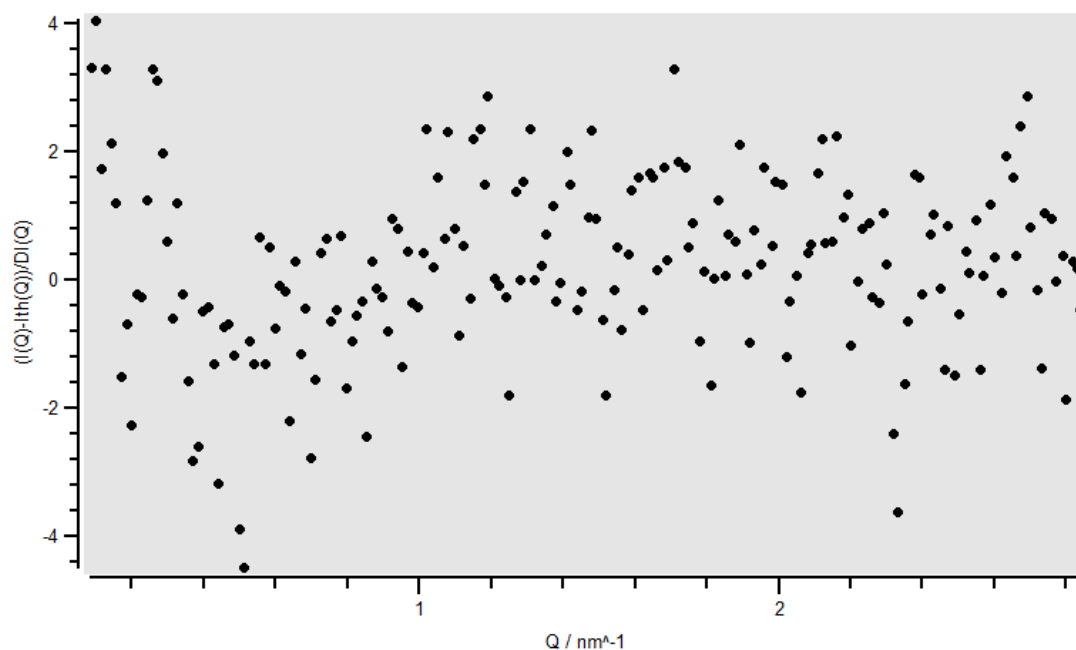


Figure 62. Distribution of the residuals; Kholodenko fit pMPAA in PBS

4.9 Summary of the results of the scattering analyses

Both acrylamides, pNAM and pMPAA, formed worm-like aggregates in aqueous solution, as confirmed by SLS, DLS and SAXS.

With respect to an application in polymer brush systems on surfaces, this could be a problem, if the polymerization of these monomers was carried out in water, with a RAFT reagent which is water soluble, due to the fact that the generated polymer would aggregate and the polymerization process would be inhibited. However, for the application of polymer brushes, these two polyacrylamides might give an interesting structure. Due to the fact of linear aggregation, they might form polymer bundles. **Figure 63** displays an assumption how this polymer brush system could look like.

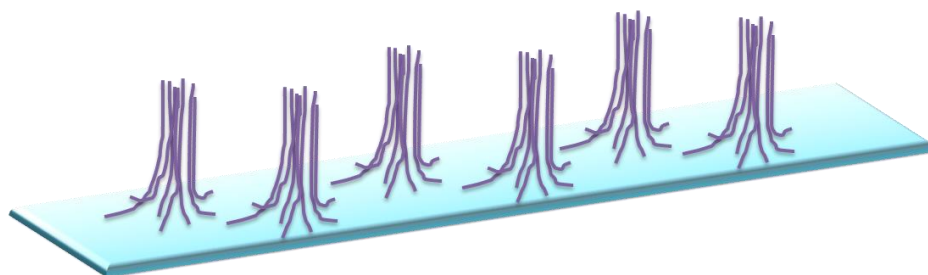
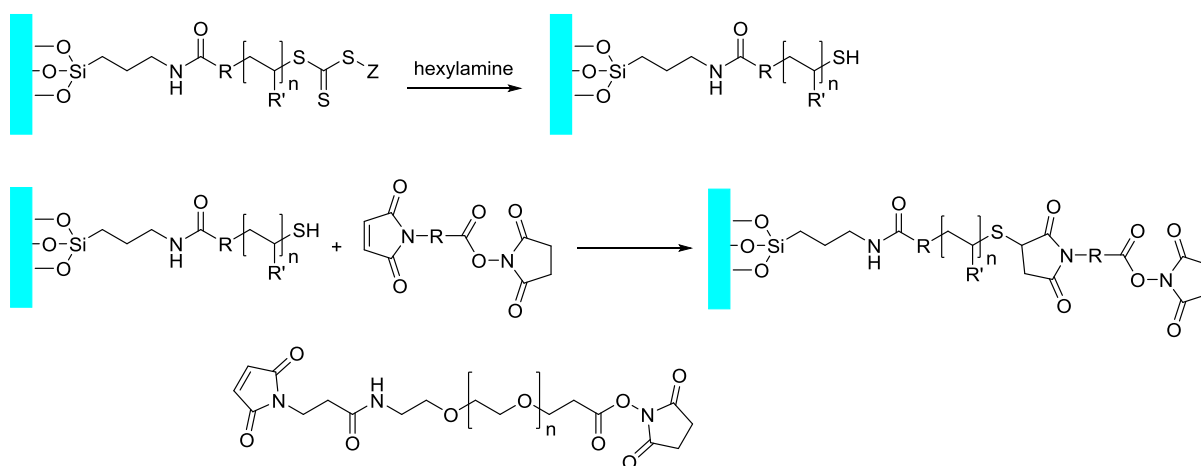


Figure 63. Assumption of the structure of pNAM/pMPAA on surfaces in aqueous environment

After the establishing of this system, measurements with atomic force spectroscopy (AFM) on- or SAXS through the glass surface, as well as computational simulations could give information validation of this assumption.

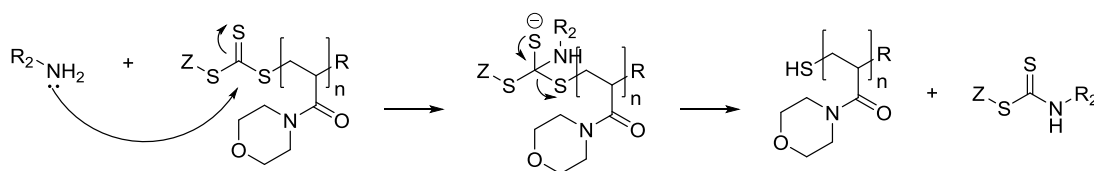
5 Modification of end groups

Since the structural experiments of these polyacrylamides were completed, the next step for the formation of the intended interface could be planned. After generating of the RAFT polymer itself, which was investigated in chapter 3, there are several ways to modify the end group of a RAFT polymer as discussed in the introduction chapter 1.3.4. Due to interest in maleimide click-chemistry, the modification to a thiol end group should be tried out first (**Scheme 28**).



Scheme 28. Aminolysis and maleimide click reaction with the linker

The first approach was an aminolysis reaction of the trithiocarbonyl moiety. Through an aminolysis reaction with hexylamine, the thiocarbonylthio group at the end of the polymer will be attacked nucleophilic by the lone electron pair of the amine⁸⁴ (**Scheme 29**).

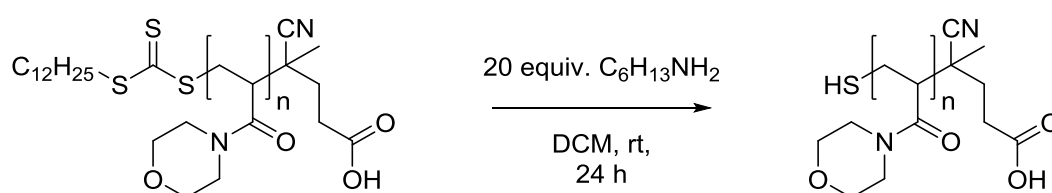


Scheme 29. Aminolysis of pNAM with trithiocarbonyl group

First, low molecular weight polymers of the four available combinations should be synthesized by RAFT polymerization. The chosen theoretical polymerization degree for these compounds was 10 monomer units. The low molecular weight might be favorable for the monitoring of the aminolysis reaction, because the trithio group shows an absorption at 410 nm wavelength and could be analyzed by UV/VIS spectroscopy. Higher molecular weight of the polymers would require higher sample amounts and possibly disturb the measurement.

5.1 Aminolysis induced end group formation to thiol groups

As mentioned before maleimide-click chemistry is a good and quantitative coupling method, aminolysis end-group formation was applied first, to obtain free thiol groups for the implementation of this coupling reaction.



Scheme 30. Aminolysis of CDTPA-pNAM

For these reactions, 1 equiv. of the polymer (CDTPA -pNAM2k, -pMPAA2k / DDMAT -pNAM2k, -pMPAA2k) was dissolved in dichloromethane (DCM) and degassed with argon. 20 equiv. of hexylamine was added dropwise, and stirred for 24 h at room temperature⁷⁶. Afterwards, the polymer was precipitated in petrol ether (PE) and dried under vacuum. During the drying step, the viscous polymer changed its color from transparent to dark yellow. Traces of amine contaminated the polymer and were presumably oxidized. So the crude product was purified again by precipitation in PE, but it was not possible to remove the amine quantitatively and the color changed again, although the product was stored under vacuum or argon atmosphere. This problem occurred for every polymer (pNAM2k, pMPAA2k) respectively. So the purification of the aminolysis product would have to be done by dialysis, to get rid of the amine. This would be no problem, in the scenario of brushes, because it is possible to just rinse the surface with the proper solvent. However, another difficulty occurred in parallel,

namely the formation of disulfide bonds. By contact with oxygen, the polymers with thiol end groups immediately formed disulfide bonds with another end-capped polymer, which could be characterized by a double peak in the SEC eluogram (**Figure 64**).

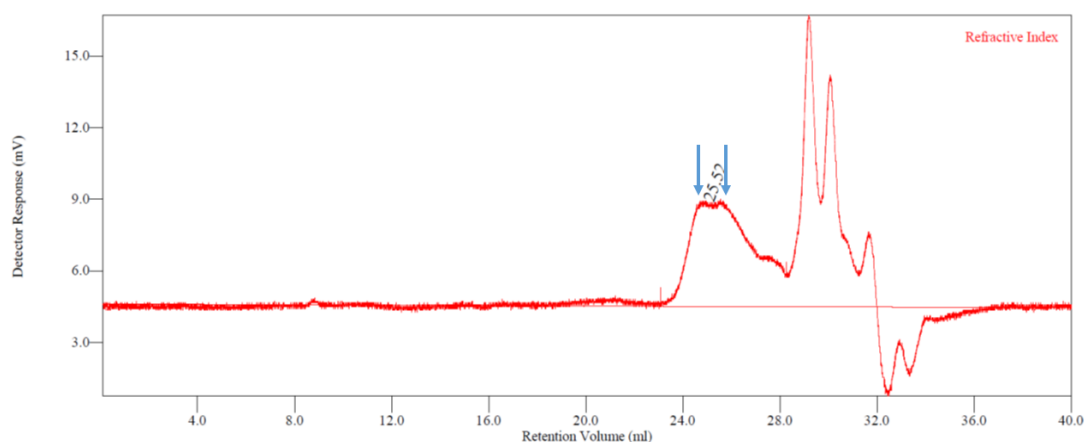
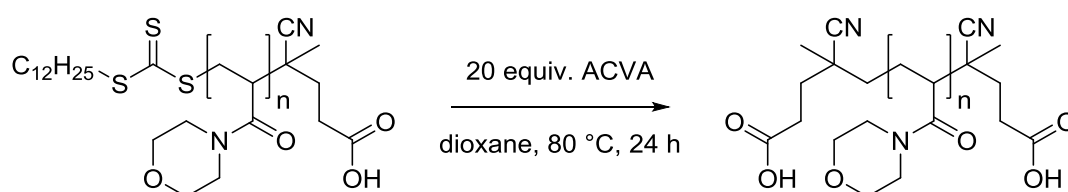


Figure 64. Eluogram (THF) of the aminolysis attempt

This “crosslinking” exhibited a bigger problem for the polymer brush system with end functionality. Although there are common methods for disulfide bond reduction, there have to be considered some drawbacks. As the intended interface, should be biocompatible, the classic way to reduce the disulfide bonds with zinc in acetic acid does not even enter the equation. Zinc, which could remain in too high concentrations within the generated brushes, is able to inhibit cell mechanisms or is even toxic for them⁸⁵. To overcome this problem there are few prospects; working under argon atmosphere, like in an argon glovebox, but not everybody owns such systems. Another prospect is the usage of biocompatible reducing agents like tris(2-carboxyethyl)phosphine (TCEP)⁸⁶, or the direct implementation of a click-chemistry reagent with the free thiol group, during the aminolysis reaction. Due to the problems with handling this end group modification pathway, another, more convenient pathway was examined.

5.2 Radical induced end group formation with 4, 4'-azobis (4-cyanovaleric acid) (ACVA)

Another possibility for end-group modification in RAFT polymers according to literature⁷⁶ is the use of a high excess of functional azo initiator. For this attempt, first polymers of NAM and MPAA with 10 kDa were synthesized with CDTPA (pNAM10k, pMPAA10k) and 1 equiv. of these polymers was dissolved in dioxane and 20 equiv. ACVA was added. This mixture was heated up to 80 °C for a time of 24 h under argon atmosphere (**Scheme 31**)⁸⁷.



Scheme 31. Radical induced end group modification of CDTPA-pNAM with ACVA

Attenuated total reflection (ATR) infrared spectroscopy was attempted to analyze the end-group modified product, but showed no significant bands for the loss of the thiocarbonyl group. Therefore the reaction mixture was analyzed by UV/VIS spectroscopy, before and after the reaction, to depict the change in absorption, with constant concentration. As mentioned before, the thiocarbonylthio group showed an absorption spectra from 410 nm downwards in the UV range (**Figure 65**; black graph CDTPA-pNAM).

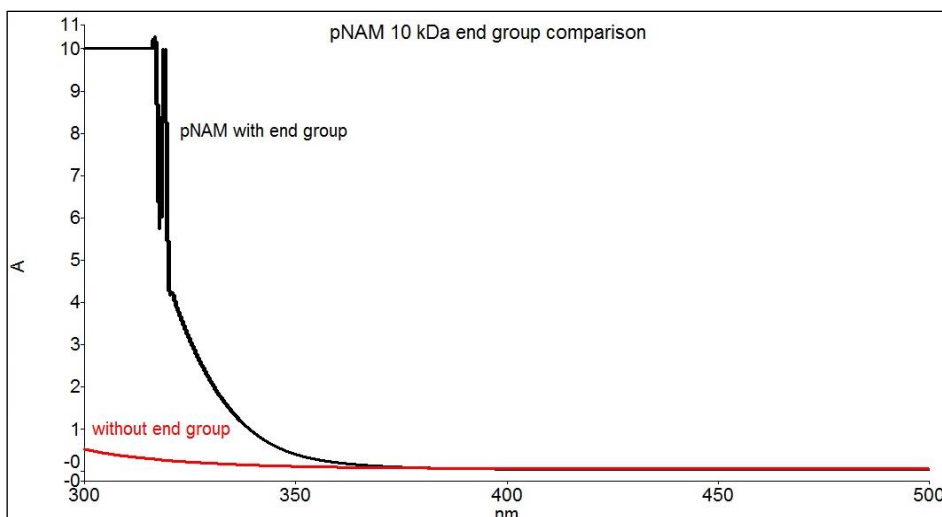


Figure 65. UV/Vis Spectra of pNAM 10 kDa with (black) and without (red) end group

After the reaction with pNAM10k (**Figure 65**; red graph)), nearly no absorption was left in the area of thiocarbonyl absorption. The reason for that, was the removal of the thiocarbonyl group. For the reaction with pMPAA10k a little lower concentration was chosen to have a better view in the spectra. It was obvious for the pMPAA polymer that the removal of the end group was not as quantitative as for the pNAM10k polymer (**Figure 66**), because there was still absorption visible in the UV-range. Subsequently for pMPAA the reaction time has to be increased, to get fully rid of the thiocarbonyl group.

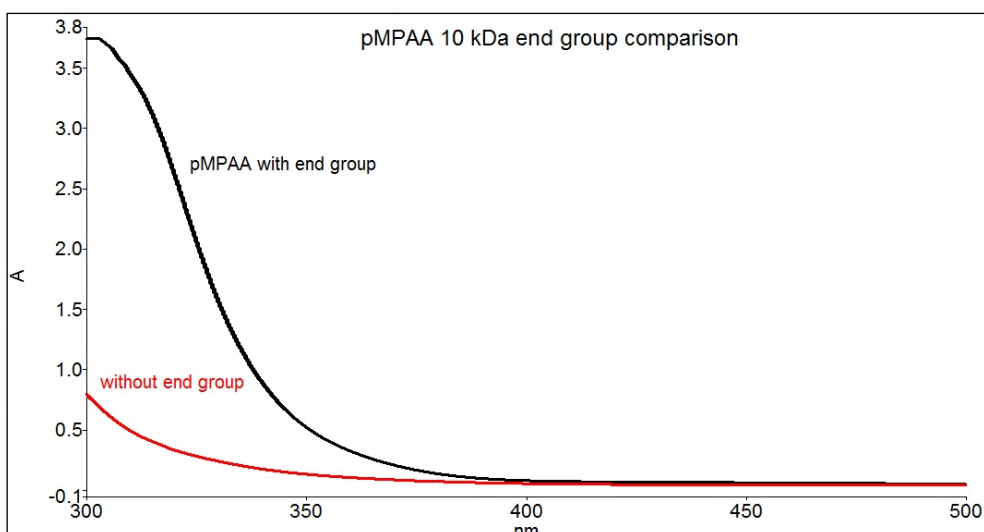
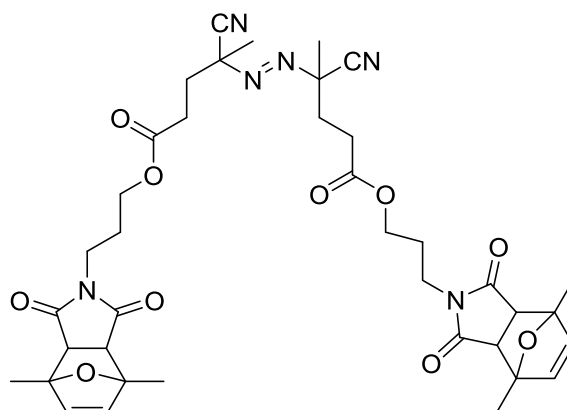


Figure 66. UV/Vis Spectra of pNAM 10 kDa with (black) and without (red) end group

As a positive aspect these polymers could be purified by precipitation again, and showed no traces of the used azoinitiator. These results made this end group transformation much more suited for further coupling reactions with biomolecules, compared to the previously described aminolysis attempt with zinc as reducing agent.

5.3 Summary of the results for end group modification

Two possibilities of end group formation were attempted for the use in the intended system, aminolysis and radical induced end-group formation. After the screening of the two mentioned methods, aminolysis was suspended from further use, as the free thiol was hard to handle, because of impurities of amine and probably even more, if the system is on a surface under oxygen, due to disulfide formation. The direct conversion of the free thiol by usage of maleimide click-chemistry could be possible, but due to the fact, that it is hard to handle, the functionalized surface might have to be treated with reducing agents in addition. The radical strategy showed good yields in a clean and easy way, and formed a stable end product. In a future experiment, the applied initiator, ACVA, could be modified with a protected maleimide functionality (**Scheme 32**) to substitute the need for a PEG-linker to the biomolecules that should be coupled to the polymer. ACVA has a half life time of $t_{1/2} = 10$ h at $65\text{ }^{\circ}\text{C}$ ⁸⁸ but the protecting groups will demerge at $120\text{ }^{\circ}\text{C}$ ⁷⁶; so this compound could initiate the end-group modification at $60\text{ }^{\circ}\text{C}$ and could be deprotected afterwards at higher temperatures.



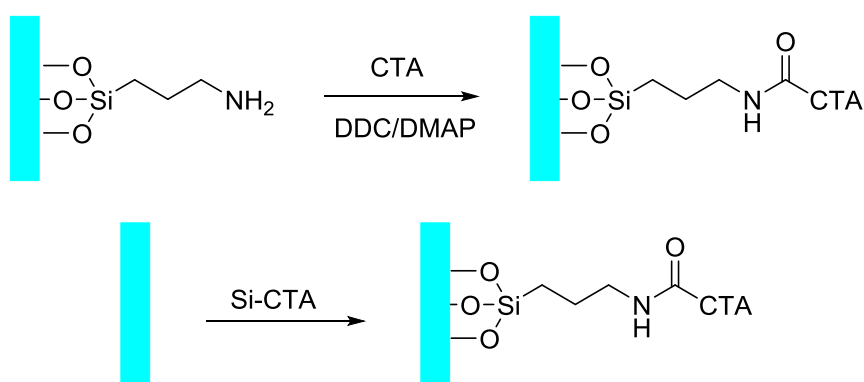
Scheme 32. ACVA functionalized with protected maleimide groups

By the deployment of this special designed thermal initiator, a linker compound could be displaced and the synthesis pathway is shortened by one step. Respectively, there are numerous initiators commercially available, so the end user could choose his/her end group by using the right initiator.

Hereby, a good pathway for end-group modification was established. The next step should be the investigation for coupling of the used RAFT reagents to the glass surface. For this attempt alkoxysilanes were chosen as starting material, and were attempted to couple with the RAFT reagents.

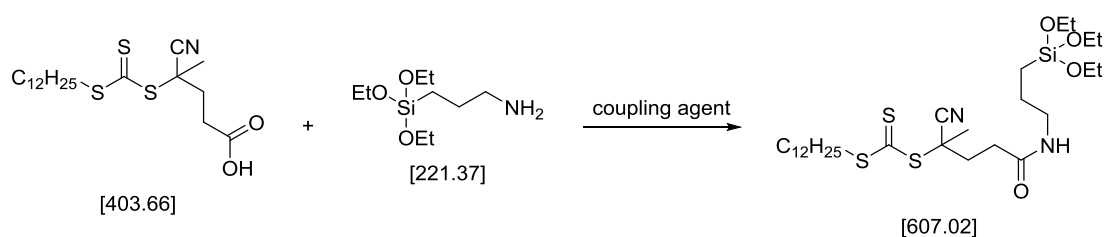
6 Synthesis of a RAFT reagent with an ethoxysilane end group

After the characterization of the free polymer in solution indicated a suitable worm-like and probably pillar-forming structure of pNAM and pMPAA in aqueous solution, the synthesis of the brush systems on glass surfaces should be investigated. In this context 2 strategies were applicable: First, coupling of a RAFT reagent with an alkoxysilane group directly to the surface or second, by coupling of the RAFT reagent to functional groups on the surface (**Scheme 33**).



Scheme 33. Immobilization approaches, prefunctionalization by APTES (top); direct functionalization with Si-CCTA (bottom)

For the direct attempt, a RAFT reagent had to be synthesized, which was able to form covalent bonds to a glass surface. For this experiment, an amide bond coupling of CDTPA and DDMAT to APTES was planned (**Scheme 34**). Literature showed examples of this coupling method, APTES to RAFT reagents with carboxylic acid end-groups, as well.^{20, 71}



Scheme 34. Amide coupling of CDTPA to APTES

For this reaction, the coupling reagents N,N'-dicyclohexylcarbodiimide (DCC) with or without 4-dimethylaminopyridine (DMAP) and EDC were tested.

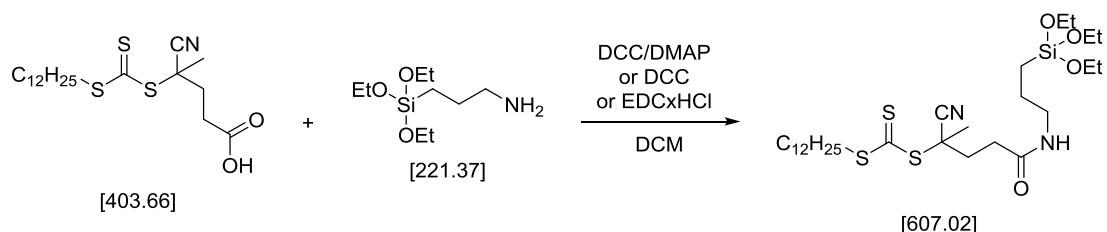
Another alternative was the coupling with alkoxy silane glycidylester, due to the fact, that these compounds and also already epoxytated glass cover slips are commercially available (**Scheme 35**).



Scheme 35. Epoxy – carboxylic acid coupling

First, the coupling with APTES was performed, according to literature of Isahak et.al.⁷¹

6.1 Screening for a suitable synthesis of 2-cyano-5-oxo-5-((3-(triethoxysilyl)propyl)amino)pentan-2-yl dodecyl carbonotrithioate (Si-CDTPA).



Scheme 36. Synthesis of Si-CDTPA via different coupling reagents

For the first synthesis of Si-CDTPA, using DCC/DMAP as coupling reagents, CDTPA was reacted with DCC/DMAP in slight excess of the catalyst. After stirring under cooling APTES was added and stirring was continued for 16 h at rt⁷¹. After purification by column chromatography the crude product was isolated in 15 % yield. The reason for the low yield might be hydrolyzation of Si-CDTPA during the chromatography and the products were attached to the silica surface. After purification by flash column chromatography, the integrals of the ¹H-NMR did not fit together for the target compound (**Figure 67**).

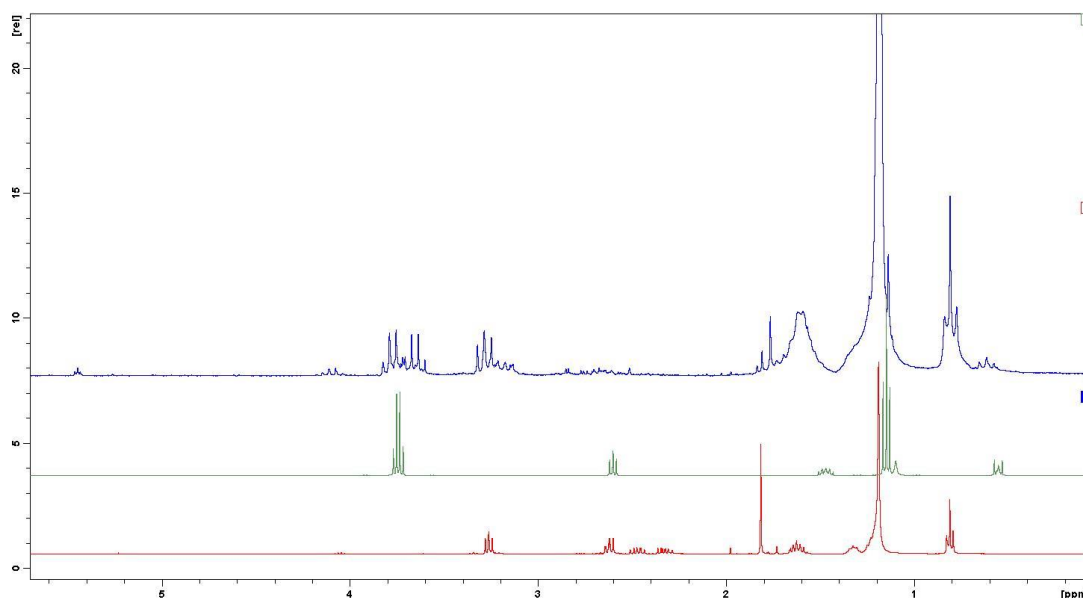


Figure 67. $^1\text{H-NMR}$ comparison of the crude product of the synthesis of Si-CDTPA (DCC/DMAP); CDTPA (red; 400 MHz), APTES (green; 400 MHz), product (blue; 200 MHz)

Some of the expected signals were visible there, like the amide bond signal at 5.51 δ ppm, or had shifted, but also signals of the RAFT reagent became lower, in terms of the cyanovaleric part of the compound, which could be explained, by simultaneous aminolysis of the reagent through APTES. Because it was also not possible to determine the loss of the real product by chromatography this reaction was repeated and hereafter used in crude for subsequent surface modification of the glass slides, without further purification.

This was the first tryout with CDTPA, but to overcome the problem of simultaneous aminolysis of the RAFT reagent, a screening with abstinence of DMAP and only using DCC and EDC as coupling reagents was applied. The next attempt was the use of DCC as coupling reagent.

For all the following screening reactions, very small scales (≈ 15 mg product) were applied, to just monitor the reaction by $^1\text{H-NMR}$. For this synthesis CDTPA was dissolved in dry DCM, molecular sieve was added and cooled, DCC dissolved in DCM was added and stirred for 15 min. APTES was then added to the mixture and then stirred for 1 h at room temperature. A TLC showed a new UV-active spot from the reaction solution. The solvent was removed under reduced pressure and the reaction

mixture was filtrated over silica. The solvent was removed again, and an $^1\text{H-NMR}$ was measured from this mixture (**Figure 68**).

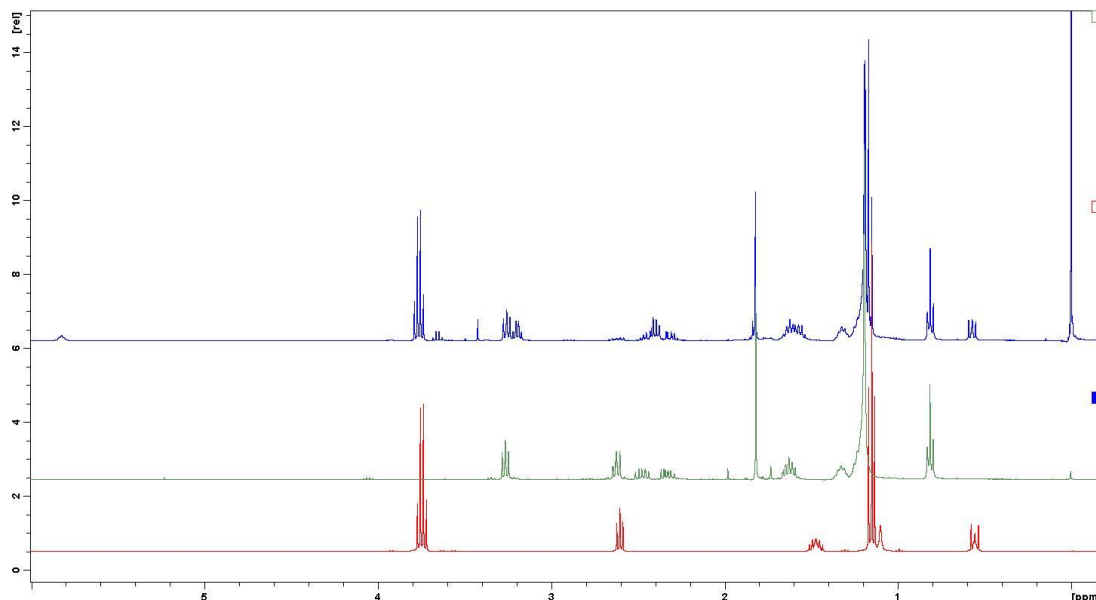


Figure 68. $^1\text{H-NMR}$ of Si-CDTPA (DCC); APTES (red), CDTPA (green); Si-CDTPA crude spectra (blue)

Here again some of the $-\text{CH}_2-$ signals of APTES shifted, an amide peak was visible at 5.89 δ ppm and the amine peak at 1.17 δ ppm vanished, which gave information that the target compound could be in the mixture. But the integrals also did not fit to the pure compound. So another attempt was applied using EDC as coupling reagent.

For this attempt, the procedure was the same as the one mentioned before, except of the use of 1 equiv. of EDCxHCl instead of DCC. TLC showed a new UV active spot as well. So the mixture was filtrated over a 100 mg silica column with PE:EE = 1:1 and after the removal of the solvent under reduced pressure, an $^1\text{H-NMR}$ was taken from the mixture (**Figure 69**)

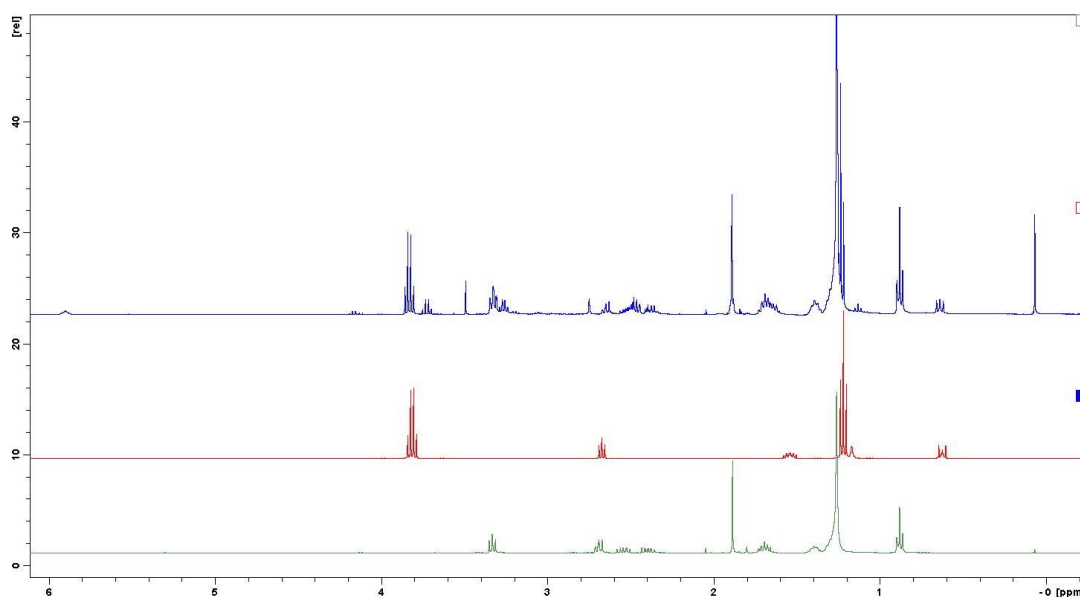


Figure 69. $^1\text{H-NMR}$ of Si-CDTPA (EDC); APTES (red), CDTPA (green); Si-CDTPA crude spectra (blue)

The interpretation of the spectra equals the one of the attempt using DCC. **Figure 70** shows an overlay of these two $^1\text{H-NMR}$ spectra, and shows that the outcome is nearly identical.

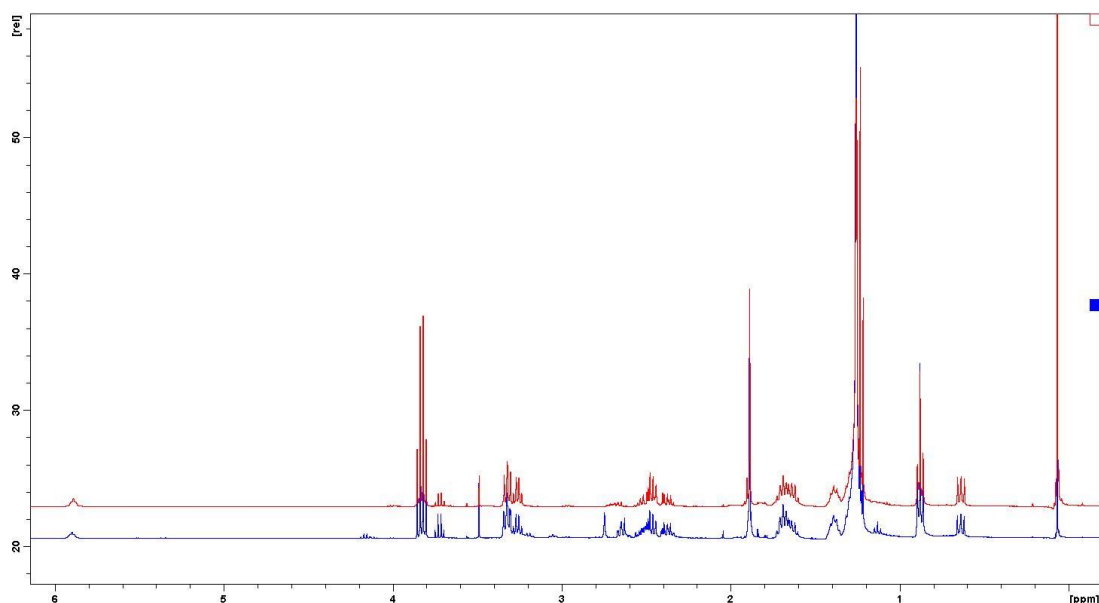
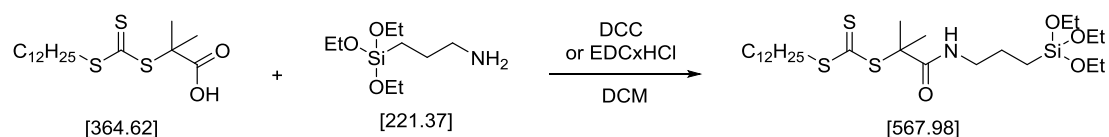


Figure 70. Comparison of the $^1\text{H-NMR}$ spectra of the DCC (red) and EDC (blue) attempt for Si-CDTPA

To conclude, it was not possible, to determine the better synthetic route by these three different coupling attempts. Due to the fact that it was not possible to separate or purify the product by common methods, like liquid column chromatography or distillation, these mixtures were used crude for subsequent surface modifications, as it was also indicated in literature²⁰. The benchmark of which method had worked out better, was done partially by functionalization of a SiO₂ surface and characterization via XPS measurement.

6.2 Screening for a synthesis of dodecyl (2-methyl-1-oxo-1-((3-(triethoxysilyl)propyl)amino)propan-2-yl) carbonotrithioate (Si-DDMAT)



Scheme 37. Synthesis of Si-DDMAT via different coupling reagents

The first coupling attempt was applied by the use of DCC as coupling reagent. DDMAT was dissolved in dry DCM, under argon atmosphere, with molecular sieve within the solution. DCC dissolved in dry DCM was added under cooling and stirred for 15 min. Then APTES was added and stirred for 1 h. TLC showed a new possible UV-active product spot. Afterwards the solvent was removed under reduced pressure and the crude mixture was filtered over silica. Subsequently the solvent was removed again under vacuum, and an ¹H-NMR was measured (**Figure 71**).

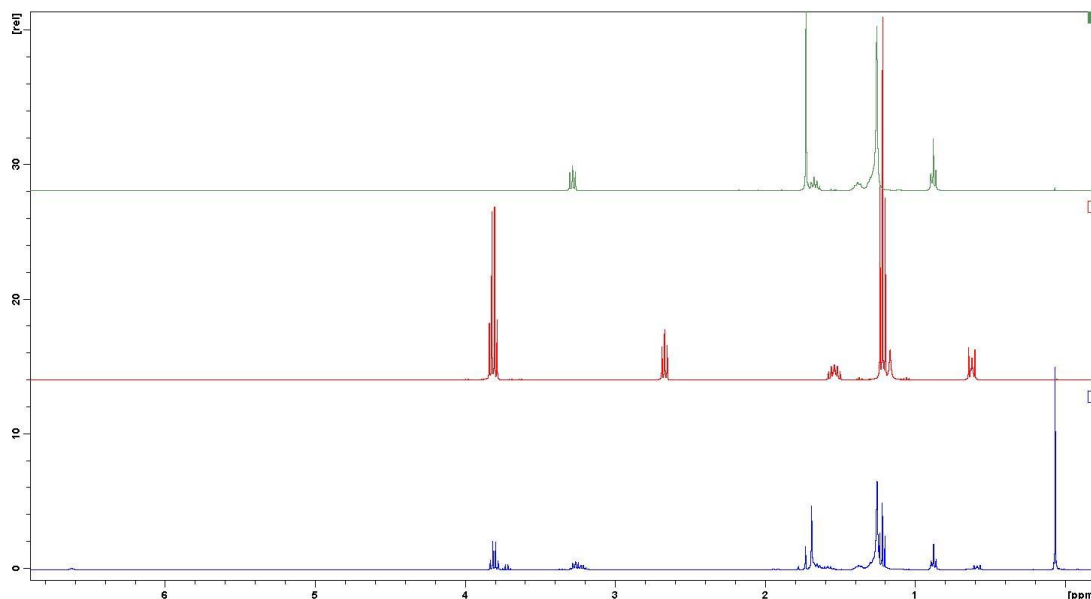


Figure 71. $^1\text{H-NMR}$ of Si-DDMAT (DCC); APTES (red), DDMAT (green); Si-DDMAT crude spectra (blue)

One could see from the $^1\text{H-NMR}$, that an amide peak exists at 6.62 δ ppm and the peak from the $-\text{CH}_3$ group at 1.69 δ ppm (nearest ^1H -signal to the newly formed amide group), shifts from the original DDMAT spectrum, the $-\text{CH}_2-$ signals from the propyl group of APTES shifted too, and the amine signal vanished. However, although the signal shifts looked promising, the integral values from $^1\text{H-NMR}$ did not fit properly for the target Si-CTA after chromatography. Column chromatography seemed to be a too destructive method for purification.

Also an attempt for the coupling via EDCxHCl was applied, for this screening experiment. The synthesis method was according to the on mentioned before, except of usage of 1 equiv. EDCxHCl except of DCC. After stirring for 1 h, TLC showed a new possible product spot at the same location as for the previous experiment, and the product mixture was, after removal of the solvent under reduced pressure, filtered over 100 mg silica in PE:EE = 1:1. The solvent was evaporated again, and $^1\text{H-NMR}$ was measured (**Figure 72**).

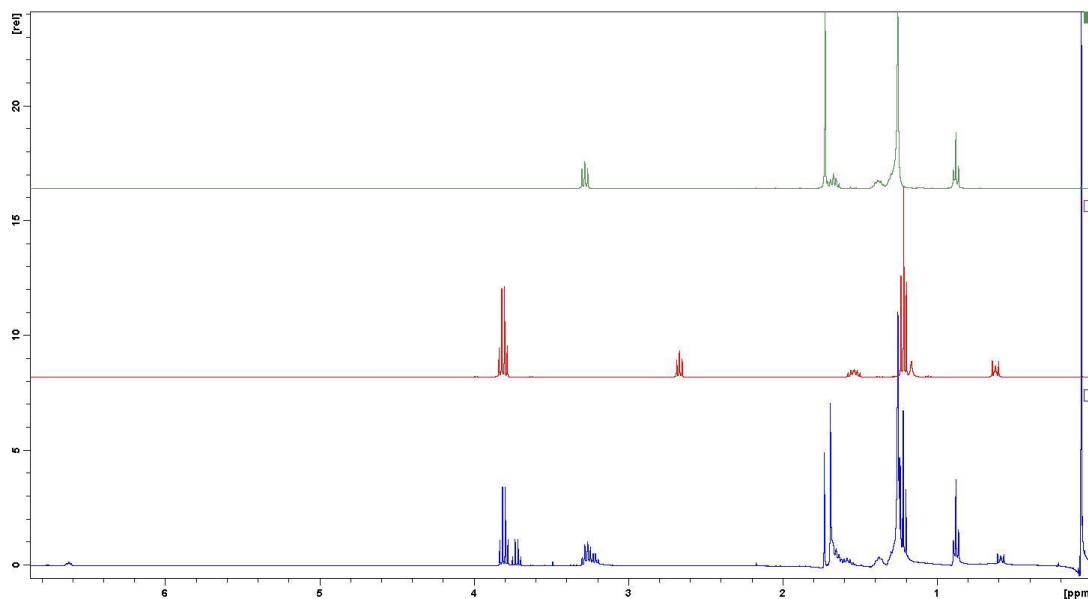


Figure 72. $^1\text{H-NMR}$ of Si-DDMAT (DCC); APTES (red), DDMAT (green); Si-DDMAT crude spectra (blue)

For the evaluation of the spectrum of this synthetic pathway, the same signal composition as from the method before was obtained, still without integral fit to a pure product. This could be seen in the overlay of both spectra in **Figure 73**.

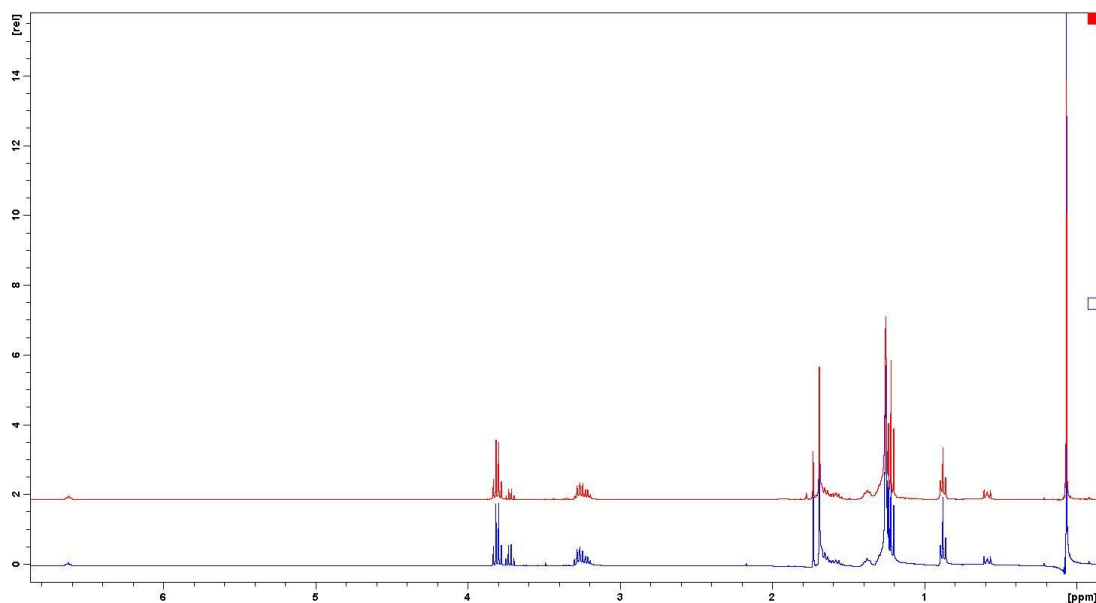
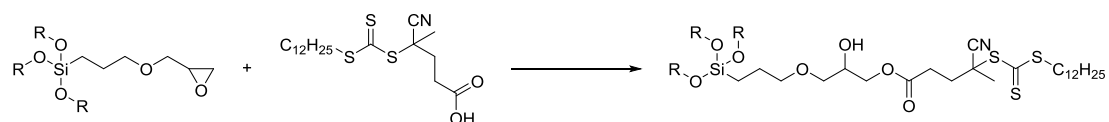


Figure 73. Comparison of the $^1\text{H-NMR}$ spectra of the DCC (red) and EDC (blue) attempt for Si-DDMAT

To conclude, in case of the DCC and EDC coupling method, it was also not possible, to determine the better synthetic route by these analyses. The benchmark of which method had worked out better, was done partial by functionalization of a SiO₂ surface and characterization via XPS measurement.

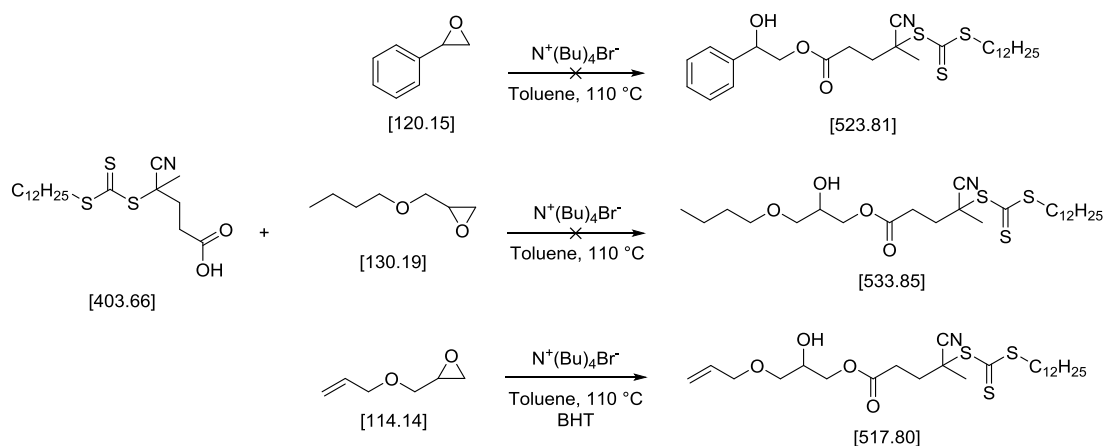
6.3 Screening for alternative coupling methods

As the coupling of the CTAs to an amino-functionalized silane did not work out properly, alternative methods using for example an epoxy containing silane examined.



Scheme 38. Epoxy – carboxylic acid coupling

Due to the fact, that there were some glycidylester and epoxy compounds with alkoxy-silane functionalities commercially available, a screening with dummy compounds without alkoxy-silane group was applied first, to do research on their coupling ability. The screening was performed with CDTPA and with an aromatic epoxide, an aliphatic glycidylester and an olefinic glycidylester (**Scheme 39**).



Scheme 39. Epoxy – carboxylic reactions of CDTPA with styrene oxide (top), an aliphatic (middle) and an olefinic glycidylester (bottom)

According to Kim et al⁸⁹., for the synthesis with styrene oxide, the epoxide and a slight excess of CDTPA was dissolved in toluene and 5 mol% of tetrabutylammonium bromide was added as catalyst. The mixture was heated to 110 °C for 5 h. The reaction mixture was worked up and separated via liquid column chromatography and the obtained fractions were analyzed by ¹H-NMR.

Unfortunately, the desired target product could not be obtained by this method. Maybe different catalysts or reaction temperatures are needed, so further research was quitted.

For the synthesis with 2-(butoxymethyl)oxirane, the reaction procedure was equivalent to the synthesis before, except of the use of 1 equiv. of 2-(butoxymethyl)oxirane instead of styrene oxide. After 5 h reaction time the reaction mixture was worked up and separated via liquid column chromatography and every collected fraction (monitored by TLC) was analyzed by ¹H-NMR respectively.

But the requested compound could not be identified within these collected fractions analyzed by ¹H-NMR. So this attempt was not pursued further more.

For the synthesis pathway with Allyl glycidyl ether, the synthetic procedure was the same as before, except of the use of 1 equiv. of 2-((allyloxy)methyl)oxirane and also 5 mol% of butylated hydroxytoluene (BHT) to stabilize the allylic group. After a reaction time of 5 h the mixture was worked up und monitored in the same way mentioned before. The product mixture could not be separated completely from CDTPA, but from the mixture ¹H-NMR, the yield could be calculated (**Figure 74**)

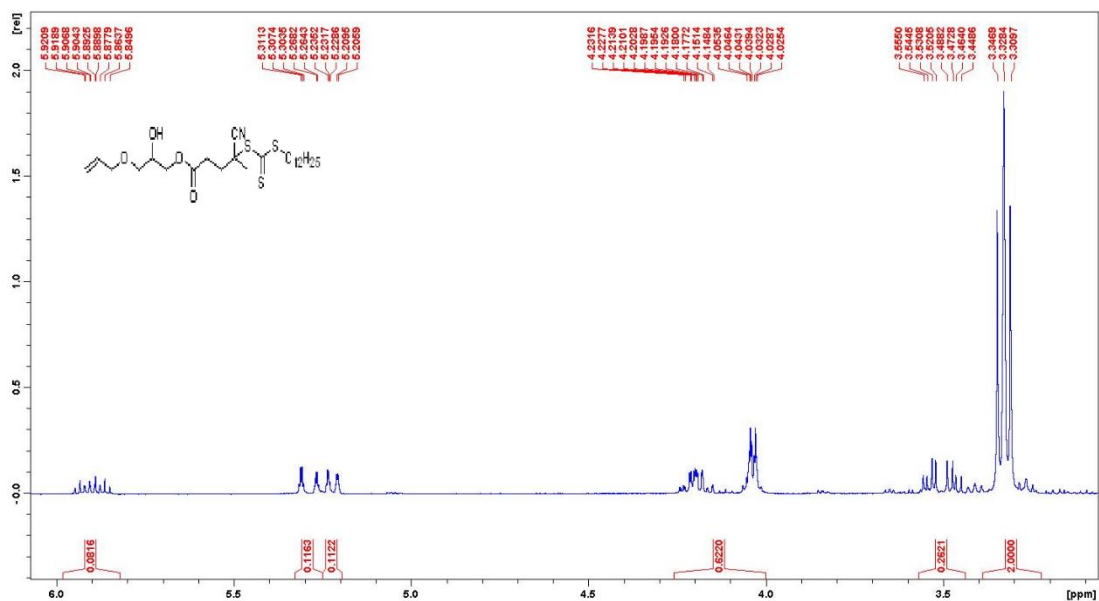


Figure 74; ¹H-NMR calculation of the epoxide conversion

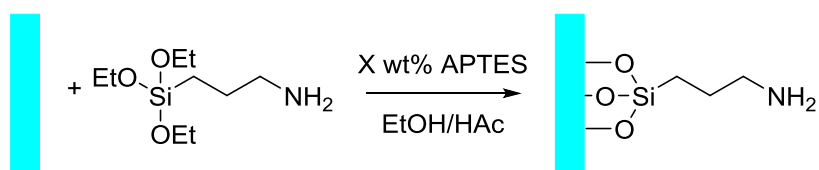
The relation of the integrals for the olefinic signals and for the opened epoxides fitted well and the signal of a duplet of duplets for the two terminal olephinic hydrogens signal at 5.25 δ ppm was set in ratio to the t signal of the –CH₂-S- signal at 3.33 δ ppm which resulted in 11.4 % yield calculated by ¹H-NMR.

In this case the reaction worked out, but in very small yields. However, after optimization with a better catalyst⁸⁹, this method might give a prospective chance for the preparation of a surface linker for the CTA.

Up to now, the Si-CTA could not be purified by common methods and have to be used in crude, but before their application on substrate, the conditions for the surface functionalization should be investigated by the simple modification of glass surfaces with APTES alone.

7 Analysis of coating homogeneity using APTES for functionalization of glass surfaces

For the first attempts to functionalize glass surfaces, with any alkoxy silane reagents, a screening was applied by the use of APTES for the coupling reaction on the SiO₂ surface. For this experiment, 3 wt%, 4 wt% and 5 wt% of APTES in a solution of Ethanol (EtOH) and 1:10 diluted acetic acid (HAc) in a ratio of EtOH:HAc_{diluted} = 97:3 were prepared.⁹⁰



Scheme 40. Functionalization of glass with APTES

The glass cover slips were first cleaned in toluene, acetone and water under supersonification. Then they were activated by piranha acid (H₂SO_{4conc.} : H₂O₂ (30 %) = 7:3) at 80 °C for a time 1 h, rinsed with water and ethanol, dipped into the APTES solution for a time of 24 h under shaking, argon atmosphere and room temperature. After this reaction time, the samples were taken out of the solution, rinsed with EtOH and acetone, and subsequently dried by an argon stream. These samples were stored under argon until further analysis.

For the determination of the coating homogeneity, the first analysis was the identification of the static and dynamic contact angles. For this measurement a water droplet of 15 μL was deposited on the surface and monitored by a goniometer. The static contact angle (CA) was determined first and afterwards the platform of specimen holder was tilted until the rolling of the droplet. **Figure 75** shows the contact angles of unmodified glass, **Figure 76** and **Figure 77** the CAs of the samples prepared with 3 and 5 %wt APTES.

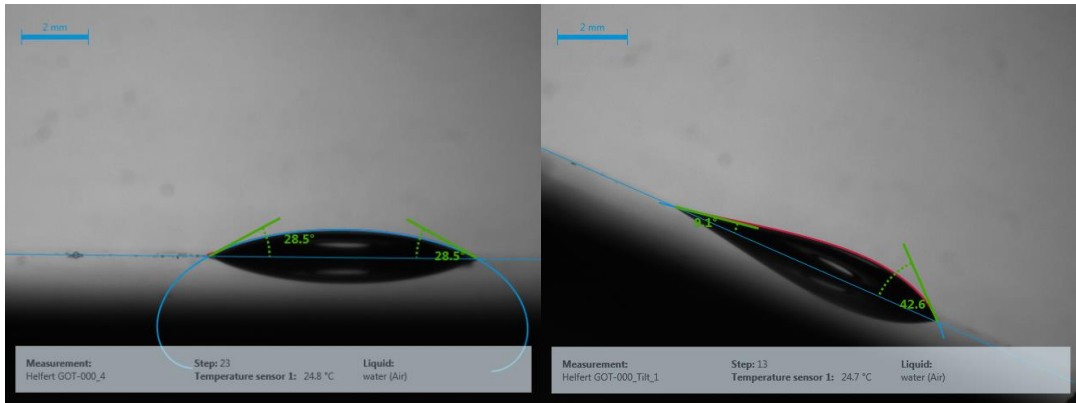


Figure 75. Static CA of unmodified glass (left); dynamic CA (right)

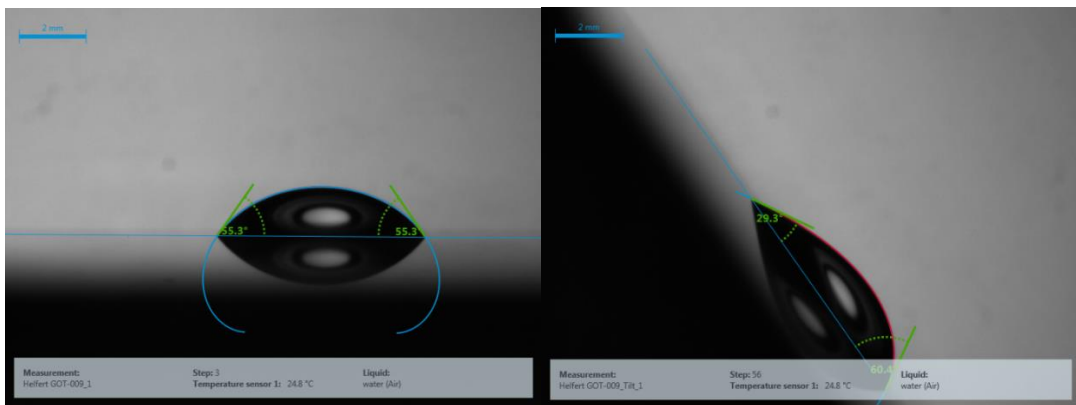


Figure 76. Static CA of APTES functionalized glass (3 wt%) (left); dynamic CA (right)

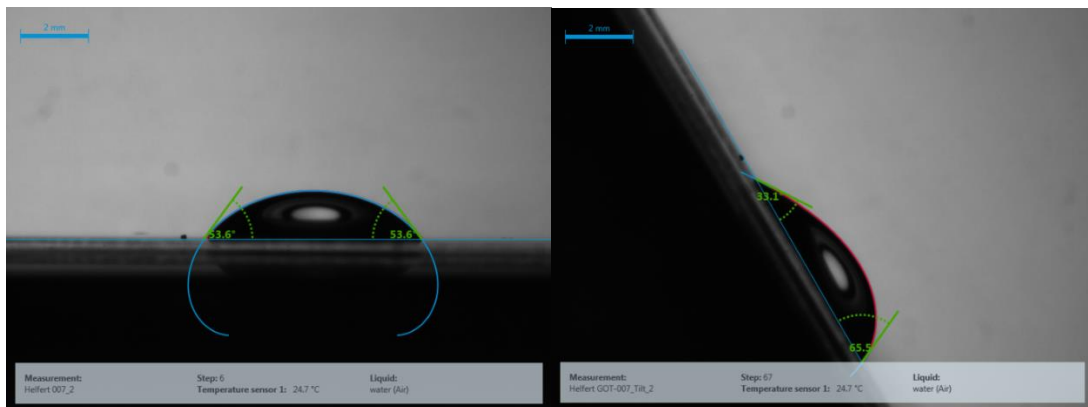


Figure 77. Static CA of APTES functionalized glass (5 wt%) (left); dynamic CA (right)

Table 2. CA measurement of glass and APTES functionalization

Sample	Static CA [°]	± [°]	Advancing CA [°]	Receding CA [°]	CA hysteresis θ [°]
Glass	28.14	±1.06	42.6	9.1	33.5
APTES 3%	55.00	±0.25	60.4	29.3	31.1
APTES 5%	53.80	±0.77	65.5	31.1	34.4

From the change of the contact angles it was obvious, that some reaction has occurred and modified the glass surface (**Table 2**). For pure glass a static CA (sCA) of 28.14 ° and a dynamic CA (dCA) hysteresis of 33.5 ° was found and for the APTES modified glass sample in 3 wt% solution, values of 55 ° for sCA and 31.1 ° in dCA hysteresis. For the sample out of 5 wt% APTES solution a sCA of 53.8 ° and a dCA hysteresis of 34.4 ° was determined. The difference between the unmodified and the functionalized samples was visible, but the comparison of the two functionalized samples was difficult. With CA measurement it was not possible to determine what actually happened, because surface roughness for example could also change the affinity to the liquid drop. To make these changes visible, the amine groups were coupled with a fluorophore dye (Alexa Fluor® 680 NHS Ester; ThermoFischer) and monitored by TIRF-microscopy.

Therefore 5 mg of the fluorophore was dissolved in 1 mL of PBS buffer. On the cleaned aminopropyl functionalized cover slips, a lab-tek-chamber® was fixed and on the spot, separated by this chamber, 100 μ L of the PBS dye solution was deposited. For the NHS coupling reaction the surface area was incubated for a time of 15 min. Subsequently the dye solution was washed with PBS buffer solution and the samples were examined under the TIRFM (**Figure 78– Figure 80**)

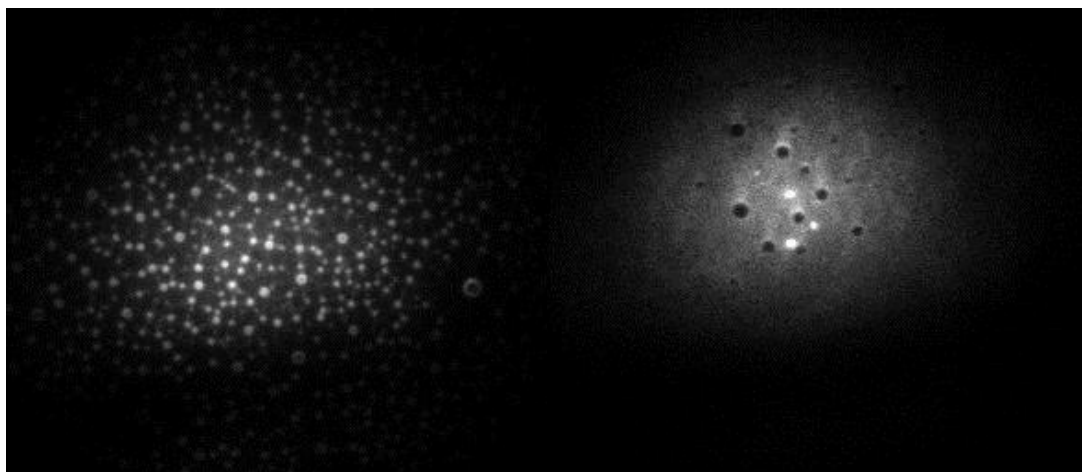


Figure 78. TIRFM image of APTES 3 wt% functionalization

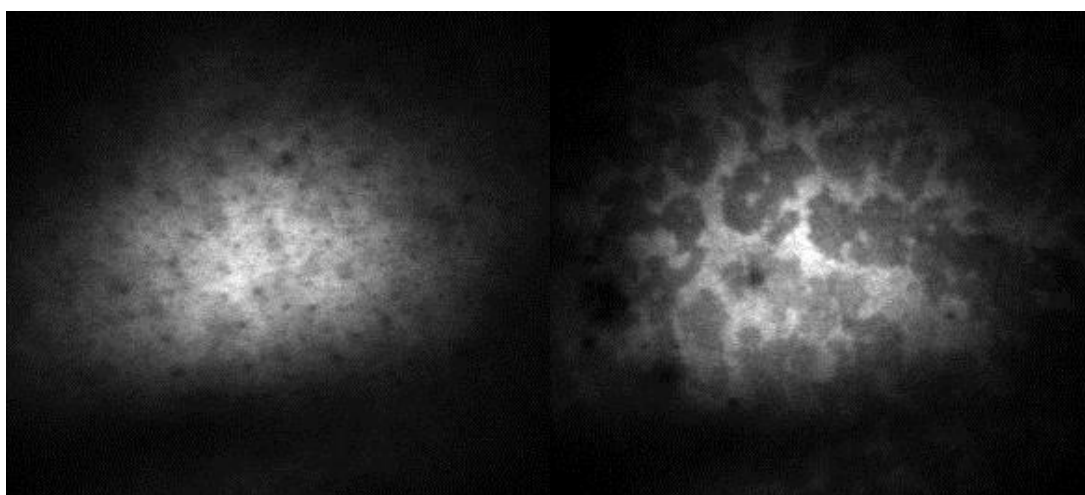


Figure 79. TIRFM image of APTES 4 wt% functionalization



Figure 80. TIRFM image of APTES 5 wt% functionalization

From the pictures obtained by TIRFM, it was obvious that the functionalization in 5 wt% APTES worked out in high yield. Actually the bright spot of **Figure 80** was not visible at the beginning and became brighter over time. The reason for that was the high concentration of the fluorophore, which was quenching itself at high concentrations and therefore developing the fluorescence over time.

In terms of monolayer surface homogeneity, a dip coating experiment was carried out. Therefore the samples were dipped into the 5 wt% solution of APTES in EtOH/HAc and withdrawn out of solution with constant velocity (**Figure 81**).

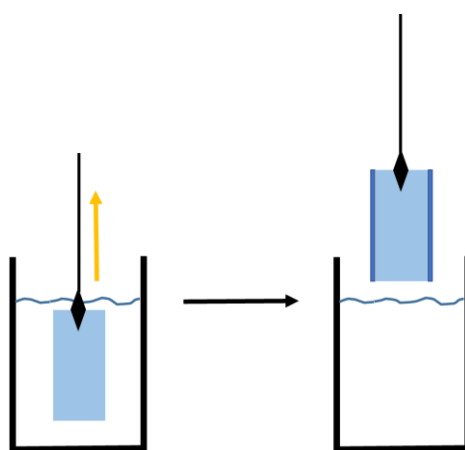


Figure 81. Scheme of a dip coating process

Two different velocities were applied for this experiment: 10 mm min^{-1} for the slow withdrawn sample and 30 mm min^{-1} for a fast withdrawn sample for comparison. The procedures for both samples were identical except of withdrawing speed. For this process a sample was mounted on the dip coater and dipped into the prepared APTES solution. In solution, the sample was in abundance for 30 s before the withdrawing at adjusted speed started. After the complete withdrawal, the sample was rinsed with ethanol and acetone immediately and dried under an argon stream. These samples were coupled with a fluorophore with the same procedure mentioned before and investigated with TIRFM (**Figure 82**).

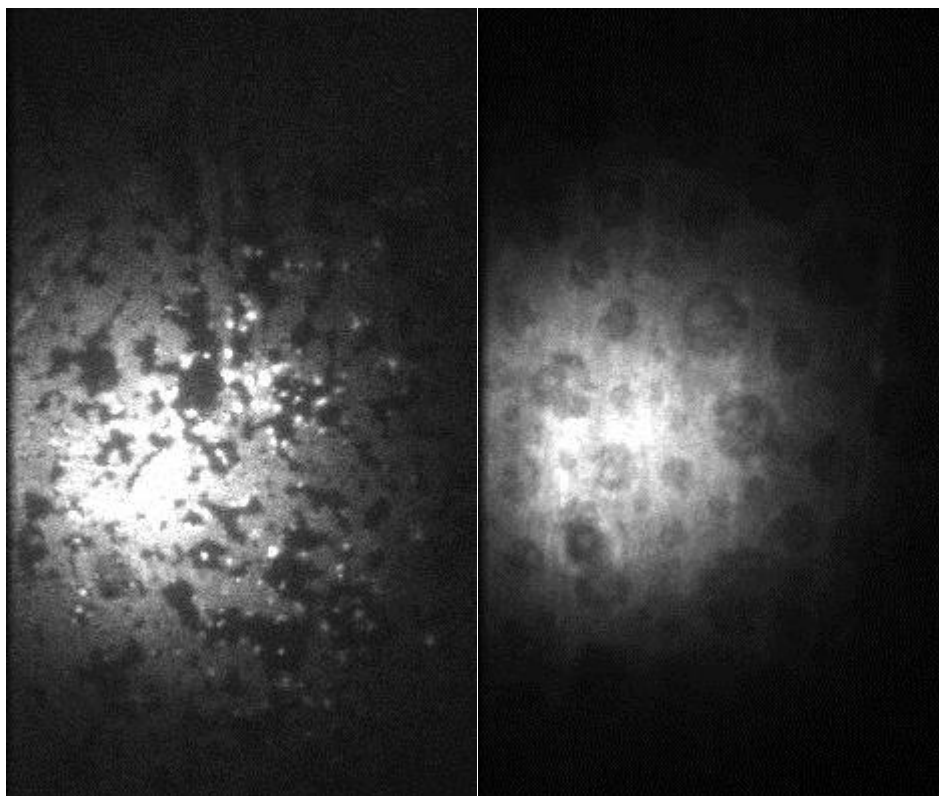


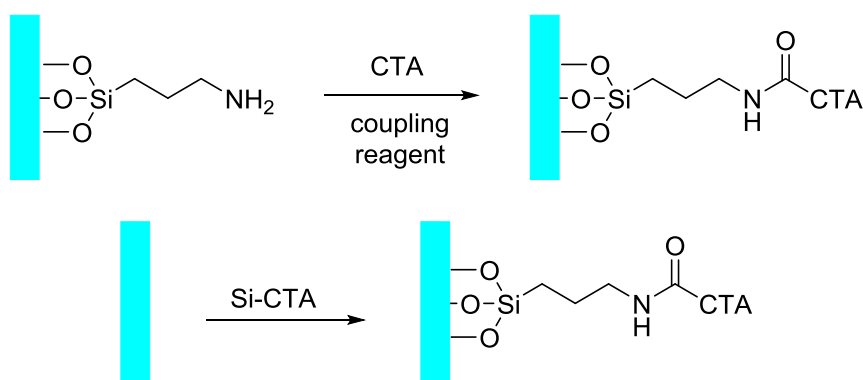
Figure 82. TIRFM pictures of the dip-coating approaches; withdrawing speed 10 mm min⁻¹ (left); 30 mm min⁻¹ (right)

From these pictures it could be derived, that the coating was not as homogenous and functionalized as the sample which dwelled 24 h in the 5 wt% solution of APTES. To make this method practicable, surface tension and wettability of the APTES solution would have to be adjusted. But due to the fact that the other approach of 24 h in 5 wt% APTES solution worked out in high quantities, investigation of dip coating as method was not continued.

For further experiments the concentration of 5 wt% of alkoxy silane compounds in solution should be applied for the functionalization of the surfaces, due to its outstanding result. The next step should be the coupling of a RAFT agent to the surface with respect to the results achieved so far.

8 Modification of the SiO₂ surface with RAFT reagents

As mentioned in chapter 1, there are two different approaches to functionalize the glass surface with one of the CTAs by amide bond coupling. First is the pre-functionalization of the surface with APTES and afterwards coupling to the CTA (pathway (1)). Second, is the synthesis of a CTA with an alkoxy silane end-group and subsequently direct functionalization of the surface via this Si-CTA (pathway (2)) (**Scheme 41**).



Scheme 41. Immobilization approaches, pre-functionalization by APTES (top, pathway (1)); direct functionalization (bottom; pathway (2))

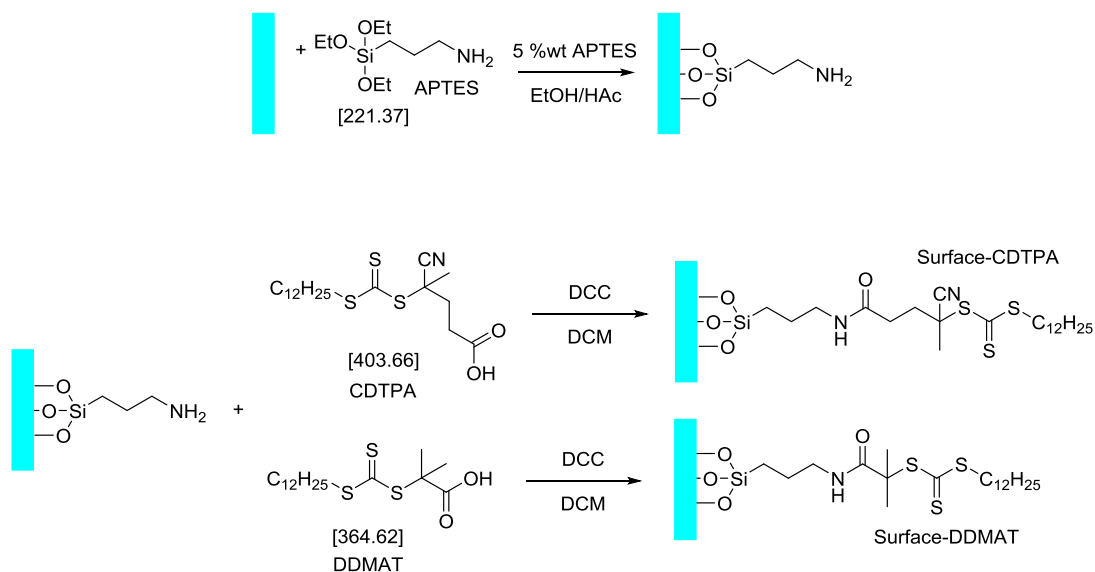
Both of these approaches were carried out and analyzed with contact angle, ellipsometry and partially with X-ray photoelectron spectroscopy using a silicon wafer reference. Furthermore, a macro-RAFT attempt was carried out, by pre-functionalization with 3-(trimethoxysilyl)propyl methacrylate and grafting of the CTA onto this compound on the surface (macro-RAFT pathway).

8.1 Pre-functionalization of the surface with APTES and coupling to the RAFT reagent; pathway (1)

For the following approaches, not only glass cover slips were used as starting material, but also a silicon wafer was applied as reference. The necessity for that is based on the bad refractive index of glass for ellipsometric measurements and also its non-conducting behavior for XPS measurements. A silicon wafer has an approximate SiO₂ layer of ≈ 20 nm on the surface, which can be functionalized in the same way like a

glass SiO₂ surface. On this note, every reaction was applied with a corresponding Si wafer reference in the same solution.

In this first pathway, two steps of functionalization are necessary. First, the functionalization with aminopropyl groups with APTES, second, the coupling to the CTA (**Scheme 42**)²³.



Scheme 42. Pre-functionalization with APTES (top), then coupling to CTA (bottom)

In this approach, a glass cover slip and a silicon wafer sample was cleaned with organic solvents and water by supersonification, and activated with piranha acid for 1 h at 80 °C, for every experiment, respectively. Subsequently, the samples were rinsed with water, EtOH, and acetone, and dried under an argon stream. Small glass cylinders (volume of 1 mL) were attached to the surfaces, using a two component dental glue (**Figure 83**), to perform the coating and coupling reaction within these small volumes to save chemicals and time.



Figure 83. Set up for the surface modifications on glass cover slips

These volumes were filled with 5 wt% solution of degassed APTES in EtOH/HAc (97:3; HAc 1:10 diluted in water), covered and stored under inert atmosphere. The silicon wafer references were analyzed via ellipsometry before the surface modification, to determine their particular SiO₂ layer. After 24 h reaction time, the samples were rinsed with EtOH and acetone, and dried under argon stream.

Afterwards a 5 wt% solution of the CDTPA or DDMAT coupling solution was prepared. Therefore 1 equiv. of CTA was dissolved in DCM, and cooled. Under cooling 1 equiv. of DCC was added in a way that a 5 wt% solution of the starting materials in solution was established. This solutions were degassed and filled into the volumes, for a reaction time of 1 h. Subsequently, the solution was removed and the surface was rinsed with DCM, EtOH and acetone, and dried under argon stream. The small cylinders were removed by usage of a scalpel and residues of the glue were stripped off. Before analysis of these surfaces, they were cleaned by supersonification in organic solvents and dried under an argon stream.

8.1.1 Analysis of the surfaces, generated by pathway (1)

As mentioned before, both samples were analyzed by static and dynamic contact angle measurements, ellipsometry and XPS. The first measurement method applied, was the layer thickness determination by ellipsometry. The measured layer thicknesses of

the silicon wafer references after the coupling approach with the CTAs are illustrated in **Table 3**. The glass samples could not be measured by this method, due to the unfavorable refractive index of the material.

Table 3. Layer thickness measurement via ellipsometry of pathway (1)

Sample	Layer thickness [Å]	Confidence _{95 %} [Å]
Blank; SiO ₂ layer thickness	14.09	± 0.16
Additional layer thickness after CDTPA functionalization	7.38	± 0.51
Blank; SiO ₂ layer thickness	13.80	± 0.39
Additional layer thickness after DDMAT functionalization	7.14	± 0.19

These results showed for both samples similar results of about 7 Å layer thickness. Because the layer thickness was measured in dry state, the results of the ellipsometric seemed to be reasonable²⁰. In the next step the samples were analyzed via contact angle measurement **Figure 84** of unmodified substrate and **Figure 85** of APTES functionalized substrate are depicted here for comparison.

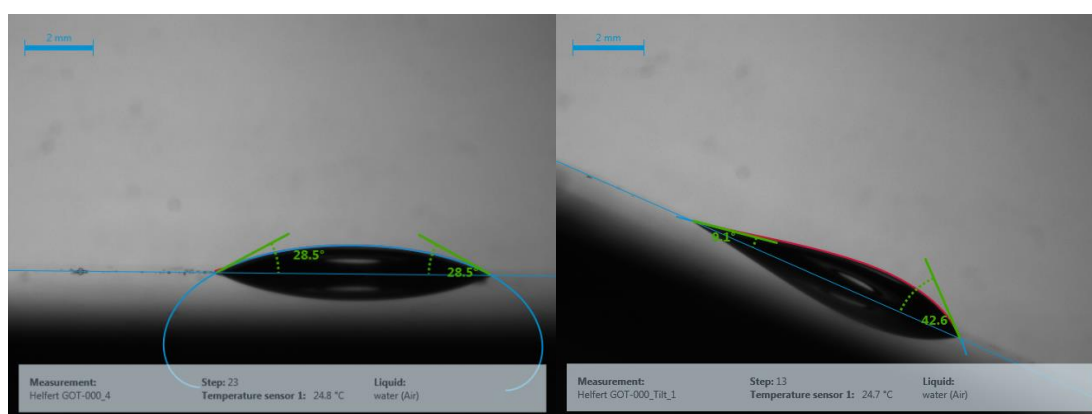


Figure 84. Static CA of unmodified glass (left); dynamic CA (right)

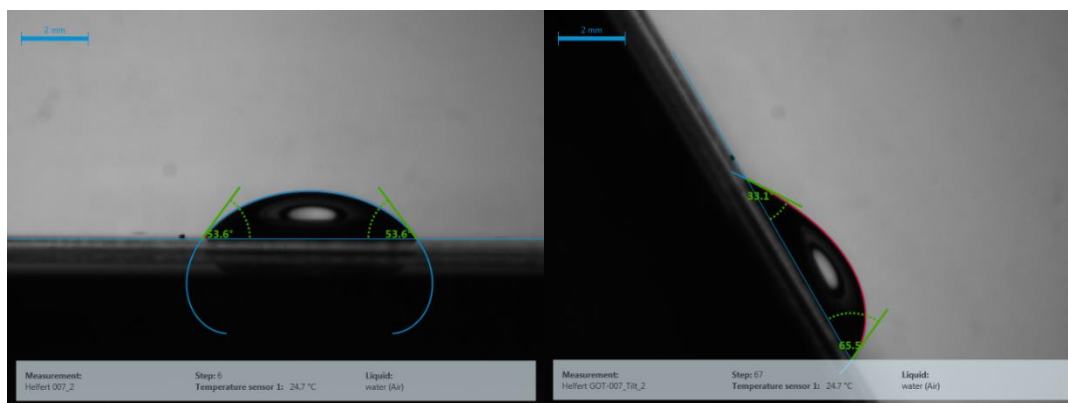


Figure 85. Static CA of APTES functionalized glass 5 wt% (left); dynamic CA (right)

After the coupling of the surface immobilized APTES to the CTAs, the static contact angles increased by a small amount, so the surface became more hydrophobic. Nevertheless, the dynamic contact angles and their hysteresis changed in a greater extend and were comparable to the Si references (**Figure 86 – Figure 87** and **Table 4**).

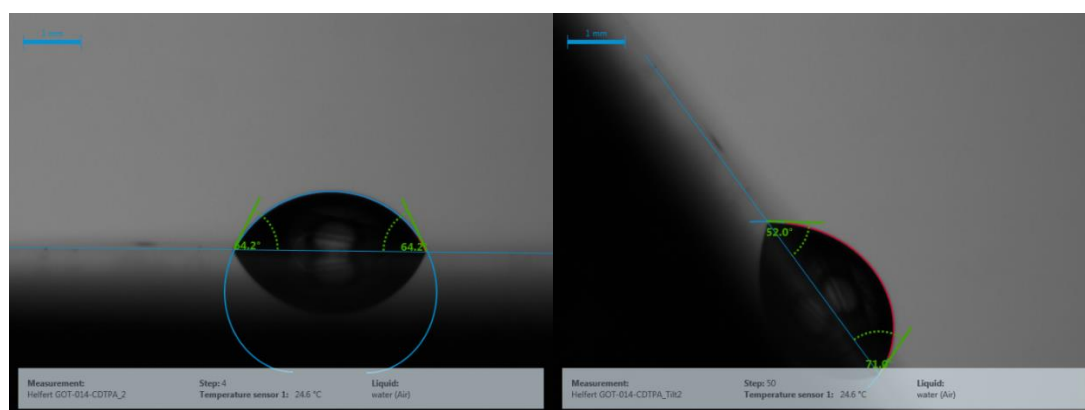


Figure 86. Pathway (1); static CA of CDTPA functionalized glass (left); dynamic CA (right)

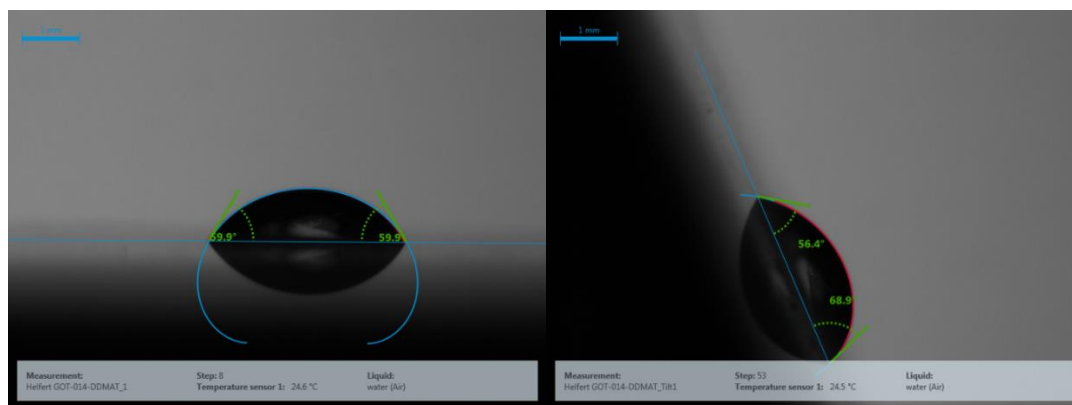


Figure 87. Pathway (1); static CA of CDTPA functionalized glass (left); dynamic CA (right)

Table 4. Results of CA measurements for pathway (1)

Sample	Static CA [°]	± [°]	Advancing CA [°]	Receding CA [°]	CA hysteresis Θ [°]
Glass	28.14	± 1.06	42.6	9.1	33.5
Surface-APTES	53.80	± 0.77	65.5	31.1	34.4
Surface-CDTPA	64.09	± 0.22	71.0	52.0	19.0
Surface-DDMAT	59.86	± 0.20	68.9	56.4	12.5

The results from the CA measurements of Si-Wafer and glass samples were absolutely comparable and looked rather promising, due to their strong change in CA-hysteresis, which indicated a difference in adhesion of the surface. To determine the atomic composition of the surface, XPS measurements were performed, since XPS is an analytical method to obtain semi-quantitative information of molecules attached to surfaces. To compare the results of silicon wafer reference samples and the glass substrate samples, both samples for the two CTAs were analyzed and in addition one unmodified glass sample was measured as reference (**Table 5**).

Table 5. Results of the XPS measurement of pathway (1)

Sample	Element [at%]							Ratio []
	C	K	N	Na	O	Si	Zn	C/N
Glass blank	28.6	1.2	-	0.7	40.2	28.3	0.9	-
Glass CDTPA	48.8	-	-	-	23.5	27.7	-	-
Si CDTPA	50.9	-	-	-	21.7	27.5	-	-
Glass DDMAT	46.4	-	0.3	-	26.4	27.0	-	169.9
Si DDMAT	50.2	-	1.3	-	22.5	26.0	-	38.6

It is obvious from the XPS measurement that no sulfur was found on the surfaces. Partially also no nitrogen was found on the surface. The problem with this approach could have been the set-up in the cylinders, glued to the surface. Due to the fact, that the solution could not be stirred, it might have occurred, that hydrolyzed DCC impurities sedimented on the surface and almost no functionalization took place.

As a test another cycle of samples, glass and silicon wafer, were prepared again, according to the same procedure, but out of solution using only CDTPA as CTA. The glass and silicon wafer samples were washed with organic solvents under supersonification, activated with piranha acid and functionalized with APTES over a time of 24 h under shaking, completely covered with the solution. Subsequently, the samples were rinsed with EtOH, acetone and DCM and immediately dipped into a 5 wt% coupling solution of CTA and DCC, prepared as mentioned before. These samples were analyzed by ellipsometry (data shown in **Table 6**) first, and afterwards measured by XPS (data shown in **Table 7**).

Table 6. Layer thickness measurement via ellipsometry of pathway (1) of sample preparation II

Sample	Layer thickness [Å]	Confidence ₉₅ % [Å]
Blank; SiO ₂ layer thickness	13.59	± 0.05
Additional layer thickness after CDTPA functionalization	9.46	± 0.35

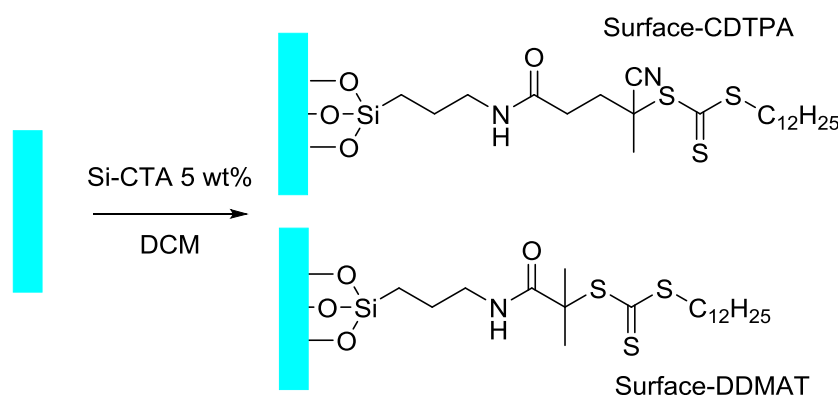
Table 7. Results of the XPS measurement of pathway (1) sample preparation II

Sample	Element (at%)				
	C	N	O	S	Si
Si CDTPA	20.6	3.0	30.0	<0.1	46.4
Glass CDTPA	38.6	1.9	29.7	<0.1	29.8

Although a greater layer thickness of this sample, prepared in solution without cylindrical reaction chambers, was determined, XPS measurement confirmed the absence of sulfur of the expected compounds. In summary, this pathway did not lead to the targeted surface functionalization of the glass or silicon reference with the CTA.

8.2 Coupling of the ethoxysilane-RAFT reagent directly to the surface; pathway (2)

For this approach, also a glass sample and a silicon wafer sample were applied for the direct functionalization process and analyzed by contact angle measurement, ellipsometry and XPS. The glass and the silicon wafer substrates were cleaned in toluene, acetone and water under supersonification and activated by piranha acid at 80 C for 1 h. The established crude Si-CTA mixture was dissolved in EtOH/HAc (97:3; HAc 1:10 diluted in water), in a way that 5 wt% solution was generated and the samples were brought into the solution for a time of 24 h.



Scheme 43. Direct CTA functionalization of a substrate surface; pathway (2)

The crude Si-CTA solutions were prepared according to the procedures mentioned in chapter 6. 1 equiv. of CTA was dissolved in DCM under ice cooling, 1 equiv. of DCC or was dissolved in DCM and added dropwise to the CTA solution under ice cooling. After a stirring time of 15 min 1 equiv. of APTES was added and stirred for 1 h under room temperature. The solvent was removed under reduced pressure and the crude Si-CTA residue was used for the functionalization of the samples surfaces.

After activation of the substrates, these samples were rinsed with water, EtOH and acetone, and dried under argon stream. The silicon wafer samples were analyzed by ellipsometry to determine the present SiO₂ layer and subsequently all samples were dipped into the Si-CTA solution for a time of 24 h.

After this reaction time, the samples were rinsed with EtOH, cleaned under supersonification in acetone and dried under argon stream, before they were analyzed in the next step.

8.2.1 Analysis of the surfaces, generated by pathway (2)

The analysis procedures of the generated samples, were the same as described in chapter 8.1.1. First the wafer references were surveyed via ellipsometry, then contact angle measurement and XPS was applied. The results of ellipsometric measurements are depicted in **Table 8**.

Table 8. Layer thickness measurement via ellipsometry of pathway (2)

Sample	Layer thickness [Å]	Confidence _{95 %} [Å]
Blank; SiO ₂ layer thickness	18.78	± 0.08
Additional layer thickness after CDTPA functionalization	6.69	± 0.25
Blank; SiO ₂ layer thickness	15.14	± 0.71
Additional layer thickness after DDMAT functionalization	10.63	± 0.20

The ellipsometric measurement determined an additional layer thicknesses of 6 to 11 Å after the functionalization reaction. For the DDMAT functionalization it looked very promising with an additional layer thickness of 10.6 Å. Subsequently the contact angle measurements were performed of these samples (**Figure 89**, **Figure 90** and **Table 9**).

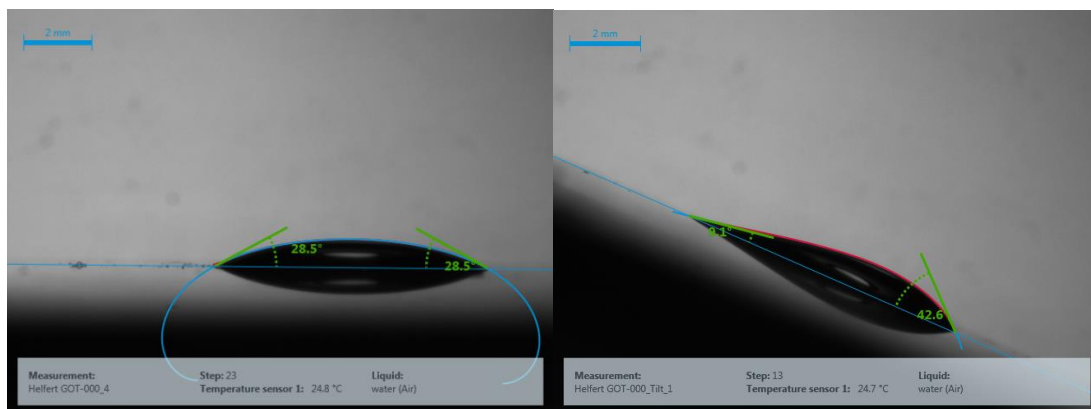


Figure 88. Static CA of unmodified glass (left); dynamic CA (right)

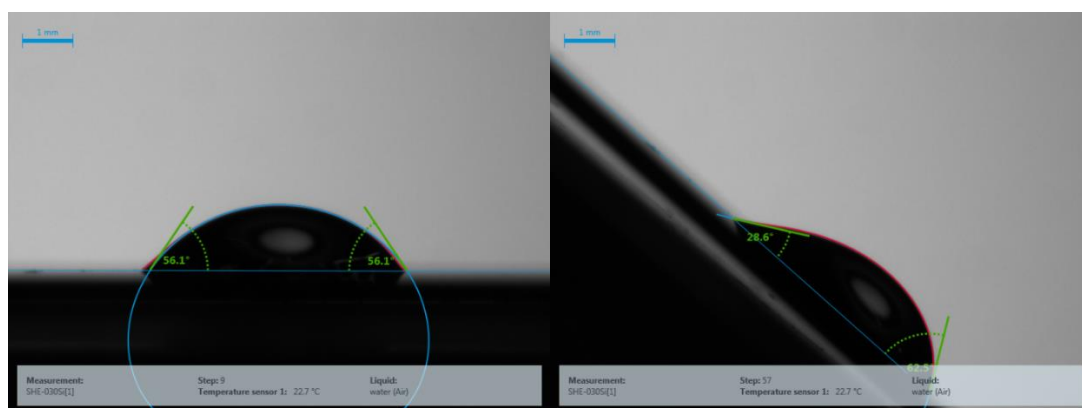


Figure 89. Pathway (2); static CA of CDTPA functionalized substrate (left); dynamic CA (right)

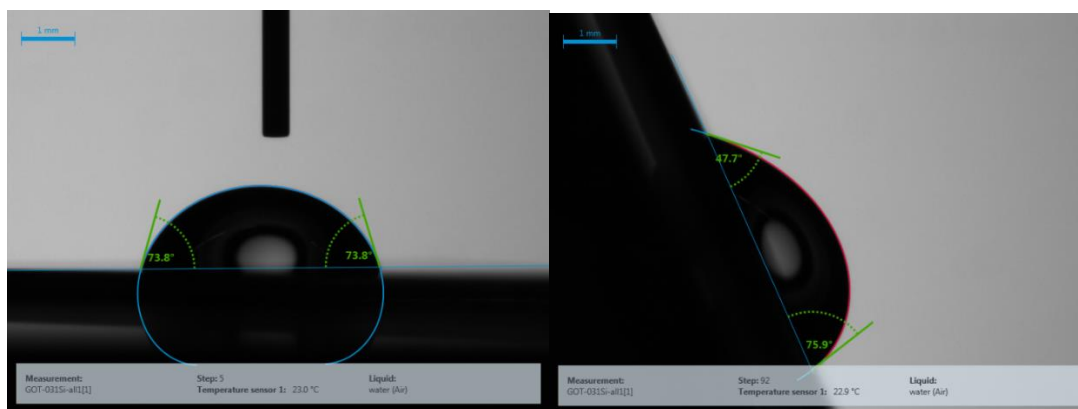


Figure 90. Pathway (2); static CA of DDMAT functionalized substrate (left); dynamic CA (right)

Table 9. Results of CA measurements for pathway (2)

Sample	Static CA [°]	± [°]	Advancing CA [°]	Receding CA [°]	CA hysteresis Θ [°]
Glass	28.14	± 1.06	42.6	9.1	33.5
Surface-APTES	53.80	± 0.77	65.5	31.1	34.4
Surface-CDTPA	56.07	± 0.20	62.4	28.1	34.3
Surface-DDMAT	73.74	± 0.50	75.3	47.6	27.7

The contact angle measurement of the CDTPA approach looked very similar to the functionalization with APTES, with a value of 53.8 °, to 56.07 °. For the DDMAT approach, the surface became a little more hydrophobic, with a CA increasing to 73.74 °, in comparison with preparation of pathway (1). For a better interpretation of the results, XPS measurements were performed of these samples (**Table 10**).

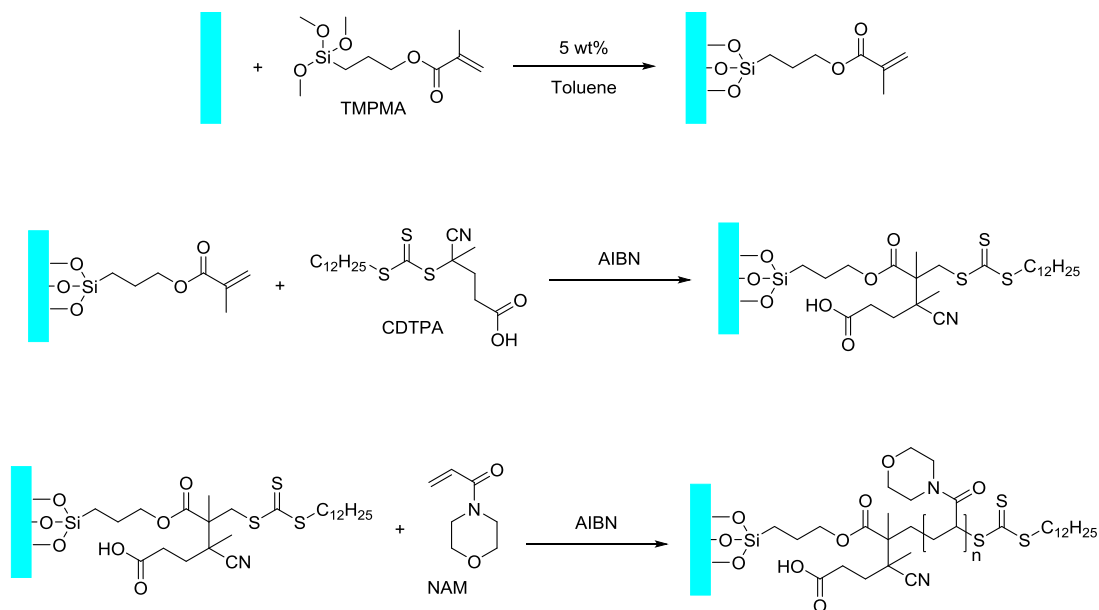
Table 10. Results of the XPS measurements for pathway (2)

Sample	Element (at%)							Ratio []	
	C	Cl	N	Na	O	S	Si	S/N	C/N
Glass CDTPA	32.1	0.7	4.4	0.7	38.5	1.1	22.5	0.25	7.2
Si CDTPA	31.6	1.2	6.1		32.1	1.1	27.9	0.18	5.2
Glass DDMAT	39.5	1.2	5.5	0.3	31.8	3.2	18.6	0.58	7.2
Si DDMAT	40.9	1.5	5.2		25.3	2.7	24.4	0.51	7.9

On these two samples, Sulphur was detected by XPS measurement. For CDTPA 1.1 at% S and for DDMAT between 2.7 and 3.2 at% S. The important fact of these measurement is the ratio of S / N, which should be 3 / 2 (1.5) for a perfect CDTPA monolayer and 3 / 1 (3) for a DDMAT monolayer. Both samples only yielded 1 / 6 of these values. The reason for that might be residues of APTES in the coating solution, which coupled to the surface first and increased the nitrogen share on the surface. Another problem could be the aminolysis reaction as mentioned in chapter 6, which will decrease the sulfur share on the surface. So with this approach, it was not possible to characterize the surface configuration completely. It could not be fully determined if CTA was on the surface and in which form it was coupled to it.

8.3 Functionalization of the surface with 3-(trimethoxysilyl)propyl methacrylate (TMPMA); pathway via macro-RAFT

Another approach was applied, by functionalization of the surface with TMPMA, subsequently prepolymerization of CDTPA, to the methacrylate on the surface, and generation of brushes via macro-RAFT polymerization (**Scheme 44**).



Scheme 44. Macro-RAFT approach with TMPMA, CDTPA and NAM for the synthesis of polymer brushes on the glass surface

Two silicon wafer substrates were cleaned as described in the chapters 8.1 and 8.2 and was analyzed via ellipsometry for the determination of the SiO_2 layer. Subsequently the substrates were dipped into a 5 wt% solution of TMPMA in toluene for a time of 24 h. Afterwards the substrates were measured again via ellipsometry and contact angle. A solution of CDTPA and AIBN 1:1 in dioxane was prepared and the substrates were brought into this solution. This mixture was degassed with argon and initiated at 80 °C for a time of 1 h for the pre-polymerization. Afterwards the silicon wafer references were analyzed again via ellipsometry and CA measurement. The results of this experiment are depicted in **Table 11** and **Table 12**.

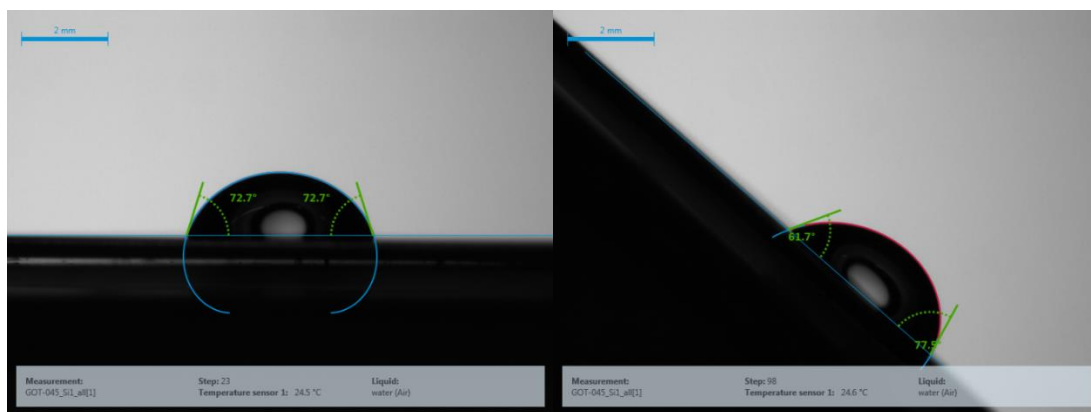


Figure 91. Static CA of TMPMA functionalized substrate (left); dynamic CA (right)

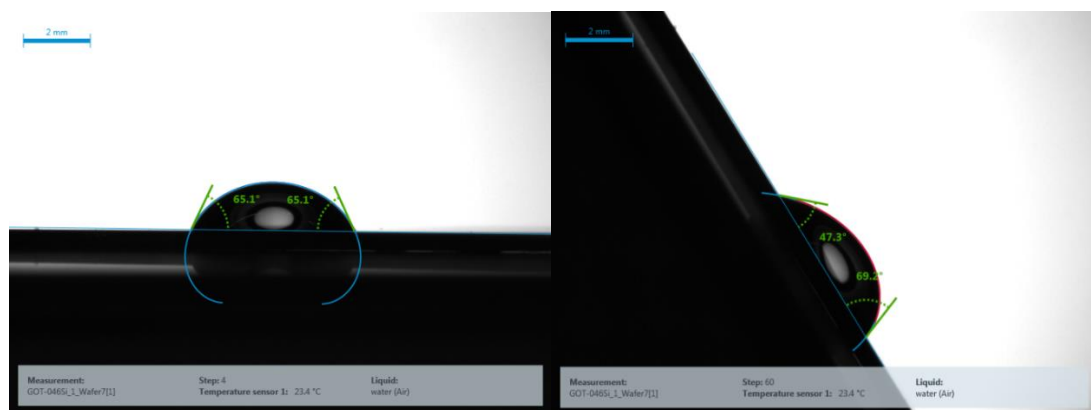


Figure 92. Static CA of CDTPA functionalized substrate (left); dynamic CA (right)

Table 11. Results of CA measurements for the macro-RAFT pathway

Sample	Static CA [°]	± [°]	Advancing CA [°]	Receding CA [°]	CA hysteresis Θ [°]
Glass	28.14	± 1.06	42.6	9.1	33.5
Surface-TMPMA	73.34	± 1.23	77.9	61.5	16.4
Surface-CDTPA	65.06	± 0.08	69.1	47.3	21.8

Table 12. Layer thickness measurement via ellipsometry of macro-RAFT pathway

Sample	Layer thickness [Å]	Confidence _{95 %} [Å]
Blank; SiO ₂ layer thickness	16.81	± 0.09
Additional layer thickness after TMPMA functionalization	12.32	± 0.56
Additional layer thickness after CDTPA functionalization	11.67	± 0.69
Blank; SiO ₂ layer thickness	13.20	± 0.24
Additional layer thickness after TMPMA functionalization	15.86	± 0.52
Additional layer thickness after CDTPA functionalization	15.76	± 1.08

The contact angle changed but it was obvious from these two results of the ellipsometric measurement that the macro-RAFT attempt, did not work out, because the organic layer actually became smaller. So this approach was not further investigated.

8.4 Summary of the modification pathways 1, 2 and macro-RAFT for the functionalization of SiO₂ surfaces with CTA reagents

Three different pathways of functionalization of the substrates were applied. The pre-functionalization with APTES and coupling to the CTA, the coupling of the CTA to APTES and the direct functionalization of the substrate with this Si-CTA and the macro-RAFT approach. None of these approaches gave a suitable result for the functionalization of the surfaces with the used CTA as could be seen especially from XPS measurements, where no / almost no / or Sulphur only with a wrong S / N ratio could be detected on the glass and Si-wafer surfaces. So a different functionalization model should be purchased.

Table 13. Summary of the analytical results of pathway (1), with pre-functionalization

Ellipsometry Sample		Layer thickness [Å]		Confidence _{95%} [Å]	
Blank; SiO ₂ layer thickness		14.09		± 0.16	
Additional layer thickness after CDTPA functionalization		7.38		± 0.51	
Blank; SiO ₂ layer thickness		13.80		± 0.39	
Additional layer thickness after DDMAT functionalization		7.14		± 0.19	
CA Sample	Static CA [°]	± [°]	Advancing CA [°]	Receding CA [°]	CA hysteresis Θ [°]
Glass	28.14	± 1.06	42.6	9.1	33.5
Surface-APTES	53.80	± 0.77	65.5	31.1	34.4
Surface-CDTPA	64.09	± 0.22	71.0	52.0	19.0
Surface-DDMAT	59.86	± 0.20	68.9	56.4	12.5
XPS Sample	Element (at%)				
	C	N	O	S	Si
Si CDTPA	20.6	3.0	30.0	<0.1	46.4
Glass CDTPA	38.6	1.9	29.7	<0.1	29.8

Table 14. Summary of the analytical results of pathway (2), with direct functionalization

CA Sample	Static CA [°]	± [°]	Advancing CA [°]	Receding CA [°]	CA hysteresis Θ [°]
Glass	28.14	± 1.06	42.6	9.1	33.5
Surface-APTES	53.80	± 0.77	65.5	31.1	34.4
Surface-CDTPA	56.07	± 0.20	62.4	28.1	34.3
Surface-DDMAT	73.74	± 0.50	75.3	47.6	27.7

Ellipsometry Sample		Layer thickness [Å]						Confidence _{95 %} [Å]	
Blank; SiO ₂ layer thickness		18.78						± 0.08	
Additional layer thickness after CDTPA functionalization		6.69						± 0.25	
Blank; SiO ₂ layer thickness		15.14						± 0.71	
Additional layer thickness after DDMAT functionalization		10.63						± 0.20	
XPS Sample	Element (at%)							Ratio []	
	C	Cl	N	Na	O	S	Si	S/N	C/N
Glass CDTPA	32.1	0.7	4.4	0.7	38.5	1.1	22.5	0.25	7.2
Si CDTPA	31.6	1.2	6.1		32.1	1.1	27.9	0.18	5.2
Glass DDMAT	39.5	1.2	5.5	0.3	31.8	3.2	18.6	0.58	7.2
Si DDMAT	40.9	1.5	5.2		25.3	2.7	24.4	0.51	7.9

Table 15. Summary of the analytical results of the macro-RAFT pathway

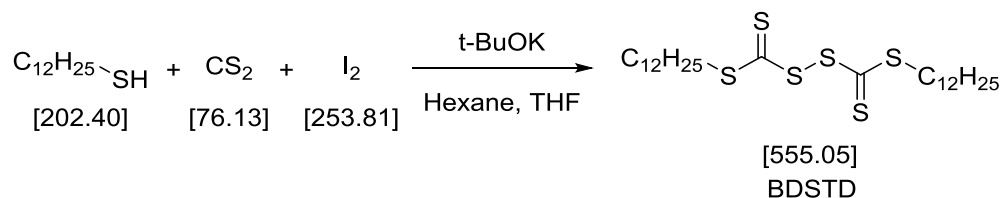
CA Sample	Static CA [°]	± [°]	Advancing CA [°]	Receding CA [°]	CA hysteresis Θ [°]
Glass	28.14	± 1.06	42.6	9.1	33.5
Surface-TMPMA	73.34	± 1.23	77.9	61.5	16.4
Surface-CDTPA	65.06	± 0.08	69.1	47.3	21.8

Ellipsometry Sample	Layer thickness [Å]	Confidence_{95 %} [Å]
Blank; SiO ₂ layer thickness	16.81	± 0.09
Additional layer thickness after TMPMA functionalization	12.32	± 0.56
Additional layer thickness after CDTPA functionalization	11.67	± 0.69
Blank; SiO ₂ layer thickness	13.20	± 0.24
Additional layer thickness after TMPMA functionalization	15.86	± 0.52
Additional layer thickness after CDTPA functionalization	15.76	± 1.08

Experimental part

2 Synthesis of the RAFT reagents

2.1.1 Synthesis of bis-(dodecylsulfanylthiocarbonyl)-disulfide (BDSTD)



	Weight [g]	Molar amount [mmol]	Molecular weight [g/mol]	Equiv. []	Volume [mL]
Potassium- <i>tert</i> -butanolate	8.36	74.5	112.18	1.04	-
Dodecanethiol	14.54	71.8	202.40	1	-
Carbon disulfide	5.66		76.15	1.03	-
Iodine	9.54		253.8	0.52	
Hexane	-	-	-	-	240
THF	-	-	-	-	70

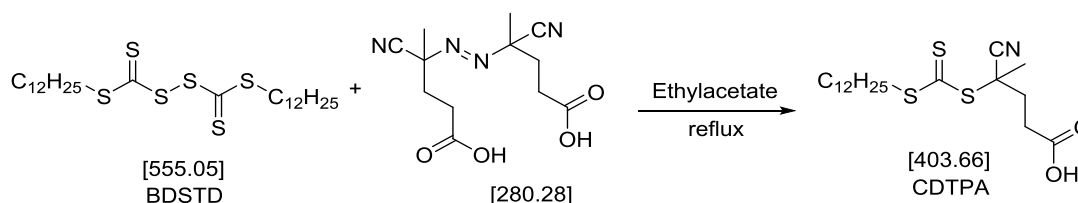
1.04 equivalents of potassium *tert*-butanolate (8.36 g; 74.5 mmol) were dissolved in a hexane/THF (240 mL / 70 mL) mixture and cooled down to 5 °C with an ice/water bath. 1 equiv. of dodecanethiol (14.54 g; 71.8 mmol) was added dropwise and the solution becomes a white emulsion. This emulsion was stirred for 30 min at 5 °C and afterwards 1.03 equiv. of carbon disulfide (5.66 g, 74.3 mmol) was added dropwise to the mixture. The formed yellow foam was stirred for 4 h at room temperature, then 0.52 equiv. of iodine (9.54 g; 37.6 mmol) dissolved in THF were added dropwise. The mixture was then stirred overnight. The mixture was dissolved completely in hexane and this organic phase was extracted with brine, thiosulfate solution and brine again, and afterwards dried with sodium sulfate. The solvent was removed via vacuum distillation

and the product was obtained as yellow oil, which crystallizes at lower temperatures to an orange solid with a yield of 87 % (17.31 g).

¹H-NMR (400 Mhz, CDCl₃):

δ ppm	0.88	(t; 6H; J = 7.05 Hz; (-S-....-C ⁽¹²⁾ H ₃) ₂)
	1.19 – 1.47	(m; 36H; (-S-...C ⁽³⁾⁻⁽¹¹⁾ H ₂ -) ₂)
	1.69	(q; 4H; J = 7.80 Hz (-S-...C ⁽²⁾ H ₂ -) ₂)
	2.68	
	2.94	(3 x t; 4H; J = 7.42 Hz; (-S-C ⁽¹⁾ H ₂ -) ₂)
	3.30	

2.1.2 Synthesis of 4-cyano-4-(((dodecylthio) carbonothioyl) thio)pentanoic acid (CDTPA)



	Weight [g]	Molar amount [mmol]	Molecular weight [g/mol]	Equiv. []	Volume [mL]
BDSTD	9.00	16.21	555.05	1	-
4,4'-(Diazene-1,2-diyl)bis(4-cyanopentanoic acid)	7.73	27.58	280.28	1.7	-
EE	-	-	-	-	85

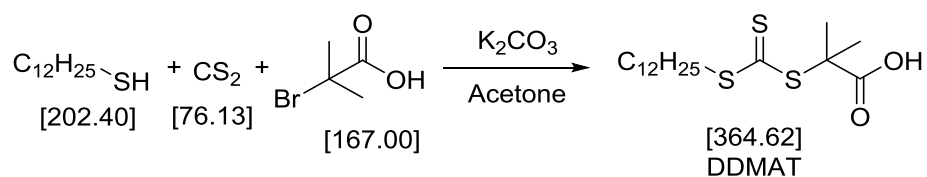
1 equiv. of bis-(dodecylsulfanylthiocarbonyl)-disulfide (9 g; 16.21 mmol) was dissolved in ethylacetate (85 mL) and the solution was degassed from oxygen with argon for 15 min. Under inert gas atmosphere the mixture was refluxed and 1.7 equiv of 4,4'-(diazene-1,2-diyl)bis(4-cyanopentanoic acid) (7.73 g, 27.58 mmol) were added dose

wise under argon counter flow. The mixture was stirred and refluxed overnight. The solvent was removed via vacuum distillation and the residue was recrystallized from diethyl ether. The product was purified via liquid column chromatography over silica with PE/EE = 1:1 to yield the product as a yellow solid in 41 % yield (5.36 g).

$^1\text{H-NMR}$ (400 Mhz, CDCl_3):

δ ppm	0.88	(t; 3H; J = 7.06 Hz; (-S-....-C ₍₁₂₎ H ₃))
	1.19 – 1.45	(m; 18H; (-S-...-C ₍₃₎₋₍₁₁₎ H ₂ -))
	1.69	(q; 2H; J = 7.43 Hz (-S-...C ₍₂₎ H ₂ -))
	1.89	(s; 3H; (-C ^{(4)'} -C ^{(5)'} H ₃))
	2.34 – 2.73	(m; 4H; (-C ^{(2)'} H ₂ -C ^{(3)'} H ₂ -))
	3.33	(t; 2H; J = 7.48 Hz; (-C ⁽¹⁾ H ₂ -S-))

2.2 Synthesis of 2-(((dodecylthio)carbonothioyl)thio)-2-methylpropanoic acid (DDMAT)



	Weight [g]	Molar amount [mmol]	Molecular weight [g/mol]	Equiv. []	Volume [mL]
Dodecanethiol	2.78	13.74	202.40	1	-
Potassium carbonate	3.98	28.80	138.20	2.1	-
Carbon disulfide	1.04	13.66	76.13	1	-
2-Bromo-2-methylpropanoic acid	2.29	13.71	167.00	1	-
Acetone	-	-	-	-	100

1 equiv. of dodecanethiol (2.78 g, 13.74 mmol) and 2.1 equiv. of potassium carbonate (3.98 g, 28.8 mmol) as the base was dissolved in acetone (100 mL) and stirred for 1 h. Then 1 equiv. of carbon disulfide (1.04 g, 13.66 mmol) was added dropwise and the mixture was stirred for further 1 h. Following 1 equiv. of 2-bromo-2-methylpropanoic acid (2.29 g, 13.71 mmol) was dissolved in acetone and added dropwise to the reaction mixture. This solution was stirred overnight and then acetone was removed via vacuum distillation. The residue was taken up with chloroform and extracted twice with 0.5 M HCl and once with brine. Chloroform was removed again via vacuum distillation and the residue was recrystallized from petroleum ether. The product was once again dissolved in ethylacetate, washed again with 0.5 M HCl and brine, and dried over sodium sulfate. After filtration the solvent was removed and the product was purified via liquid column chromatography over silica with PE:EE = 1:1 to yield the product as a yellow solid in a yield of 41 % (2.05 g).

$^1\text{H-NMR}$ (400 Mhz, CDCl_3):

δ ppm	0.88	(t; 3H; J = 7.03 Hz; (-S-....-C ₍₁₂₎ H ₃))
	1.12 – 1.43	(m; 18H; (-S-...-C ₍₃₎₋₍₁₁₎ H ₂ -))
	1.67	(q; 2H; J = 7.42 Hz (-S-...C ₍₂₎ H ₂ -))
	1.73	(s; 6H; (-S-C'(C'H ₃) ₂ -))
	3.28	(t; 2H; J = 7.37 Hz; (-C ⁽¹⁾ H ₂ -S-))

3 Kinetic studies of RAFT polymerization method

3.1 Reaction kinetics of RAFT polymerization of NAM and MPAA using CDTPA as CTA

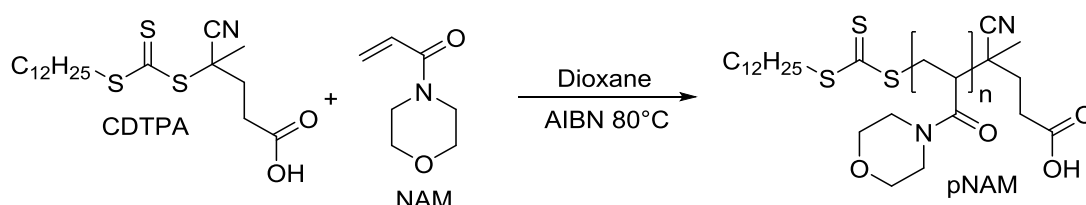
General procedure for RAFT polymerizations

500 mg of the monomer, CTA in a ratio to the monomer corresponding to the target molecular weight, AIBN in a ratio of 7.5 to the CTA and 100 mg of naphthalene as internal standard were dissolved in abs. dioxane (2 mmol mL^{-1} monomer in solution). The solution was degassed with argon for a time of 20 min, a sample of 0.1 mL was taken out of solution and subsequently the reaction mixture placed into a pre-heated heating block at 80 °C, for a time of 3 h. For the kinetic studies, samples of 0.1 mL were taken in time steps of $t = 0 \text{ s}$, 30 s, 60 s, 2 min, 5 min, 10 min, 20 min, 40 min, 1 h, 1.5 h, 2 h and 3 h, and analyzed by $^1\text{H-NMR}$. After this reaction time, the solution

was precipitated in cold PE, and the residue was dissolved again in dioxane. This precipitation step was performed three times for every polymerization, respectively. Afterwards, the product was dried at 40 °C under reduced pressure over night. The dry product was analyzed via GPC, for the determination of the MW corresponding to PS standards. The monomer conversion was determined via ¹H-NMR.

3.1.1 Synthesis of a 20 kDa and 40 kDa pNAM homopolymer by CDTPA as RAFT reagent for kinetic studies

3.1.1.1 Synthesis of a 20 kDa pNAM homopolymer by CDTPA as RAFT reagent



	Weight [mg]	Molar amount [mmol]	Molecular weight [g/mol]	Equiv. []	Volume [mL]
CDTPA	10.32	0.026	403.67	1	-
AIBN	0.59	0.004	164.21	0.14	-
Naphtalene	99.86	0.779	128.17	-	-
NAM	500.44	3.545	141.17	138.67	-
Dioxane	1830	-	-	-	-

The synthesis was performed according to the general procedure for RAFT polymerizations. A ratio of monomer:CTA of 138.66:1 and a ratio of CTA:initiator of 7.12:1 was applied. The conversion was determined via ¹H-NMR by comparison of the constant naphthalene signals to the olefinic signal of NAM. M_n, M_w and dispersity were determined via THF GPC. The product was isolated as white-slightly yellow powder.

¹H-NMR (400 Mhz, CDCl₃):

δ ppm	5.65	(dd; 1H; J ₁ = 1.95 Hz; J ₂ = 10.55 Hz; (NAM, CH=CHH))
	7.41	(dt; 4H; J ₁ = 3.51 Hz; J ₂ = 9.76 HZ; (naphthalene, (=oCH=pCH=pCH=oCH=) ₂)

Monomer conversion = 99 %

M_{n, NMR} = 19800 g mol⁻¹

GPC M_{n, GPC} = 8200 g mol⁻¹
M_{w, GPC} = 11200 g mol⁻¹
Đ = 1.37

3.1.1.2 Synthesis of a 40 kDa pNAM homopolymer by CDTPA as RAFT reagent

	Weight [mg]	Molar amount [mmol]	Molecular weight [g/mol]	Equiv. []	Volume [mL]
CDTPA	5.15	0.013	403.67	1	-
AIBN	0.32	0.002	164.21	0.15	
Naphtalene	100.43	0.784	128.17	-	-
NAM	55.12	3.543	141.17	277.68	-
Dioxane	1830	-	-	-	-

The synthesis was performed according to the general procedure for RAFT polymerizations. A ratio of monomer:CTA of 277.68:1 and a ratio of CTA:initiator of 6.55:1 was applied. The conversion was determined via ¹H-NMR by comparison of the constant naphthalene signals to the olefinic signal of NAM. M_n, M_w and dispersity were determined via THF GPC. The product was isolated as white-slightly yellow powder.

$^1\text{H-NMR}$ (400 Mhz, CDCl_3):

δ ppm	5.65	(dd; 1H; $J_1 = 1.95$ Hz; $J_2 = 10.55$ Hz; (NAM, CH=CHH))
	7.41	(dt; 4H; $J_1 = 3.51$ Hz; $J_2 = 9.76$ HZ; (naphtalene, (=oCH=pCH=pCH=oCH=) ₂)

Monomer conversion = 97 %

$M_{n, \text{NMR}} = 38400 \text{ g mol}^{-1}$

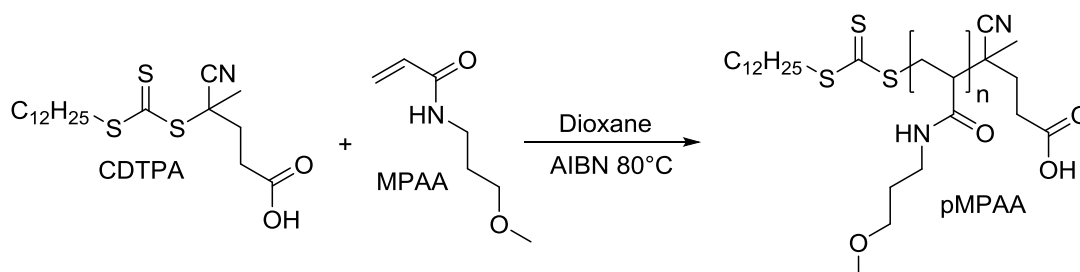
GPC $M_{n, \text{GPC}} = 16600 \text{ g mol}^{-1}$

$M_{w, \text{GPC}} = 22600 \text{ g mol}^{-1}$

$\text{Đ} = 1.36$

3.1.2 Synthesis of a 20 kDa and 40 kDa pMPAA homopolymer by CDTPA as RAFT reagent for kinetic studies

3.1.2.1 Synthesis of a 20 kDa pMPAA homopolymer by CDTPA as RAFT reagent



	Weight [g]	Molar amount [mmol]	Molecular weight [g/mol]	Equiv. []	Volume [mL]
CDTPA	10.38	0.026	403.67	1	-
AIBN	0.57	0.004	164.21	0.13	-
Naphtalene	99.37	0.775	128.17	-	-
MPAA	500.50	3.450	143.19	135.9	-
Dioxane	1800	-	-	-	-

The synthesis was performed according to the general procedure for RAFT polymerizations. A ratio of monomer:CTA of 135.93:1 and a ratio of CTA:initiator of 7.41:1 was applied. The conversion was determined via ¹H-NMR by comparison of the constant naphthalene signals to the olefinic signal of NAM. M_n, M_w and dispersity were determined via THF GPC. The product was isolated as slightly yellow transparent high viscous paste.

¹H-NMR (400 Mhz, CDCl₃):

δ ppm	5.57	(dd; 1H; J ₁ = 1.51 Hz; J ₂ = 10.19 Hz; (MPAA, CH=CHH))
	7.41	(dt; 4H; J ₁ = 3.51 Hz; J ₂ = 9.76 HZ; (naphtalene, (=oCH=pCH=pCH=oCH=) ₂)

Monomer conversion = 95 %

M_{n, NMR} = 18900 g mol⁻¹

GPC M_{n, GPC} = 8700 g mol⁻¹
 M_{w, GPC} = 11700 g mol⁻¹
 Đ = 1.34

3.1.2.2 Synthesis of a 40 kDa pMPAA homopolymer by CDTPA as RAFT reagent

	Weight [mg]	Molar amount [mmol]	Molecular weight [g/mol]	Equiv. []	Volume [mL]
CDTPA	5.15	0.013	403.67	1	-
AIBN	0.27	0.002	164.21	0.13	-
Naphtalene	101.75	0.794	128.17	-	-
MPAA	499.83	3.491	143.19	273.61	-
Dioxane	1800	-	-	-	-

The synthesis was performed according to the general procedure for RAFT polymerizations. A ratio of monomer:CTA of 273.61:1 and a ratio of CTA:initiator of 7.76:1 was applied. The conversion was determined via $^1\text{H-NMR}$ by comparison of the constant naphthalene signals to the olefinic signal of NAM. M_n , M_w and dispersity were determined via THF GPC. The product was isolated as slightly yellow transparent high viscous paste.

$^1\text{H-NMR}$ (400 Mhz, CDCl_3):

δ ppm	5.57	(dd; 1H; $J_1 = 1.51$ Hz; $J_2 = 10.19$ Hz; (MPAA, $\text{CH}=\text{CHH}$))
	7.41	(dt; 4H; $J_1 = 3.51$ Hz; $J_2 = 9.76$ HZ; (naphtalene, $(=\text{oCH}=\text{pCH}=\text{pCH}=\text{oCH}=\text{=})_2$)

Monomer conversion = 93 %

$M_{n, \text{NMR}} = 36839 \text{ g mol}^{-1}$

GPC $M_{n, \text{GPC}} = 13400 \text{ g mol}^{-1}$

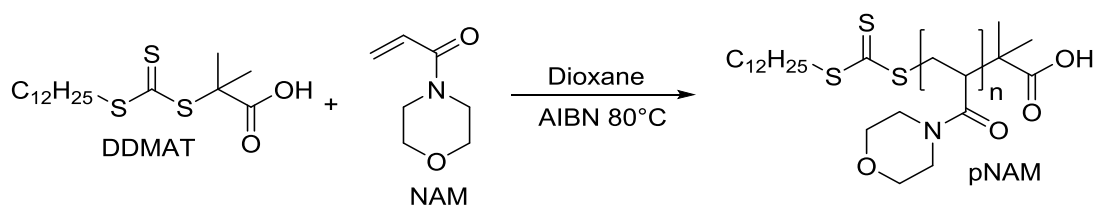
$M_{w, \text{GPC}} = 20000 \text{ g mol}^{-1}$

$\text{Đ} = 1.49$

3.2 Reaction kinetics of RAFT polymerization of NAM and MPAA using DDMAT as CTA

3.2.1 Synthesis of a 20 kDa and a 40 kDa pNAM homopolymer by DDMAT as RAFT reagent for kinetic studies

3.2.1.1 Synthesis of a 20 kDa pNAM homopolymer by DDMAT as RAFT reagent



	Weight [mg]	Molar amount [mmol]	Molecular weight [g/mol]	Equiv. []	Volume [mL]
DDMAT	8.48	0.023	364.63	1	-
AIBN	0.64	0.004	164.21	0.17	-
Naphtalene	100.4	0.783	128.17	-	-
NAM	500.39	3.545	141.17	152.41	-
Dioxane	1826	-	-	-	-

The synthesis was performed according to the general procedure for RAFT polymerizations. A ratio of monomer:CTA of 152.41:1 and a ratio of CTA:initiator of 5.97:1 was applied. The conversion was determined via $^1\text{H-NMR}$ by comparison of the constant naphthalene signals to the olefinic signal of NAM. M_n , M_w and dispersity were determined via THF GPC. The product was isolated as white-slightly yellow powder.

$^1\text{H-NMR}$ (400 Mhz, CDCl_3):

δ ppm	5.65	(dd; 1H; $J_1 = 1.95$ Hz; $J_2 = 10.55$ Hz; (NAM, CH=CHH))
	7.41	(dt; 4H; $J_1 = 3.51$ Hz; $J_2 = 9.76$ HZ; (naphtalene, (para; =CH=CH=CH=CH=) ₂)

Monomer conversion = 97 %

$M_{n, \text{NMR}} = 21200 \text{ g mol}^{-1}$

GPC $M_{n, \text{GPC}} = 8900 \text{ g mol}^{-1}$
 $M_{w, \text{GPC}} = 12100 \text{ g mol}^{-1}$
 $\text{Đ} = 1.36$

3.2.1.2 Synthesis of a 20 kDa pNAM homopolymer by DDMAT as RAFT reagent

	Weight [mg]	Molar amount [mmol]	Molecular weight [g/mol]	Equiv. []	Volume [mL]
DDMAT	4.53	0.012	364.63	1	-
AIBN	0.25	0.002	164.21	0.12	-
Naphtalene	97.48	0.760	128.17	-	-
NAM	502.44	3.556	141.17	286.48	-
Dioxane	1837	-	-	-	-

The synthesis was performed according to the general procedure for RAFT polymerizations. A ratio of monomer:CTA of 286.48:1 and a ratio of CTA:initiator of 8.16:1 was applied. The conversion was determined via $^1\text{H-NMR}$ by comparison of the constant naphthalene signals to the olefinic signal of NAM. M_n , M_w and dispersity were determined via THF GPC. The product was isolated as white-slightly yellow powder.

$^1\text{H-NMR}$ (400 Mhz, CDCl_3):

δ ppm	5.65	(dd; 1H; $J_1 = 1.95$ Hz; $J_2 = 10.55$ Hz; (NAM, CH=CHH))
	7.41	(dt; 4H; $J_1 = 3.51$ Hz; $J_2 = 9.76$ HZ; (naphtalene, (=oCH=pCH=pCH=oCH=) ₂)

Monomer conversion = 98 %

$M_{n, \text{NMR}} = 39998 \text{ g mol}^{-1}$

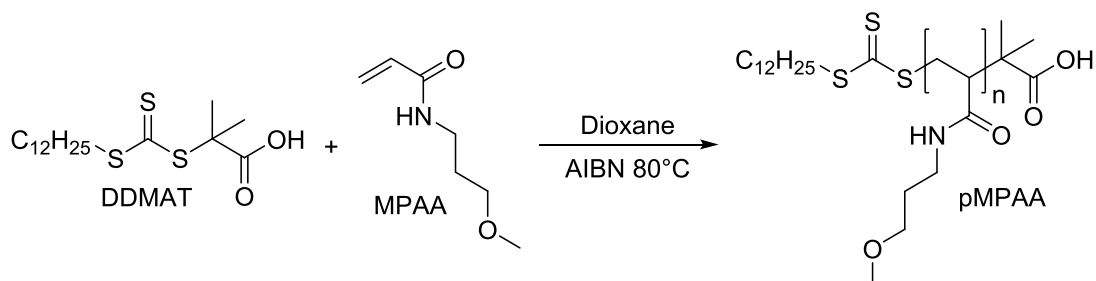
GPC $M_{n, \text{GPC}} = 16400 \text{ g mol}^{-1}$

$M_{w, \text{GPC}} = 22500 \text{ g mol}^{-1}$

$\bar{D} = 1.37$

3.2.2 Synthesis of a 20 kDa and a 40 kDa pMPAA homopolymer by DDMAT as RAFT reagent for kinetic studies

3.2.2.1 Synthesis of a 20 kDa pMPAA homopolymer by DDMAT as RAFT reagent



	Weight [mg]	Molar amount [mmol]	Molecular weight [g/mol]	Equiv. []	Volume [mL]
DDMAT	8.47	0.023	364.63	1	-
AIBN	0.47	0.003	164.21	0.12	-
Naphtalene	131.65	1.027	128.17	-	-
MPAA	500.45	3.495	143.19	152.61	-
Dioxane	1820	-	-	-	-

The synthesis was performed according to the general procedure for RAFT polymerizations. A ratio of monomer:CTA of 152.61:1 and a ratio of CTA:initiator of 8.12:1 was applied. The conversion was determined via ¹H-NMR by comparison of the constant naphthalene signals to the olefinic signal of NAM. M_n, M_w and dispersity were determined via THF GPC. The product was isolated as slightly yellow transparent high viscous paste.

¹H-NMR (400 Mhz, CDCl₃):

δ ppm	5.57	(dd; 1H; J ₁ = 1.51 Hz; J ₂ = 10.19 Hz; (MPAA, CH=CHH))
	7.41	(dt; 4H; J ₁ = 3.51 Hz; J ₂ = 9.76 HZ; (naphtalene, (=oCH=pCH=pCH=oCH=) ₂)

Monomer conversion = 79 %

$M_{n, \text{NMR}} = 17500 \text{ g mol}^{-1}$

GPC $M_{n, \text{GPC}} = 7700 \text{ g mol}^{-1}$
 $M_{w, \text{GPC}} = 11200 \text{ g mol}^{-1}$
 $\bar{D} = 1.45$

3.2.2.2 Synthesis of a 40 kDa pMPAA homopolymer by DDMAT as RAFT reagent

	Weight [mg]	Molar amount [mmol]	Molecular weight [g/mol]	Equiv. []	Volume [mL]
DDMAT	4.54	0.012	364.63	1	-
AIBN	0.25	0.002	164.21	0.12	-
Naphtalene	101.38	0.788	128.17	-	-
MPAA	502.53	3.510	143.19	285.90	-
Dioxane	1810	-	-	-	-

The synthesis was performed according to the general procedure for RAFT polymerizations. A ratio of monomer:CTA of 285.9:1 and a ratio of CTA:initiator of 8.18:1 was applied. The conversion was determined via $^1\text{H-NMR}$ by comparison of the constant naphthalene signals to the olefinic signal of NAM. M_n , M_w and dispersity were determined via THF GPC. The product was isolated as slightly yellow transparent high viscous paste.

$^1\text{H-NMR}$ (400 Mhz, CDCl_3):

δ ppm 5.57 (dd; 1H; $J_1 = 1.51 \text{ Hz}$; $J_2 = 10.19 \text{ Hz}$;
(MPAA, $\text{CH}=\text{CHH}$))
7.41 (dt; 4H; $J_1 = 3.51 \text{ Hz}$; $J_2 = 9.76 \text{ Hz}$;
(naphtalene, $(=\text{oCH}=\text{pCH}=\text{pCH}=\text{oCH}=\text{)}_2$)

Monomer conversion = 78 %

$M_{n, \text{NMR}} = 31900 \text{ g mol}^{-1}$

GPC $M_{n, GPC} = 11200 \text{ g mol}^{-1}$
 $M_{w, GPC} = 19000 \text{ g mol}^{-1}$
 $\bar{D} = 1.67$

4 Analysis of pNAM and pMPAA in solution by static light scattering, dynamic light scattering and small angle X-ray scattering

4.1 – 4.4 SLS and DLS analysis of pNAM in water

4.1.1 Synthesis of a 20 kDa pNAM homopolymer by CDTPA as RAFT reagent for the structure analysis (pNAM20k)

	Weight [mg]	Molar amount [mmol]	Molecular weight [g/mol]	Equiv. []	Volume [mL]
CDTPA	9.63	0.024	403.67	1	-
AIBN	0.57	0.003	164.21	0.15	-
Naphtalene	99.26	0.774	128.17	-	-
NAM	514.37	3.644	141.17	152.73	-
Dioxane	1835	-	-	-	-

The synthesis was performed according to the general procedure for RAFT polymerizations. A ratio of monomer:CTA of 152.73:1 and a ratio of CTA:initiator of 6.87:1 was applied. The conversion was determined via $^1\text{H-NMR}$ by comparison of the constant naphthalene signals to the olefinic signal of NAM at $t = 0 \text{ min}$ and at the end after 3 h. M_n , M_w and dispersity were determined via THF GPC. The product was isolated as white-slightly yellow powder in a yield of 43.8 % (223 mg).

$^1\text{H-NMR}$ (400 Mhz, CDCl_3):

δ ppm	5.65	(dd; 1H; $J_1 = 1.95 \text{ Hz}$; $J_2 = 10.55 \text{ Hz}$; (NAM, $\text{CH}=\text{CHH}$))
	7.41	(dt; 4H; $J_1 = 3.51 \text{ Hz}$; $J_2 = 9.76 \text{ Hz}$; (naphtalene, $(=\text{oCH}=\text{pCH}=\text{pCH}=\text{oCH}=\text{=})_2$)

Monomer conversion = 99 %

$M_{n, \text{NMR}} = 21700 \text{ g mol}^{-1}$

GPC $M_{n, \text{GPC}} = 11100 \text{ g mol}^{-1}$

$M_{w, \text{GPC}} = 13300 \text{ g mol}^{-1}$

$\bar{D} = 1.20$

4.5 – 4.8 SLS and DLA analysis of pMPAA in water

4.5.1 Synthesis of a 20 kDa pMPAA homopolymer by DDMAT as RAFT reagent for the structure analysis (pMPAA20k)

	Weight [mg]	Molar amount [mmol]	Molecular weight [g/mol]	Equiv. []	Volume [mL]
DDMAT	8.56	0.023	364.63	1	-
AIBN	0.44	0.003	164.21	0.11	-
Naphtalene	97.32	0.759	128.17	-	-
MPAA	507.98	3.548	143.19	151.12	-
Dioxane	1801	-	-	-	-

The synthesis was performed according to the general procedure for RAFT polymerizations. A ratio of monomer:CTA of 151.12:1 and a ratio of CTA:initiator of 8.76:1 was applied. The conversion was determined via $^1\text{H-NMR}$ by comparison of the constant naphthalene signals to the olefinic signal of NAM at $t = 0 \text{ min}$ and at the end after 3 h. M_n , M_w and dispersity were determined via THF GPC. The product was isolated as slightly yellow transparent high viscous paste in a yield of 46.9% (242 mg).

$^1\text{H-NMR}$ (400 Mhz, CDCl_3):

δ ppm 5.57 (dd; 1H; $J_1 = 1.51 \text{ Hz}$; $J_2 = 10.19 \text{ Hz}$;
(MPAA, $\text{CH}=\text{CHH}$))

7.41 (dt; 4H; $J_1 = 3.51 \text{ Hz}$; $J_2 = 9.76 \text{ Hz}$;
(naphtalene, $(=\text{oCH}=\text{pCH}=\text{pCH}=\text{oCH}=\text{)}_2$)

Monomer conversion = 92 %

$M_{n, \text{NMR}} = 20400 \text{ g mol}^{-1}$

GPC $M_{n, \text{GPC}} = 8500 \text{ g mol}^{-1}$
 $M_{w, \text{GPC}} = 12300 \text{ g mol}^{-1}$
 $\bar{D} = 1.45$

5 Modification of end groups

5.1 Aminolysis induced end group formation to thiol groups

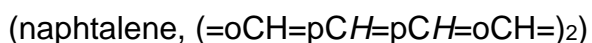
5.1.1 Synthesis of a pNAM homopolymer with 10 monomer units by CDTPA as RAFT reagent for aminolysis reaction (pNAM2k)

	Weight [mg]	Molar amount [mmol]	Molecular weight [g/mol]	Equiv. []	Volume [mL]
CDTPA	71.37	0.177	403.67	1	-
AIBN	3.75	0.023	164.21	0.13	-
Naphtalene	49.34	0.385	128.17	-	-
NAM	251.69	1.783	141.17	10.08	-
Dioxane	930	-	-	-	-

The synthesis was performed according to the general procedure for RAFT polymerizations with the half scale. A ratio of monomer:CTA of 10.08:1 and a ratio of CTA:initiator of 7.74:1 was applied. The conversion was determined via $^1\text{H-NMR}$ by comparison of the constant naphthalene signals to the olefinic signal of NAM at $t = 0 \text{ min}$ and at the end after 3 h. M_n , M_w and dispersity were determined via THF GPC. The product was isolated as slightly yellow viscous liquid in a yield of 53.6 % (173 mg).

$^1\text{H-NMR}$ (400 Mhz, CDCl_3):

δ ppm 5.65 (dd; 1H; $J_1 = 1.95 \text{ Hz}$; $J_2 = 10.55 \text{ Hz}$;
(NAM, CH=CHH))
7.41 (dt; 4H; $J_1 = 3.51 \text{ Hz}$; $J_2 = 9.76 \text{ Hz}$;



Monomer conversion = 99 %

$M_{n, NMR} = 1800 \text{ g mol}^{-1}$

5.1.2 Synthesis of a pMPAA homopolymer with 10 monomer units by CDTPA as RAFT reagent for aminolysis reaction (pMPAA2k)

	Weight [mg]	Molar amount [mmol]	Molecular weight [g/mol]	Equiv. []	Volume [mL]
CDTPA	71.16	0.176	403.67	1	-
AIBN	3.75	0.023	164.21	0.13	-
Naphtalene	53.42	0.417	128.17	-	-
MPAA	250.85	1.752	143.19	9.94	-
Dioxane	0.91	-	-	-	-

The synthesis was performed according to the general procedure for RAFT polymerizations with the half scale. A ratio of monomer:CTA of 9.94:1 and a ratio of CTA:initiator of 7.72:1 was applied. The conversion was determined via ¹H-NMR by comparison of the constant naphthalene signals to the olefinic signal of NAM at t = 0 min and at the end after 3 h. M_n , M_w and dispersity were determined via THF GPC. The product was isolated as slightly yellow viscous liquid in a yield of 49.7 % (160 mg).

¹H-NMR (400 Mhz, CDCl₃):

δ ppm	5.57	(dd; 1H; $J_1 = 1.51 \text{ Hz}$; $J_2 = 10.19 \text{ Hz}$; (MPAA, CH=CHH))
	7.41	(dt; 4H; $J_1 = 3.51 \text{ Hz}$; $J_2 = 9.76 \text{ Hz}$; (naphthalene, (=oCH=pCH=pCH=oCH=) ₂)

Monomer conversion = 98 %

$M_{n, NMR} = 1800 \text{ g mol}^{-1}$

5.2 Radical induced end group formation with 4, 4'-azobis (4-cyanovaleric acid) (ACVA)

5.2.1 Synthesis of a 10 kDa pNAM homopolymer by CDTPA as RAFT reagent for the radical endgroup formation (pNAM10k)

	Weight [mg]	Molar amount [mmol]	Molecular weight [g/mol]	Equiv. []	Volume [mL]
CDTPA	21.10	0.052	403.67	1	-
AIBN	1.20	0.007	164.21	0.14	-
Naphtalene	100.14	0.781	128.17	-	-
NAM	500.15	3.543	141.17	68.10	-
Dioxane	1821	-	-	-	-

The synthesis was performed according to the general procedure for RAFT polymerizations. A ratio of monomer:CTA of 68.1:1 and a ratio of CTA:initiator of 7.12:1 was applied. The conversion was determined via ¹H-NMR by comparison of the constant naphthalene signals to the olefinic signal of NAM at t = 0 min and at the end after 3 h. M_n, M_w and dispersity were determined via THF GPC. The product was isolated as white-slightly yellow powder in a yield of 62.4 % (325 mg).

¹H-NMR (400 Mhz, CDCl₃):

δ ppm	5.65	(dd; 1H; J ₁ = 1.95 Hz; J ₂ = 10.55 Hz; (NAM, CH=CHH))
	7.41	(dt; 4H; J ₁ = 3.51 Hz; J ₂ = 9.76 HZ; (naphtalene, (=oCH=pCH=pCH=oCH=) ₂)

Monomer conversion = 99 %

M_{n, NMR} = 10000 g mol⁻¹

GPC $M_{n, GPC} = 4100 \text{ g mol}^{-1}$
 $M_{w, GPC} = 5400 \text{ g mol}^{-1}$
 $\bar{D} = 1.31$

5.2.2 Synthesis of a 10 kDa pMPAA homopolymer by CDTPA as RAFT reagent for the radical endgroup formation (pMPAA10k)

	Weight [mg]	Molar amount [mmol]	Molecular weight [g/mol]	Equiv. []	Volume [mL]
CDTPA	21.01	0.052	403.67	1	-
AIBN	1.09	0.007	164.21	0.13	-
Naphtalene	99.95	0.78	128.17	-	-
MPAA	499.97	3.492	143.19	67.09	-
Dioxane	1802	-	-	-	-

The synthesis was performed according to the general procedure for RAFT polymerizations. A ratio of monomer:CTA of 67.09:1 and a ratio of CTA:initiator of 7.84:1 was applied. The conversion was determined via $^1\text{H-NMR}$ by comparison of the constant naphthalene signals to the olefinic signal of NAM at $t = 0 \text{ min}$ and at the end after 3 h. M_n , M_w and dispersity were determined via THF GPC. The product was isolated as slightly yellow transparent viscous paste in a yield of 56.4 % (294 mg).

$^1\text{H-NMR}$ (400 Mhz, CDCl_3):

δ ppm	5.57	(dd; 1H; $J_1 = 1.51 \text{ Hz}$; $J_2 = 10.19 \text{ Hz}$; (MPAA, $\text{CH}=\text{CHH}$))
	7.41	(dt; 4H; $J_1 = 3.51 \text{ Hz}$; $J_2 = 9.76 \text{ Hz}$; (naphtalene, $(=\text{oCH}=\text{pCH}=\text{pCH}=\text{oCH}=\text{)}_2$)

Monomer conversion = 95 %

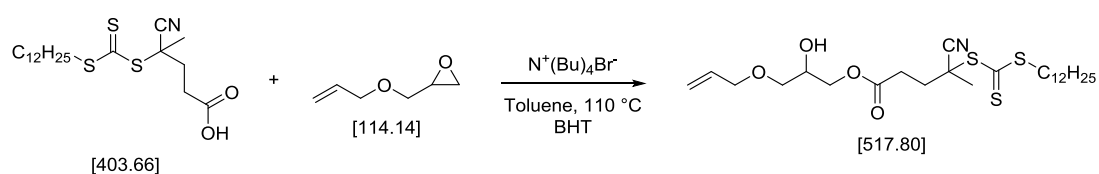
$M_{n, NMR} = 9500 \text{ g mol}^{-1}$

GPC $M_{n, GPC} = 5200 \text{ g mol}^{-1}$
 $M_{w, GPC} = 7300 \text{ g mol}^{-1}$
 $\bar{D} = 1.39$

6 Synthesis of a RAFT reagent with an ethoxysilane end group

6.3 Screening for alternative coupling methods

6.3.1 Synthesis of 3-(allyloxy)-2-hydroxypropyl 4-cyano-4-(((dodecylthio)carbonothioyl)thio)pentanoate



	Weight [mg]	Molar amount [mmol]	Molecular weight [g/mol]	Equiv. []	Volume [mL]
CDTPA	49.5	0.12	403.67	1.5	
Allyl glycidyl ether	10.0	0.09	114.12	1	
BHT	1.1	0.005	220.35	0.05	
tetrabutylammonium bromide	1.5	0.005	322.36	0.05	
toluene	-	-	-	-	3

CDTPA (49.5 mg, 0.12 mmol), allyl glycidyl ether (10 mg; 0.09 mmol), BHT (1.1 mg, 0.005 mmol) and tetrabutylammonium bromide (1.5 mg, 0.005 mmol) were dissolved in toluene (3 mL) and heated to 110 °C for a time of 5 h. Afterwards the reaction mixture was diluted with DCM, washed with saturated bicarbonate solution (2 x 5 mL) and dried over sodium sulfate. The solvent was removed under reduced pressure and the product was separated by liquid column chromatography (PE:EE = 1:1). The fractions were collected and analyzed via ¹H-NMR. The yield was calculated by comparison of the terminal allylic H-signals to the –S-CH₂- signal and gave 13 % yield

$^1\text{H-NMR}$ (400 Mhz, CDCl_3):

δ ppm	3.33	(d; 2H; $J_1 = 7.44$ Hz; ($-\text{S}-\text{CH}_2-$))
	5,22	(dd; 0.14H; $J_1 = 1.60$ Hz; $J_2 = 10.27$ Hz; ($\text{CH}=\text{CHH}$))
	5.28	(dd; 0.14H; $J_1 = 1.55$ Hz; $J_2 = 17.25$ Hz; ($\text{CH}=\text{CHH}$))

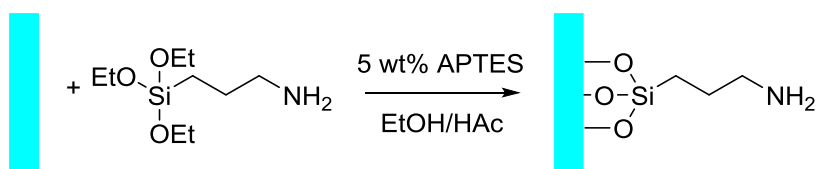
7 Analysis of coating homogeneity using APTES for functionalization of glass surfaces

7.1 General procedure for the functionalization of glass and silicon wafer surfaces

The glass cover slips or silicon wafers were cleaned in toluene, acetone and water under supersonication for a time of 5 min, respectively. Then they were activated by piranha acid ($\text{H}_2\text{SO}_{4\text{conc.}} : \text{H}_2\text{O}_2$ (30 %) = 7:3) at 80 °C for a time 1 h, afterwards rinsed with water and ethanol.

The calculated weight share of alkoxy silane compound was calculated and dissolved in a 97 : 3 mixture of EtOH / HAc (HAc; 1 : 10 diluted in deionized water), and degassed with argon for a time of 15 min. Subsequently the cleaned glass or silicon wafer was dipped into this solution for a time of 24 h. Afterwards the sample was removed, rinsed with EtOH and acetone, and dried under argon stream.

7.2 Synthesis of aminopropyl functionalized SiO_2 surfaces



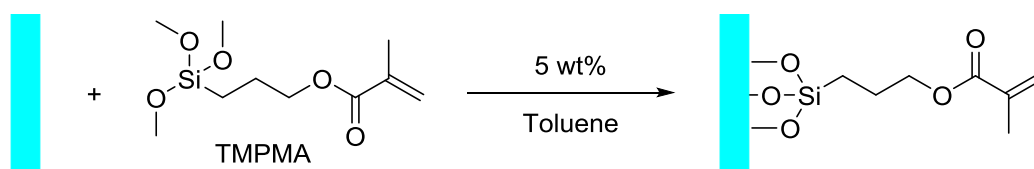
	Weight [mg]	Weight share [wt%]	Volume [mL]	Volume share [v%]
EtOH	-	-	19.4	97
HAc diluted 10:1	-	-	0.6	3
APTES	795	5	-	--

The synthesis was performed according to the general procedure for the functionalization of glass and silicon wafer surfaces. The substrate was analyzed via CA measurement and TIRFM.

Sample	Static CA [°]	± [°]	Advancing CA [°]	Receding CA [°]	CA hysteresis Θ [°]
APTES 5%	53.80	±0.77	65.5	31.1	34.4

8 Modification of the SiO₂ surfaces with RAFT reagents

8.3 Synthesis of 3-(trimethoxysilyl)propyl methacrylate (TMPMA) functionalized SiO₂ surfaces



	Weight [mg]	Weight share [wt%]	Volume [mL]	Volume share [v%]
Toluene	-	-	19.2	96
TMPMA	836	5	0.8	4

The cleaning process was performed according to the general procedure for the functionalization of glass and silicon wafer surfaces. After the cleaning process the silicon wafer sample was dipped into a degassed 5 wt% solution of TMPMA in toluene

for a time of 24 h. Afterwards, the sample was rinsed with toluene and acetone, and dried under argon stream. The sample was characterized via CA measurement and ellipsometry.

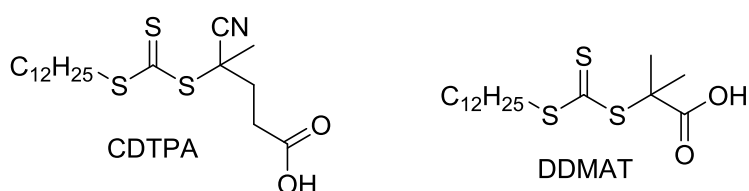
CA sample	Static CA [°]	± [°]	Advancing CA [°]	Receding CA [°]	CA hysteresis Θ [°]
Surface-TMPMA	73.34	± 1.23	77.9	61.5	16.4

Ellipsometry Sample	Layer thickness [Å]	Confidence_{95 %} [Å]
Blank; SiO ₂ layer thickness	13.20	± 0.24
Additional layer thickness after TMPMA functionalization	15.86	± 0.52

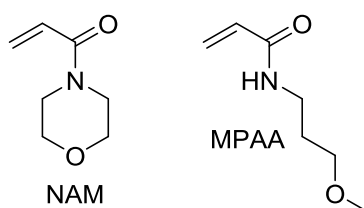
Summary

A polymer linker system for the application as covalent bonded polymer brush system in cell-biologic analysis with total internal reflection fluorescence microscopy should be investigated. Therefore, surface induced RAFT polymerization was chosen as “grafting from” polymerization method, due to the possibility to generate uniform polymer chain lengths and to introduce potential end-functionality for coupling with biomolecules. For the optical analyses with TIRFM, glass cover slips are needed, and were used as substrate for the immobilization of these, so called, RAFT reagents or chain transfer agents. After this immobilization of the RAFT reagent, polymer brushes should be generated by surface induced RAFT polymerization in an R-group attempt, for a possible end-group formation.

During this thesis, two CTA agents were synthesized, CDTPA and DDMAT, and kinetic studies of these CTA were performed with NAM and MPAA as monomers (**Scheme 45**, **Scheme 46** and **Figure 93**).



Scheme 45. The CTAs; CDTPA (left), DDMAT (right)



Scheme 46. The monomers NAM (left); MPAA (right)

Both RAFT reagents performed well with the monomers in high monomer throughput and short times to reach maximum monomer conversions, independent of small inhibition periods at the beginning. The only exception was DDMAT in combination with MPAA for a higher target molecular weight of 40 kDa. These conditions resulted in a

loss of control and a higher dispersity of $\bar{M}_w = 1.67$ compared to the other polymerization with dispersities < 1.5 .

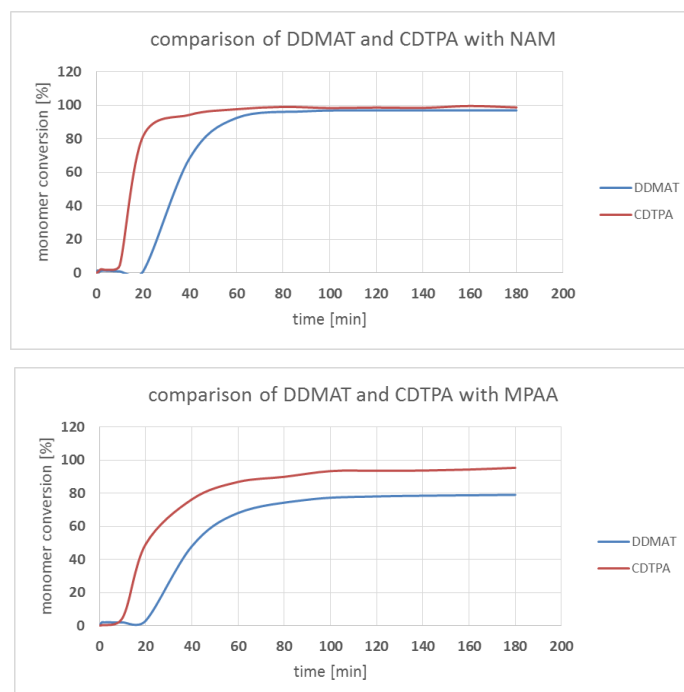


Figure 93. Comparison of CDTPA and DDMAT in their kinetical behavior

These generated pNAM and pMPAA polymers with a MW of approximately 20 kDa were investigated via SLS, DLS and SAXS to determine their size and shape in aqueous solution as well as stability of the formed structures. The results of these measurements showed, that strong aggregation occurred in aqueous solution, and that the formed aggregates exhibited a Kholodenko-worm-like shape in water (**Figure 94**) as well as PBS buffer solution.

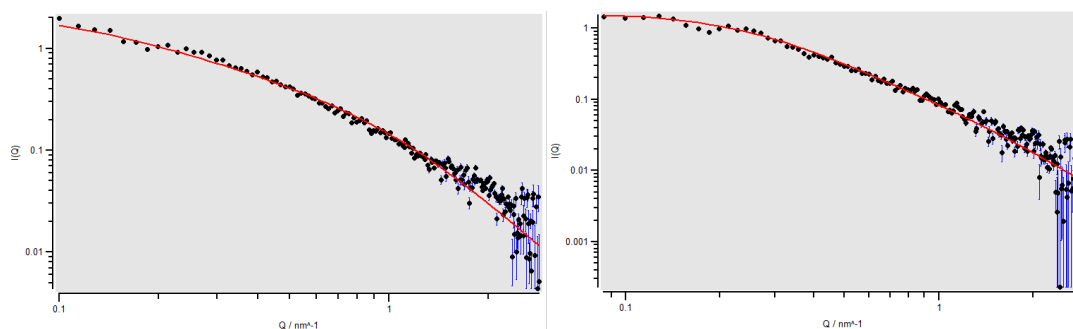
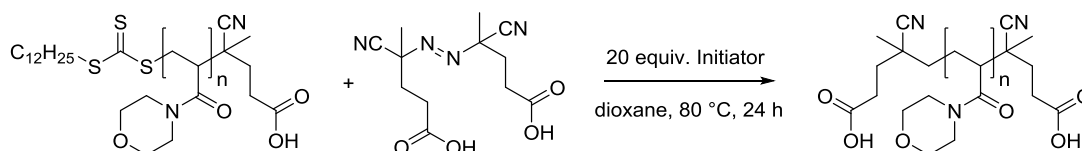


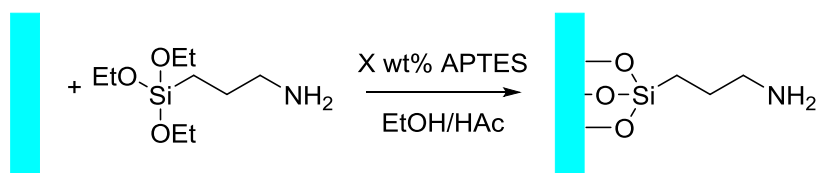
Figure 94. SAXS measurements of pNAM 20 kDa (left) and pMPAA 20 kDa (right) in water with mathematical Kholodenko worm-like fit

Furthermore, experiments for the end-group modification of pNAM and pMPAA were applied, to be able to couple polymers with biomolecules. Two different approaches were applied: Aminolysis with hexylamine and radical induced end-group formation with 4, 4'-azobis (4-cyanovaleric acid) (ACVA) as initiator. The aminolysis approach showed problems due to disulfide bond formation and was therefore not perfect for the handling of this system. Radical induced end-group formation delivered better results, due to oxygen stable products, so this method turned out to be the method of choice for further experiments (**Scheme 47**).



Scheme 47. Radical induced end group modification of CDTPA-pNAM with ACVA

For the functionalization of the glass substrate surfaces, the alkoxy silane compound that was investigated, was (3-aminopropyl)triethoxysilane. To get an idea of the homogeneity of the APTES distribution on the glass surface, a screening for the coupling of pure APTES to the glass surface at different concentrations was performed. The introduced amine groups bound to the surface by this screening experiments, were afterwards coupled with a fluorescence marker and investigated with TIRFM, to determine the highest density of amine groups, on the basis of microscopy (**Figure 95**). The results of this investigation showed that the 5 wt% solution of APTES introduced the largest amount of amine groups to the surface, over a time of 24 h.

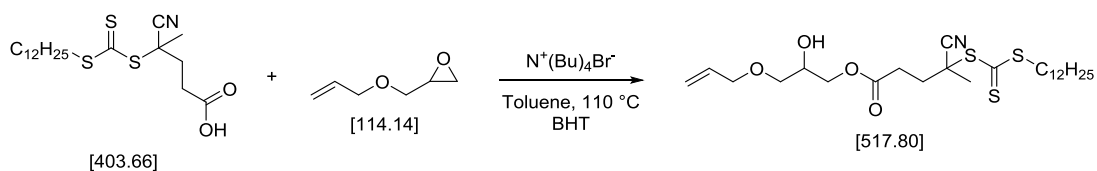


Scheme 48. Functionalization of glass with APTES



Figure 95. Comparison of the TIRFM images of the functionalization with APTES in 3 wt% (left), 4 wt% (middle) and 5 wt% solution (right)

Furthermore, a screening for a coupling method for the amide bond formation of the CTA to APTES was applied, using the coupling reagents DCC and EDC, as well as a screening for a coupling possibility to epoxy compounds via epoxy-carboxylic acid reaction. The results of the APTES coupling methods showed no mentionable difference in performance and the results of the coupling of the CTA to epoxy dummy compounds showed for the reaction with an allylic glycidylester about 11 % yield, calculated by $^1\text{H-NMR}$ (**Scheme 49**).

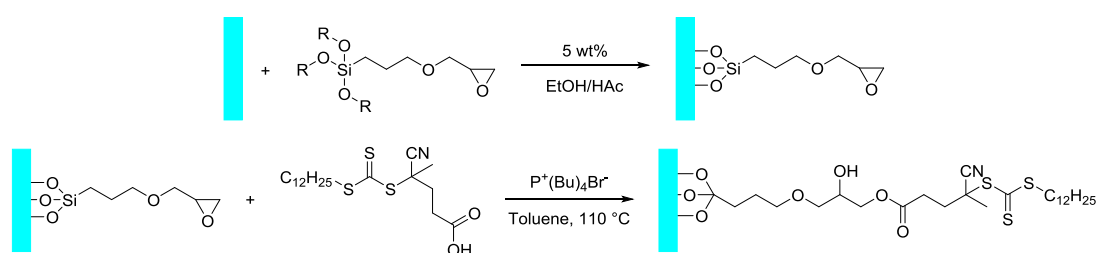


Scheme 49. Coupling of the CTA to an allylic glycidylester via epoxy-carboxylic acid reaction

For the coupling of a CTA to the substrates surface, three different pathways were applied. Pathway (1), pre-functionalization of the surface with APTES, then coupling to the CTA, pathway (2), the direct functionalization of the surface via a synthesized CTA with alkoxy silane end-group by coupling to APTES, and pathway (3), the macro-RAFT pathway with functionalization of the surface with TMPMA, pre-polymerization of the CTA to the surface. These approaches were analyzed via contact angle, ellipsometry and partially with XPS. The direct functionalization showed traces of sulfur on the surface, but the atomic ration of S / N did not fit to the anticipated surface composition. The other approaches gave no mentionable results in surface composition or additional layer thickness.

Due to the fact, that this project will be continued in a PhD thesis, there will be sufficient room for enhancement of the developed methods and for the application of the acquired data of this thesis. As the RAFT polymerization of the monomers NAM and MPAA worked out fine for the investigated CTAs, it will be of major interest to improve the surface functionalization with the RAFT agents to be able to build up a polymer brush system. Already a few considerations, also partial according to literature were discovered.

The first approach to establish the functionalization of the substrate might be the pre-functionalization of the surface with an alkoxy silane-glycidylester and coupling to the CTA via epoxy-carboxylic acid reaction mentioned in chapter 6.6 (**Scheme 50**) with a high performance catalyst⁸⁹.

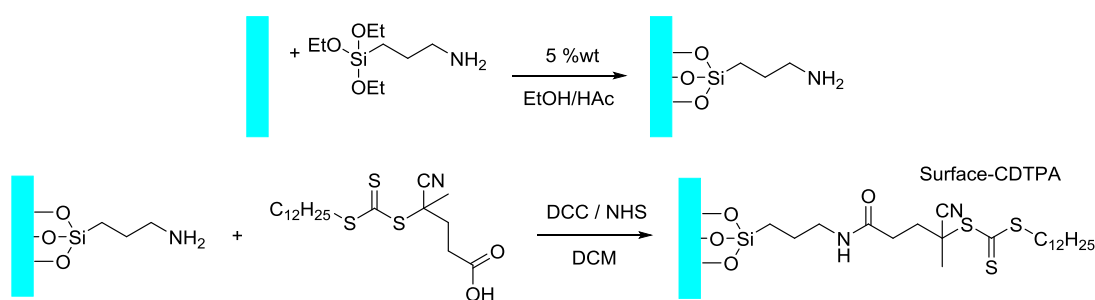


Scheme 50. Glycidyl ester pre-functionalization and epoxy carboxylic acid reaction to couple the CTA

If this approach worked, it would be possible to avoid simultaneous aminolysis reaction and it would be possible to cleave the polymer chains after the generation of brushes

by saponification. This would also give the possibility to analyze the generated brush polymers via GPC after cleavage and thus their molecular weight and dispersity.

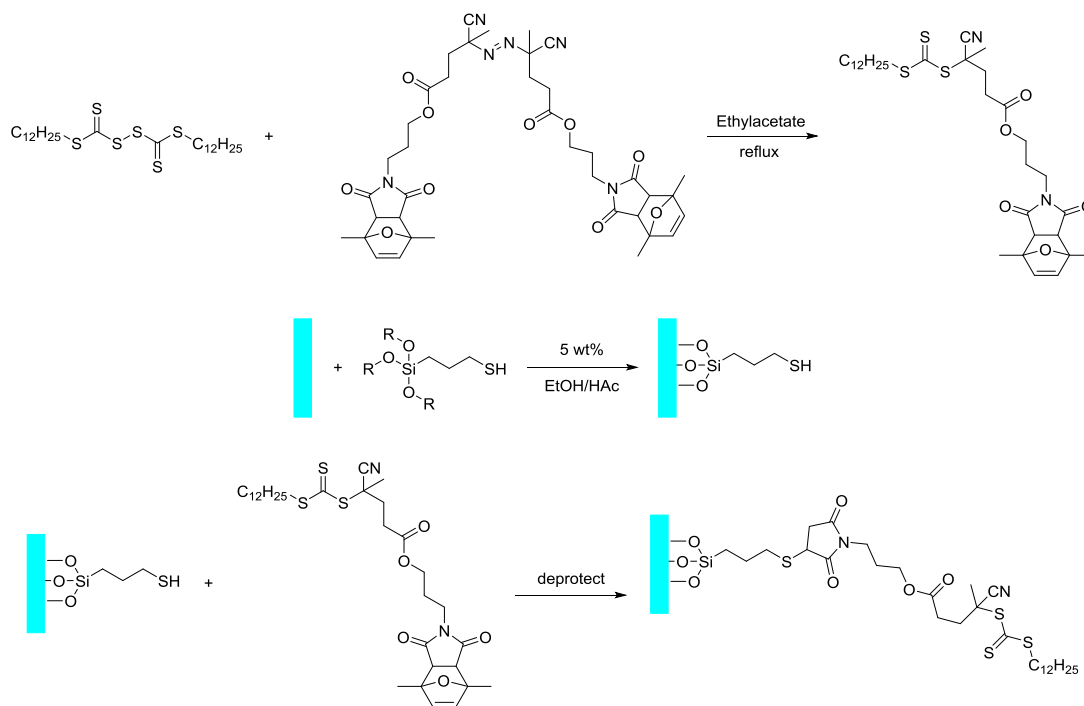
Another possibility, to improve the functionalization is the synthesis of an NHS-ester CTA first, by use of NHS in the coupling solution, pre-functionalize the surface with APTES, and couple the CTA to the substrates surface via NHS-coupling (**Scheme 51**)²³.



Scheme 51. Pre-functionalization with APTES and NHS coupling to the CTA

This method could improve the system, already tested in chapter 8.1.

The use of thiol-maleimide click reaction could also be a prospect for a good working functionalization. Therefore the substrates surface will be pre-functionalized with 3-(triethoxysilyl)propane-1-thiol and a CTA reagent with a maleimide end-group must be synthesized first and coupled to the surface. The protected maleimide azo initiator mentioned in chapter 5.3 (**Fehler! Verweisquelle konnte nicht gefunden werden.**) could be a possibility to overcome a lot of follow-up steps (**Scheme 52**).



Scheme 52. Synthesis of a maleimide end-group CTA, pre-functionalization with thiol group and click coupling to the CTA

This azo initiator could also be used also to modify the end-group of the generated polymer⁷⁶, and substitute the need for a linker to the biomolecule.

After the establishing of one of these linking systems, the generation of polymer brushes using NAM and MPAA could be applied and coupled to biomolecules for the further investigations of theses with TIRFM.

Materials, devices, analytics

Materials

Glass cover slips (Menzel Gläser 24x60 mm #1.5), dodecanethiol (Sigma-Aldrich), carbon disulfide (Loba Feinchemie), Iodine (Sigma-Aldrich), potassium-*tert*-butanolate (Sigma-Aldrich), tetrahydrofurane (VWR), ethylacetate (Fluka), hexane (VWR), ACVA (Sigma-Aldrich), AIBN (Sigma-Aldrich), dioxane (JT-Baker chemicals), naphthalene (Merck), NAM (TCI chemicals), MPAA (Sigma-Aldrich), acetone (Donau Chemie), 2-bromo-2-methylpropanoic acid (Sigma-Aldrich), potassium carbonate (Alfa Aesar), APTES (Fluka), DCC (Fluka), DMAP (Acros), EDCxHCl (Fluka), silica (Merck), Alexa Fluor® 680 NHS Ester (ThermoFischer), silicon wafer (MEMC Electr. Materials Sdn Bhd, Boron P-type)

Analytical methods

NMR

¹H-NMR spectra were recorded on a *Bruker 400 NMR*. 10 mg of sample were dissolved in deuterated solvents. For ¹H-NMR spectra a scan number of 16 was chosen.

Goniometry

Contact angle measurements were applied on a Krüss DSA 30 in combination with the provided Krüss ADVANCE 1.5.1.0 software. The device was equipped with a CCD camera with a resolution of 780x582 and could record 60 frames per second. Further a software controlled inclinable stage was installed, and this stage was improved with a custom-built housing which allowed better saturation of the atmosphere around the sample with probe liquid and protection of surrounding drafts. Static contact angles were determined by placing a drop of 15 µL Milli-Q water on the samples surface. Data analysis was performed by the Young-Laplace method of the instrument software. Dynamic contact angles were determined by tilting this 15 µL drop of water, until the drop rolled of the surface. Data analysis of receding and advancing contact angle was executed by the tangent method. The measurements of both methods were averaged.

Static and Dynamic Light Scattering

An ALV/CGS3 compact goniometer system equipped with an ALV7004 correlator was used for the determination of gyration radius (R_g) and hydrodynamic radius (R_h). The light source was a 50 mW HeNe laser and the temperature was set at 25°C. The light scattering signal was recorded for 30 seconds and 3 times for each angle from 30° to 140° with steps of 10°. The software ALVstat was used for the data analysis. Almost five different concentrations of each polymer solution were analyzed and R_g and R_h was extrapolated from the Zimm plot and the Dynamic Zimm plot, respectively, for each sample.

Small angle X-ray scattering

X-rays were used from a Bruker AXS Nanostar SAXS device (Universität Wien), equipped with an area detector (VÅNTEC 2000 gas detector). A microfocus X-ray tube system produces $\text{CuK}\alpha$ radiation with a brilliance of about $2 \cdot 10^8$ photons s^{-1} on the sample at a beam diameter of 0.5 mm. The samples were filled into quartz capillaries with an outer diameter of 1.5 mm and a wall thickness of 0.01 mm. The capillaries were air tight heat-sealed via a shrinking hose. The samples were measured under vacuum for a time of 6 h, respectively, for each sample in an angular range of 0.1 – 4°, scattering vector range of 0.08 – 2.2 nm^{-1} and sample to detector distance of 108 cm. The software SASfit was used for the analysis of the obtained scattering images.

Ellipsometry

Ellipsometric measurements were carried out using a Sentech SE 500adv which uses a He-Ne as light source and a rotating analyzer. The utilized wavelength was 632.8 nm. Data analysis was done with the supplied instrument software SE400advanced 2.16 which uses the McCracking algorithm. The used optical constants were Si ($n = 3.865$, $k = 0.02$), SiO_2 ($n = 1.465$, $k = 0$), organic layer ($n = 1.5$, $k = 0$). The measurements were done at four different spots on each samples surface, measured twice this spot, and were then averaged.

X-ray photoelectron spectroscopy

XPS measurements were conducted with a SPECS XPS-Spectrometer, equipped with a monochromatic Al K α X-ray source (μ Focus 350) and a hemispheric WAL-150 analyzer (angle of acceptance: 60 °). The glass and silicon wafer samples were fastened with Mo clamps on the specimen holder. The measurement of the survey spectra was applied with a pass energy of 100 eV and energy resolution of 500 meV, whereas for the measurement of the detail spectra a pass energy of 30 eV and for energy resolution 50 meV (excitation energy: 1486.6 eV, size of spot: 500 μ m, 93 W, angle: 51 °) Because of strong (partial) charging effects on the glass samples a Flood Gun (10 eV at 25 μ A) was used for compensation. Evaluation of the generated data was performed with CASA XPS software by use of correction of transmission (according to manufacturer information) and sensitivity parameters according to Scofield⁹¹. Charge corrections were done, the way that C-C components in the C 1s signal were found at 284.8 eV binding energy. The information of the elements is specified in atom percent (%at), with a threshold of 0.1 %at for reasonable quantification (0.3 %at for S) out of the survey spectra. The accuracy of the quantification is, depending on the element, about 10 – 20 %. The classification of the individual components was carried out after ^{92, 93}. For the quantification the average value of the chemical composition was calculated for a measurement depth of 7- 10 nm by angle integrated measurement.

Gel permeation chromatography

Molecular weight of the measured samples were determined via Viscotek 270 Dual Detector RI refractive index detector. Samples were separated with Styragel® HR 0.5 THF 7.8 x 300 mm Column (molecular weight range 0–1 K), Styragel® HR 3 THF 7.8 x 300 mm Column (molecular weight range 500–30 K) and Styragel® HR 4 THF 7.8 x 300 mm Column (molecular weight range 5 K–600 K). A Styragel® Guard Column, 20 μ m, 4.6 x 30 mm, 100–10 K precolumn was used. Calibration was performed with polystyrol standards (Polymer Standard Service) of different molecular weights. As eluent THF, stabilized with 250 ppm BHT, was used with a flow rate of 1 mL/min and columns were heated at 40 °C. Samples for THF-GPC were prepared

with a concentration of 5 mg/mL and filtered with a 0.45 μm filter. Analysis of the data was executed by OmniSec software from Malvern.

Aqueous GPC measurements were applied on a Phase 19" Modular GPC from Orange Analytics with RI detection and a Waters Ultrahydrogel 250 separation column. 1 mg of sample were dissolved in 1 mL milli-Q water and a flow rate of 1 mL min^{-1} milli-Q water was applied. Analysis of the data was executed by PARSEC software from Brookhaven Instruments. Evaluation of the measured samples according to a PEG standard (Polymer Standard Service).

Abbreviations

TCR	T cell receptor
TIRFM	Total internal reflection fluorescence microscopy
GFP	Green fluorescent protein
CRP	Controlled radical polymerization
SIP	Surface initiated polymerization
APTES	(3-aminopropyl)triethoxysilane
HEMA	2-hydroxyethyl methacrylate
rt	Room temperature
XPS	X-ray photoelectron spectroscopy
AFM	Atomic force spectroscopy
EDC	1-Ethyl-3-(3-dimethylaminopropyl)carbodiimide
DMAP	4-Dimethylaminopyridine
V40	1,1'-Azobis(cyclohexanecarbonitrile)
AIBN	Azobisisobutyronitrile
CTA	chain transfer agent

DLS	Dynamic light scattering
NIPAM	N-isopropylacrylamide
LCST	Lower critical solution temperature
AGA	N-acryloyl glucosamine
PEG	Polyethylene glycol
CDTPA	4-cyano-4-(((dodecylthio)carbonothioyl)thio)pentanoic acid
DDMAT	2-(((dodecylthio)carbonothioyl)thio)-2-methylpropanoic acid
Si-CTA	Alkoxy-silane functionalized CTA
NMR	Nucleus magnetic resonance
SEC	Size exclusion chromatography
PE	Petrol ether
Đ	Dispersity
SLS	Static light scattering
DLS	Dynamic light scattering
SAXS	Small angle X-ray scattering
R _g	Radius of gyration
R _H	Hydrodynamic radius
PBS buffer	phosphate buffered saline buffer
DCM	Dichloromethane
PE	Petrol ether
TCEP	Tris(2-carboxyethyl)phosphine
ACVA	4,4'-Azobis(4-cyanovaleric acid)

DCC	N,N'-Dicyclohexylcarbodiimide
DMAP	4-Dimethylaminopyridine
EE	Ethylacetate
PS	Polystyrene
BHT	Butylated hydroxytoluene
EtOH	Ethanol
HAc	Acetic acid
CA	Contact angle
NHS	N-Hydroxysuccimide
RAFT	Reversible addition fragmentation chain transfer polymerization
ATRP	Atom-transfer radical polymerization
MW	Molecular weight
THF	Tetrahydrofuran
Std	Standard
TMPMA	3-(trimethoxysilyl)propyl methacrylate
FRP	Free Radical Polymerisation
PRE	Persistent radical effect
SFRP	Stable free radical polymerization
APTES	(3-aminopropyl) triethoxysilane

Literature

- (1) Krishnamoorthy, M.; Hakobyan, S.; Ramstedt, M.; Gautrot, J. E. "Surface-Initiated Polymer Brushes in the Biomedical Field: Applications in Membrane Science, Biosensing, Cell Culture, Regenerative Medicine and Antibacterial Coatings"; *Chemical Reviews* 2014, **114** (21), 10976-11026.
- (2) Xu, F. J.; Neoh, K. G.; Kang, E. T. "Bioactive surfaces and biomaterials via atom transfer radical polymerization"; *Progress in Polymer Science* 2009, **34** (8), 719-761.
- (3) Raynor, J. E.; Capadona, J. R.; Collard, D. M.; Petrie, T. A.; García, A. J. "Polymer brushes and self-assembled monolayers: Versatile platforms to control cell adhesion to biomaterials (Review)"; *Biointerphases* 2009, **4** (2), FA3-FA16.
- (4) Ayres, N. "Polymer brushes: Applications in biomaterials and nanotechnology"; *Polymer Chemistry* 2010, **1** (6), 769-777.
- (5) Bünsow, J.; Kelby, T. S.; Huck, W. T. S. "Polymer Brushes: Routes toward Mechanosensitive Surfaces"; *Accounts of Chemical Research* 2010, **43** (3), 466-474.
- (6) Radhakrishnan, B.; Ranjan, R.; Brittain, W. J. "Surface initiated polymerizations from silica nanoparticles"; *Soft Matter* 2006, **2** (5), 386-396.
- (7) Li, W.; Nakayama, M.; Akimoto, J.; Okano, T. "Effect of block compositions of amphiphilic block copolymers on the physicochemical properties of polymeric micelles"; *Polymer* 2011, **52** (17), 3783-3790.
- (8) Yamazaki, A.; Winnik, F. M.; Cornelius, R. M.; Brash, J. L. "Modification of liposomes with N-substituted polyacrylamides: identification of proteins adsorbed from plasma"; *Biochimica et Biophysica Acta (BBA) - Biomembranes* 1999, **1421** (1), 103-115.
- (9) Feng, W.; Chen, R.; Brash, J. L.; Zhu, S. "Surface-Initiated Atom Transfer Radical Polymerization of Oligo(ethylene glycol) Methacrylate: Effect of Solvent on Graft Density"; *Macromolecular Rapid Communications* 2005, **26** (17), 1383-1388.
- (10) Perruchot, C.; Khan, M. A.; Kamitsi, A.; Armes, S. P.; von Werne, T.; Patten, T. E. "Synthesis of Well-Defined, Polymer-Grafted Silica Particles by Aqueous ATRP"; *Langmuir* 2001, **17** (15), 4479-4481.
- (11) Jones, D. M.; Huck, W. T. S. "Controlled Surface-Initiated Polymerizations in Aqueous Media"; *Advanced Materials* 2001, **13** (16), 1256-1259.
- (12) Marx, K. A. "Quartz Crystal Microbalance: A Useful Tool for Studying Thin Polymer Films and Complex Biomolecular Systems at the Solution-Surface Interface"; *Biomacromolecules* 2003, **4** (5), 1099-1120.
- (13) Homola, J.; Yee, S. S.; Gauglitz, G. "Surface plasmon resonance sensors: review"; *Sensors and Actuators B: Chemical* 1999, **54** (1-2), 3-15.
- (14) Lutolf, M. P.; Hubbell, J. A. "Synthetic biomaterials as instructive extracellular microenvironments for morphogenesis in tissue engineering"; *Nat Biotech* 2005, **23** (1), 47-55.
- (15) Cole, M. A.; Voelcker, N. H.; Thissen, H.; Griesser, H. J. "Stimuli-responsive interfaces and systems for the control of protein-surface and cell-surface interactions"; *Biomaterials* 2009, **30** (9), 1827-1850.
- (16) Lichter, J. A.; Van Vliet, K. J.; Rubner, M. F. "Design of Antibacterial Surfaces and Interfaces: Polyelectrolyte Multilayers as a Multifunctional Platform"; *Macromolecules* 2009, **42** (22), 8573-8586.
- (17) Schierholz, J. M.; Beuth, J. "Implant infections: a haven for opportunistic bacteria"; *Journal of Hospital Infection* 2001, **49** (2), 87-93.
- (18) Tsujii, Y.; Ohno, K.; Yamamoto, S.; Goto, A.; Fukuda, T., Structure and Properties of High-Density Polymer Brushes Prepared by Surface-Initiated Living

Radical Polymerization. in *Surface-Initiated Polymerization I*, Jordan, R., Ed. Springer Berlin Heidelberg: Berlin, Heidelberg, 2006; pp 1-45.

(19) Barbey, R.; Lavanant, L.; Paripovic, D.; Schüwer, N.; Sugnaux, C.; Tugulu, S.; Klok, H.-A. "*Polymer Brushes via Surface-Initiated Controlled Radical Polymerization: Synthesis, Characterization, Properties, and Applications*"; Chemical Reviews 2009, **109** (11), 5437-5527.

(20) Zamfir, M.; Rodriguez-Emmenegger, C.; Bauer, S.; Barner, L.; Rosenhahn, A.; Barner-Kowollik, C. "*Controlled growth of protein resistant PHEMA brushes via S-RAFT polymerization*"; Journal of Materials Chemistry B 2013, **1** (44), 6027-6034.

(21) Phan, T. N. T.; Jestin, J.; Gimes, D., Nitroxide-Mediated Polymerization from Surfaces. in *Controlled Radical Polymerization at and from Solid Surfaces*, Vana, P., Ed. Springer International Publishing: Cham, 2016; pp 1-27.

(22) Ahmad, R.; Mocaer, A.; Gam-Derouich, S.; Lamouri, A.; Lecoq, H.; Decorse, P.; Brunet, P.; Mangeney, C. "*Grafting of polymeric platforms on gold by combining the diazonium salt chemistry and the photoiniferter method*"; Polymer 2015, **57**, 12-20.

(23) Matsuzaka, N.; Nakayama, M.; Takahashi, H.; Yamato, M.; Kikuchi, A.; Okano, T. "*Terminal-Functionality Effect of Poly(N-isopropylacrylamide) Brush Surfaces on Temperature-Controlled Cell Adhesion/Detachment*"; Biomacromolecules 2013, **14** (9), 3164-3171.

(24) Qiu, J.; Charleux, B.; Matyjaszewski, K. "*Controlled/living radical polymerization in aqueous media: homogeneous and heterogeneous systems*"; Progress in Polymer Science 2001, **26** (10), 2083-2134.

(25) Moad, G.; Rizzardo, E.; Thang, S. H. "*Toward Living Radical Polymerization*"; Accounts of Chemical Research 2008, **41** (9), 1133-1142.

(26) Fischer, H. "*The Persistent Radical Effect: A Principle for Selective Radical Reactions and Living Radical Polymerizations*"; Chemical Reviews 2001, **101** (12), 3581-3610.

(27) Braunecker, W. A.; Matyjaszewski, K. "*Controlled/living radical polymerization: Features, developments, and perspectives*"; Progress in Polymer Science 2007, **32** (1), 93-146.

(28) Matyjaszewski, K.; Spanswick, J. "*Controlled/living radical polymerization*"; Materials Today 2005, **8** (3), 26-33.

(29) Shipp, D. A. "*Reversible-Deactivation Radical Polymerizations*"; Polymer Reviews 2011, **51** (2), 99-103.

(30) Shipp, D. A. "*Living Radical Polymerization: Controlling Molecular Size and Chemical Functionality in Vinyl Polymers*"; Journal of Macromolecular Science, Part C: Polymer Reviews 2005, **45** (2), 171-194.

(31) Matyjaszewski, K.; Xia, J. "*Atom Transfer Radical Polymerization*"; Chemical Reviews 2001, **101** (9), 2921-2990.

(32) Phuong, L. T.; Moad, G.; Rizzardo, E.; Thang, S. H. Polymerization with living characteristics. 1998.

(33) Chiefari, J.; Chong, Y. K.; Ercole, F.; Krstina, J.; Jeffery, J.; Le, T. P. T.; Mayadunne, R. T. A.; Meijs, G. F.; Moad, C. L.; Moad, G.; Rizzardo, E.; Thang, S. H. "*Living Free-Radical Polymerization by Reversible Addition-Fragmentation Chain Transfer: The RAFT Process*"; Macromolecules 1998, **31** (16), 5559-5562.

(34) Pascale, C.; Dominique, C.; Samir, Z.; Xavier, F.; Ghenwa, B. Method for block polymer synthesis by controlled radical polymerisation from dithiocarbamate compounds. 1999.

(35) Moad, G.; Rizzardo, E.; Thang, S. H. "*Living Radical Polymerization by the RAFT Process: A Third Update*"; Australian Journal of Chemistry 2012, **65** (8), 985-1076.

- (36) Matyjaszewski, K., General Concepts and History of Living Radical Polymerization. in *Handbook of Radical Polymerization*, John Wiley & Sons, Inc: 2003; pp 361-406.
- (37) Moad, G.; Rizzardo, E.; Thang, S. H. "Radical addition-fragmentation chemistry in polymer synthesis"; *Polymer* 2008, **49** (5), 1079-1131.
- (38) Lowe, A. B.; McCormick, C. L. "Reversible addition-fragmentation chain transfer (RAFT) radical polymerization and the synthesis of water-soluble (co)polymers under homogeneous conditions in organic and aqueous media"; *Progress in Polymer Science* 2007, **32** (3), 283-351.
- (39) Moad, G.; Rizzardo, E.; Thang, S. H. "Living Radical Polymerization by the RAFT Process"; *Australian Journal of Chemistry* 2005, **58** (6), 379-410.
- (40) Smith, A. E.; Xu, X.; McCormick, C. L. "Stimuli-responsive amphiphilic (co)polymers via RAFT polymerization"; *Progress in Polymer Science* 2010, **35** (1-2), 45-93.
- (41) Moad, G. R., E., Thang, S. H., "A RAFT Tutorial"; *The stream chemiker* 2011, **XXV** (1).
- (42) Perrier, S.; Barner-Kowollik, C.; Quinn, J. F.; Vana, P.; Davis, T. P. "Origin of Inhibition Effects in the Reversible Addition Fragmentation Chain Transfer (RAFT) Polymerization of Methyl Acrylate"; *Macromolecules* 2002, **35** (22), 8300-8306.
- (43) Barner-Kowollik, C.; Buback, M.; Charleux, B.; Coote, M. L.; Drache, M.; Fukuda, T.; Goto, A.; Klumperman, B.; Lowe, A. B.; McLeary, J. B.; Moad, G.; Monteiro, M. J.; Sanderson, R. D.; Tonge, M. P.; Vana, P. "Mechanism and kinetics of dithiobenzoate-mediated RAFT polymerization. I. The current situation"; *Journal of Polymer Science Part A: Polymer Chemistry* 2006, **44** (20), 5809-5831.
- (44) Moad, G. "Mechanism and Kinetics of Dithiobenzoate-Mediated RAFT Polymerization – Status of the Dilemma"; *Macromolecular Chemistry and Physics* 2014, **215** (1), 9-26.
- (45) Chong, Y. K.; Moad, G.; Rizzardo, E.; Thang, S. H. "Thiocarbonylthio End Group Removal from RAFT-Synthesized Polymers by Radical-Induced Reduction"; *Macromolecules* 2007, **40** (13), 4446-4455.
- (46) Moad, G.; Rizzardo, E.; Thang, S. H. "End-functional polymers, thiocarbonylthio group removal/transformation and reversible addition-fragmentation-chain transfer (RAFT) polymerization"; *Polymer International* 2011, **60** (1), 9-25.
- (47) Gody, G.; Maschmeyer, T.; Zetterlund, P. B.; Perrier, S. "Pushing the Limit of the RAFT Process: Multiblock Copolymers by One-Pot Rapid Multiple Chain Extensions at Full Monomer Conversion"; *Macromolecules* 2014, **47** (10), 3451-3460.
- (48) Rosselgong, J.; Williams, E. G. L.; Le, T. P.; Grusche, F.; Hinton, T. M.; Tizard, M.; Gunatillake, P.; Thang, S. H. "Core Degradable Star RAFT Polymers: Synthesis, Polymerization, and Degradation Studies"; *Macromolecules* 2013, **46** (23), 9181-9188.
- (49) Huang, J.; Koepsel, R. R.; Murata, H.; Wu, W.; Lee, S. B.; Kowalewski, T.; Russell, A. J.; Matyjaszewski, K. "Nonleaching Antibacterial Glass Surfaces via "Grafting Onto": The Effect of the Number of Quaternary Ammonium Groups on Biocidal Activity"; *Langmuir* 2008, **24** (13), 6785-6795.
- (50) Mendes, P. M. "Stimuli-responsive surfaces for bio-applications"; *Chemical Society Reviews* 2008, **37** (11), 2512-2529.
- (51) Dörfler, H.-D., Lichtstreuung an kolloiden und makromolekularen Systemen. in *Grenzflächen- und Kolloidchemie*, VCH Verlagsgesellschaft mbH.: 1994; pp 412-451.
- (52) Dörfler, H.-D., Strukturuntersuchung an kolloiden, makromolekularen und amphiphilen Systemen. in *Grenzflächen- und Kolloidchemie*, VCH Verlagsgesellschaft mbH.: 1994; pp 539-577.

- (53) Schreiber, P. D. F. Static and Dynamic Light Scattering (SLS/DLS). <http://www.soft-matter.uni-tuebingen.de/index.html?dls.html> (accessed 23.03.2017).
- (54) Schärftl, W. "*Light scattering from Polymer Solutions and Nanoparticle Dispersions*". Springer-Verlag Berlin Heidelberg: 2007; p 191.
- (55) Dynamic light scattering. https://en.wikipedia.org/wiki/Dynamic_light_scattering (accessed 23.03.2017).
- (56) Louis, C. P. M. d. S.; Daniela, U.; Marleen, M.; Ernst, J. R. S., Organic Surface Modification of Silicon Nanowire-Based Sensor Devices. 2011.
- (57) Veinot, J., Surface Passivation and Functionalization of Si Nanocrystals. in *Silicon Nanocrystals; Fundamentals, Synthesis and Applications*, Lorenzo Pavesi, R. T., Ed. Wiley VCH Verlag GmbH & Co. KGaA: 2010; pp 155-172.
- (58) Xiaosong Li, S. P.-K., Marta Alvarez, Ulrich jonas, Modification of Surfaces by Photosensitive Silanes. in *Surface Design: Applications in Bioscience and Nanotechnology*, R. Förch, H. S., A. T. A. Jenkins, Ed. WILEY-VCH verlag & GmbH & Co. KGaA: 2009; pp 207-220.
- (59) John C. Rivière, H. B., Introduction. in *Surface and Thin Film Analysis*, Gernot Friedbacher, H. B., Ed. Wiley VCH Verlag GmbH & Co. KGaA: 2011; pp 1-6.
- (60) Rulon E. Johnson Jr., R. H. D., Wetting of Low-Energy Surfaces. in *Wettability*, Berg, J. C., Ed. Taylor & Francis Group: 1993; pp 1-73.
- (61) GmbH, K. Schematic diagram of contac angle. <https://www.kruss.de/services/education-theory/glossary/contact-angle/> (accessed 24.03.2017).
- (62) Nosonovsky, M.; Ramachandran, R. "*Geometric Interpretation of Surface Tension Equilibrium in Superhydrophobic Systems*"; Entropy 2015, **17** (7), 4684.
- (63) Bernd Gruska, K. H., UV-VIS-IR Ellipsometry (ELL). in *Surface and Thin Film Analysis*, Gernot Friedbacher, H. B., Ed. Wiley VCH Verlag GmbH & Co. KGaA: 2011; pp 393-405.
- (64) Henning Bubert, J. C. R., Wolfgang S.M. Werner, X-ray Photoelectron Spectroscopy (XPS). in *Surface and Thin Film Analysis*, Gernot Friedbacher, H. B., Ed. Wiley VCH Verlag GmbH & Co. KGaA: 2011; pp 9-41.
- (65) Axelrod, D., Total Internal Reflection Fluorescence Microscopy. in *Optical Imaging and Microscopy*, Peter Török, J.-J. K., Ed. Springer-Verlag Berlin Heidelberg: 2007; pp 195-233.
- (66) M. Jübner, A. S., K. Bender, Surface Chemistry in Forensic-Toxicological analysis. in *Surface Design: Applications in Bioscience and Nanotechnology*, R. Förch, H. S., A. T. A. Jenkins, Ed. WILEY-VCH verlag & GmbH & Co. KGaA: 2009; pp 183-206.
- (67) Sevcsik, E.; Brameshuber, M.; Fölser, M.; Weghuber, J.; Honigmann, A.; Schütz, G. J. "*GPI-anchored proteins do not reside in ordered domains in the live cell plasma membrane*"; Nature Communications 2015, **6**, 6969.
- (68) Schönherr, H., Coupling Chemistries for the Modification and Functionalization of Surfaces to Create Advanced Biointerfaces in *Surface Design: Applications in Bioscience and Nanotechnology*, R. Förch, H. S., A. T. A. Jenkins, Ed. WILEY-VCH verlag & GmbH & Co. KGaA: 2009; pp 3-28.
- (69) E. Benetti, M. N., S. Zapotocny, G. J. Vancso, Stimuli-responsive Polymer Brushes. in *Surface Design: Applications in Bioscience and Nanotechnology*, R. Förch, H. S., A. T. A. Jenkins, Ed. WILEY-VCH verlag & GmbH & Co. KGaA: 2009; pp 125-144.
- (70) Tischer, T.; Gralla-Koser, R.; Trouillet, V.; Barner, L.; Barner-Kowollik, C.; Lee-Thedieck, C. "*Direct Mapping of RAFT Controlled Macromolecular Growth on Surfaces via Single Molecule Force Spectroscopy*"; ACS Macro Letters 2016, **5** (4), 498-503.

- (71) Isahak, N.; Sanchez, J.; Perrier, S.; Stone, M. J.; Payne, R. J. "Synthesis of polymers and nanoparticles bearing polystyrene sulfonate brushes for chemokine binding"; *Organic & Biomolecular Chemistry* 2016, **14** (24), 5652-5658.
- (72) Stenzel, M. H.; Zhang, L.; Huck, W. T. S. "Temperature-Responsive Glycopolymers Synthesized via RAFT Polymerization Using the Z-group Approach"; *Macromolecular Rapid Communications* 2006, **27** (14), 1121-1126.
- (73) Moad, G.; Chong, Y. K.; Postma, A.; Rizzardo, E.; Thang, S. H. "Advances in RAFT polymerization: the synthesis of polymers with defined end-groups"; *Polymer* 2005, **46** (19), 8458-8468.
- (74) Schachner, M. *Synthese polymerer Wirkstoffträgersysteme mittels RAFT Polymerisation*. master thesis, Technische Universität Wien, Vienna, 2012.
- (75) Northrop, B. H.; Frayne, S. H.; Choudhary, U. "Thiol-maleimide "click" chemistry: evaluating the influence of solvent, initiator, and thiol on the reaction mechanism, kinetics, and selectivity"; *Polymer Chemistry* 2015, **6** (18), 3415-3430.
- (76) Willcock, H.; O'Reilly, R. K. "End group removal and modification of RAFT polymers"; *Polymer Chemistry* 2010, **1** (2), 149-157.
- (77) Skey, J.; O'Reilly, R. K. "Facile one pot synthesis of a range of reversible addition-fragmentation chain transfer (RAFT) agents"; *Chemical Communications* 2008, (35), 4183-4185.
- (78) Galinsky, G.; Burchard, W. "Starch Fractions as Examples for Nonrandomly Branched Macromolecules. 3. Angular Dependence in Static Light Scattering"; *Macromolecules* 1997, **30** (15), 4445-4453.
- (79) Fuetterer, T.; Nordskog, A.; Hellweg, T.; Findenegg, G. H.; Foerster, S.; Dewhurst, C. D. "Characterization of polybutadiene-poly(ethyleneoxide) aggregates in aqueous solution: A light-scattering and small-angle neutron-scattering study"; *Physical Review E* 2004, **70** (4), 041408.
- (80) Kholodenko, A. L. "Analytical calculation of the scattering function for polymers of arbitrary flexibility using the dirac propagator"; *Macromolecules* 1993, **26**, 4179-4183.
- (81) Breßler, I. SASfit Manual. <http://sasfit.ingobressler.net/manual/KholodenkoWorm>.
- (82) Kratky, O.; Porod, G. "Röntgenuntersuchung gelöster Fadenmoleküle"; *Recueil des Travaux Chimiques des Pays-Bas* 1949, **68** (12), 1106-1122.
- (83) Buchholz, E.; Fox, M. A.; Whitesell, J. K.; Glauner, F.; Lichtenthäler, J.; Müller-Becker, S.; Wolf, K. "Organische Chemie: Grundlagen, Mechanismen, bioorganische Anwendungen". Spektrum Akademischer Verlag: 1995.
- (84) Xu, J.; He, J.; Fan, D.; Wang, X.; Yang, Y. "Aminolysis of Polymers with Thiocarbonylthio Termini Prepared by RAFT Polymerization: The Difference between Polystyrene and Polymethacrylates"; *Macromolecules* 2006, **39** (25), 8616-8624.
- (85) Bozym, R. A.; Chimienti, F.; Giblin, L. J.; Gross, G. W.; Korichneva, I.; Li, Y.; Libert, S.; Maret, W.; Parviz, M.; Frederickson, C. J.; Thompson, R. B. "Free zinc ions outside a narrow concentration range are toxic to a variety of cells in vitro"; *Experimental biology and medicine* (Maywood, N.J.) 2010, **235** (6), 741-750.
- (86) Winther, J. R.; Thorpe, C. "Quantification of Thiols and Disulfides"; *Biochimica et biophysica acta* 2014, **1840** (2), 10.1016/j.bbagen.2013.03.031.
- (87) Perrier, S.; Takolpuckdee, P.; Mars, C. A. "Reversible Addition-Fragmentation Chain Transfer Polymerization: End Group Modification for Functionalized Polymers and Chain Transfer Agent Recovery"; *Macromolecules* 2005, **38** (6), 2033-2036.
- (88) Bouchékif, H.; Narain, R. "Reversible Addition-Fragmentation Chain Transfer Polymerization of N-Isopropylacrylamide: A Comparison between a Conventional and a Fast Initiator"; *The Journal of Physical Chemistry B* 2007, **111** (38), 11120-11126.

- (89) Kim, J. W. C., Dae Won; Park, Gyoosoon; Kim, Sung Hong; Ra, Choon Sup "Efficient Ring Opening Reaction of Epoxides with Oxygen Nucleophiles Catalyzed by Quaternary Onium Salt"; Bulletin of the Korean Chemical Society 2013, **Volume 34** (Issue 8), 2286-2290.
- (90) Garoff, H.; Ansorge, W. "Improvements of DNA sequencing gels"; Analytical Biochemistry 1981, **115** (2), 450-457.
- (91) Scofield, J. H. "Hartree-Slater subshell photoionization cross-sections at 1254 and 1487 eV"; Journal of Electron Spectroscopy and Related Phenomena 1976, **8** (2), 129-137.
- (92) G. Beamson, D. B., High Resolution XPS of Organic Polymers: The Scienta ESCA300 Database Wiley: 1992; p Appendices 3.1 and 3.2.
- (93) C.D. Wagner, A. V. N., A. Kraut-Vass, S.W. Gaarenstroom, C. J. Powell, J.W. Allison, J.R. Rumble NIST Standard reference Database 20. <https://srdata.nist.gov/xps/>.